О распределении грозовой активности и роли молнии в глобальной электрической цепи

Е.А.Мареев
Институт прикладной физики РАН,
Нижний Новгород
evgeny.mareev@gmail.com

Особая благодарность: Е.М.Володину, В.А.Ракову, Н.Н.Слюняеву

План

- Введение (физика молнии).
- Мониторинг молниевой активности.
- Статистика пиковых токов молнии.
- Параметризация молнии. Распределение вспышек по земному шару. Эль-Ниньо.
- Молнии и климат. Глобальная электрическая цепь.

Оптические наблюдения интенсивной молнии с помощью высокоскоростной камеры

Триггерная молния (Rocket-and-wire triggered lightning experiments)

Отрицательный разряд *облако-земля*

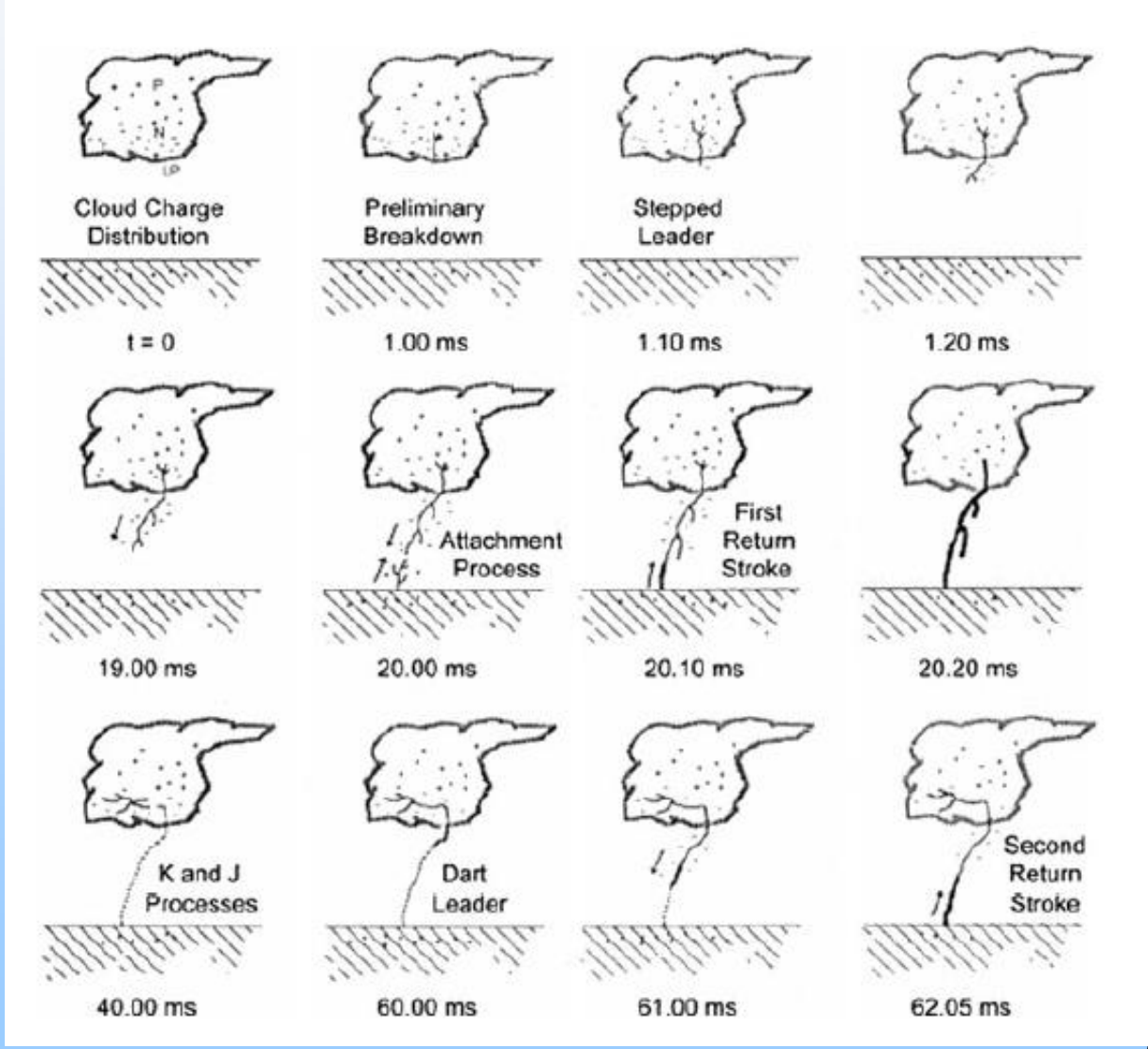

"Lightning: Physics and Effects" (V.A. Rakov and M.A. Uman, 2003, Cambridge University Press)

Этапы развития главной стадии молнии (Базелян, Горин, Левитов, 1978)

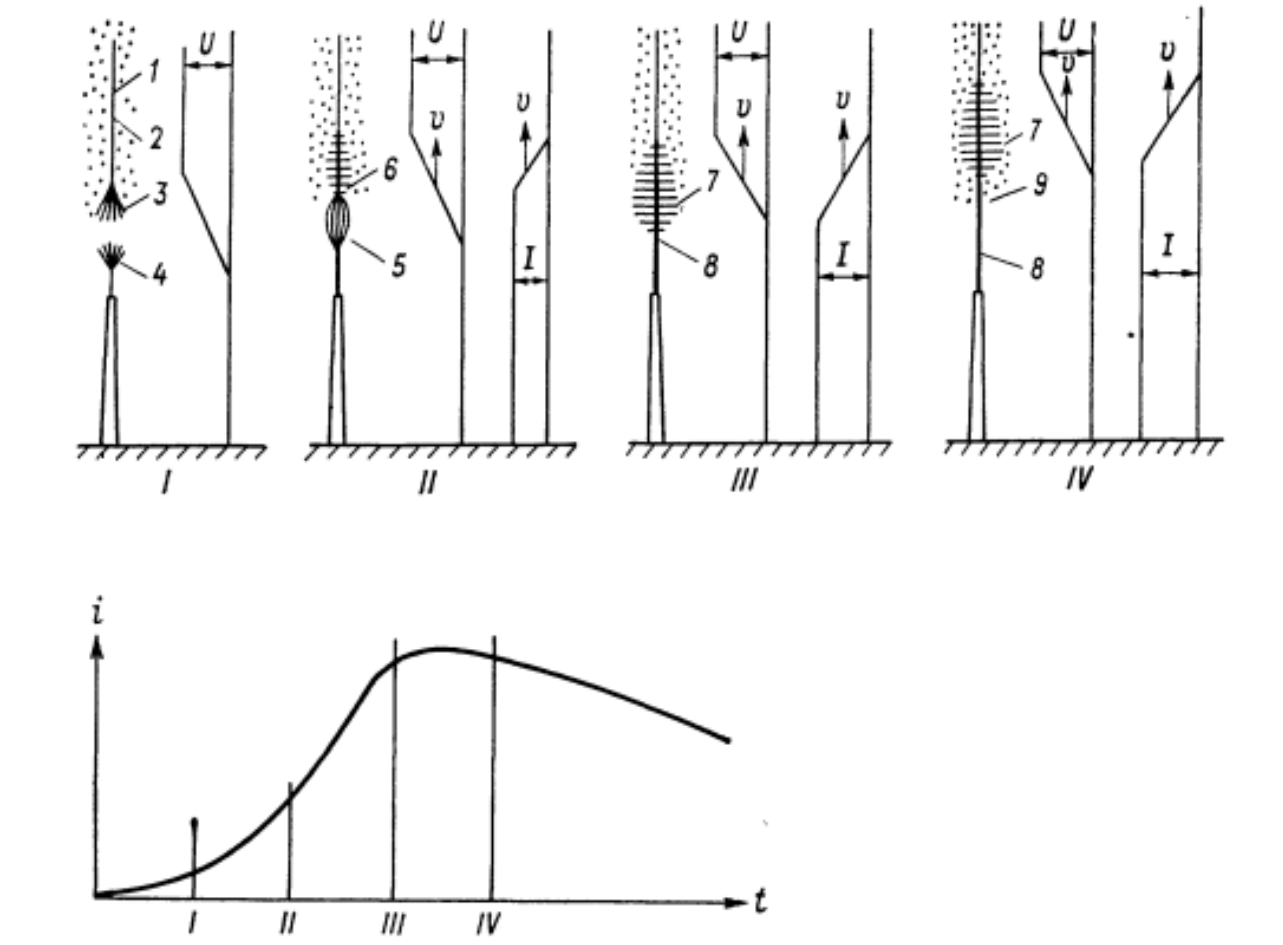

Эксперименты с искусственным облаком

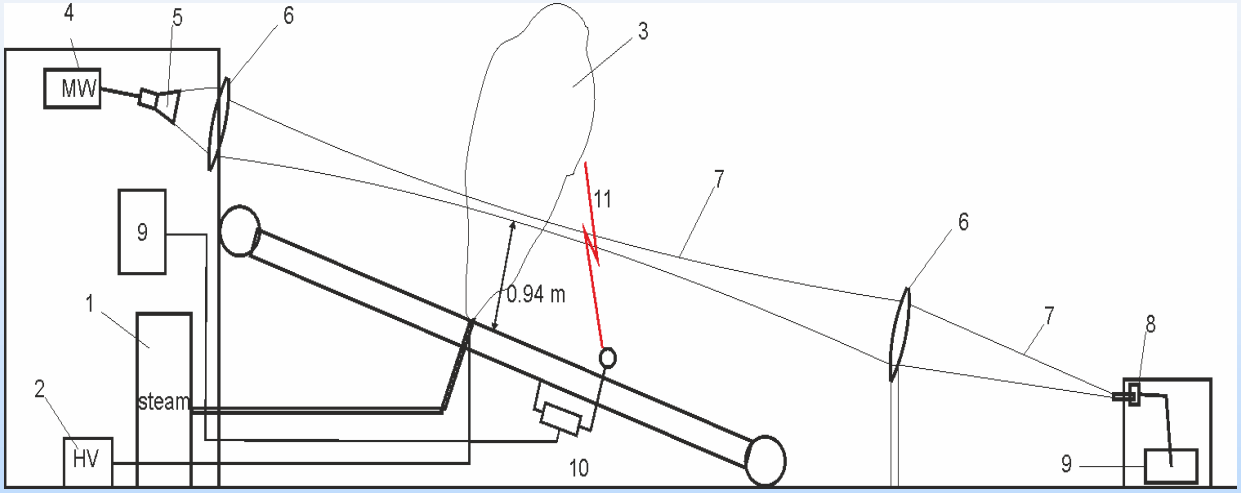

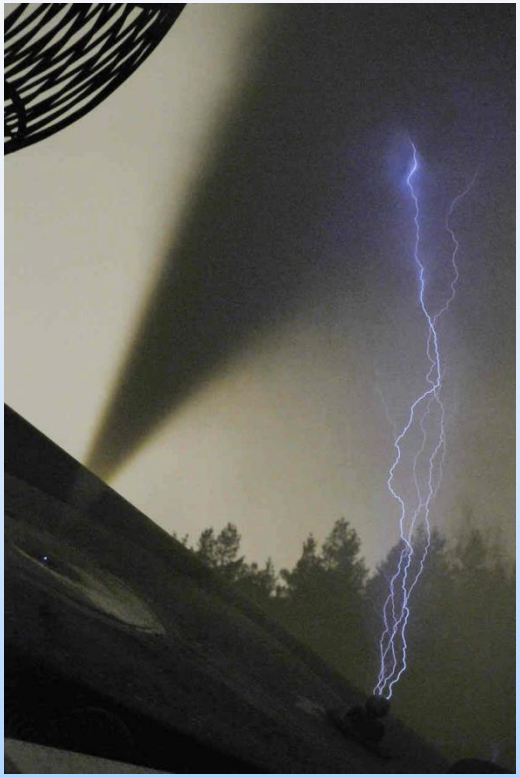

1 – парогенератор, 2 – высоковольтный источник питания, 3 – заряженное аэрозольное облако, 4 – СВЧ генератор, 5 – излучающий рупор, 6 – линзы, 7 - СВЧ пучок, 8 – детектор, 9 – осциллографы, 10 – измерительный шунт, 11 – искровой разряд облако-земля

Встреча нисходящего отрицательного лидера и восходящего положительного

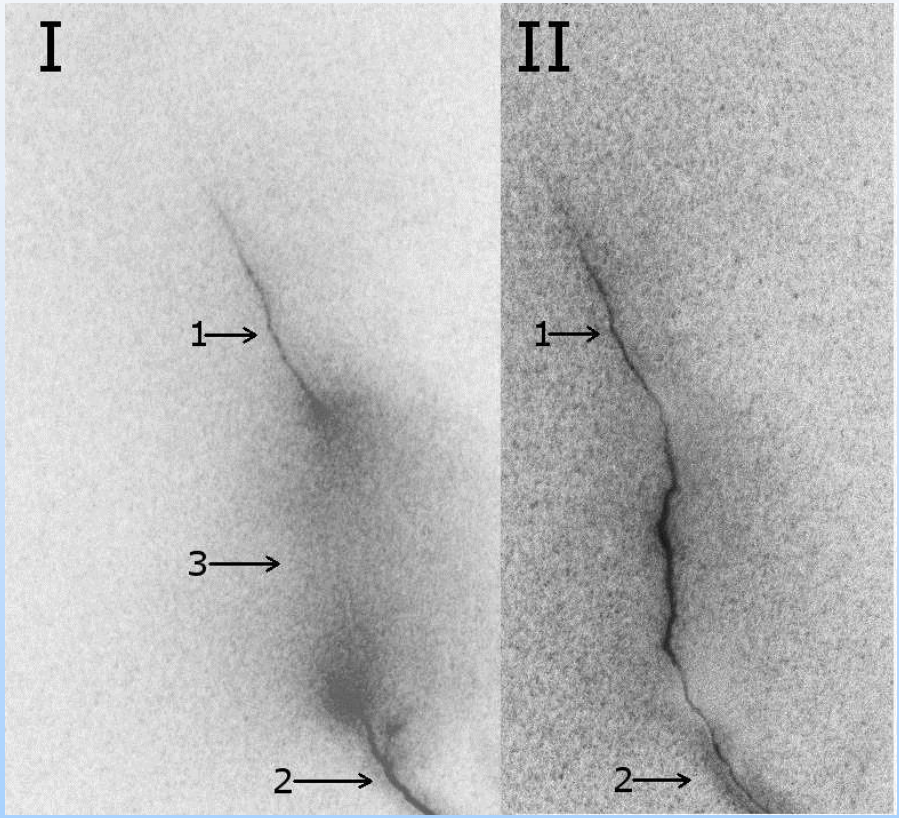

Kostinsky et al., JGR (2016)

Two 4Picos frames showing the break-through phase (I) and later return-stroke stage (II) of a negative discharge to ground generated by the cloud of artificially-charged water droplets. The exposure time for each frame is 100 ns and the time interval between frames is 2 μs. Labeled are the electrodeless downward negative leader 1, upward positive leader 2, and the common streamer zone 3. Image (II) was considerably fainter than image (I) and was contrast-enhanced more than image (I), to improve its visualization. AGP stands for “above the grounded plane”

Природа ступеней лидера

Biagi et al., JGR, 2010

V. A. Rakov, The Physics of Lightning, Surveys in Geophysics, 2013

Petersen and Beasley, JGR, 2013

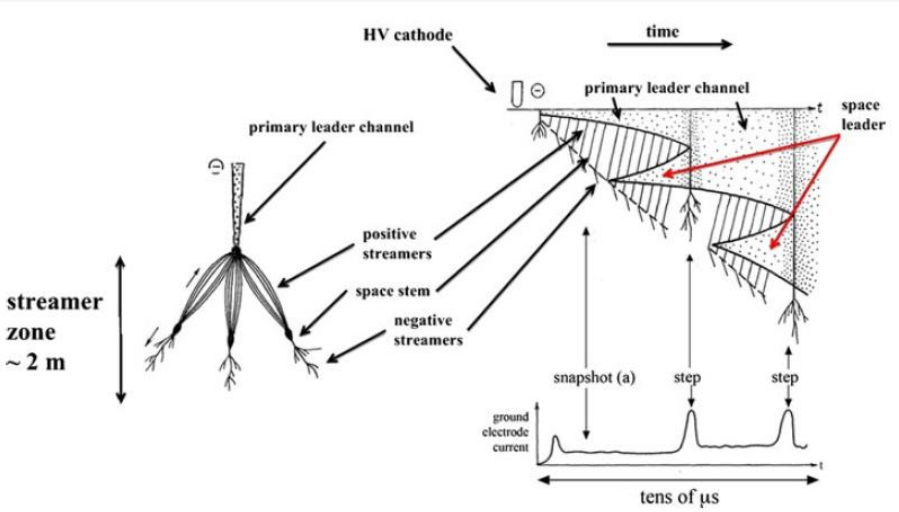

Illustration of the development of negative stepped leader in a long laboratory spark, based on a description given by Gorin et al. (1976). It schematically shows a snap-shot (*left*) and a time-resolved optical picture (*upper right*) including an initial impulsive corona from the negative high-voltage electrode and the first two steps, along with the corresponding current through the gap (*lower right*). Adapted from Biagi et al. (2010)

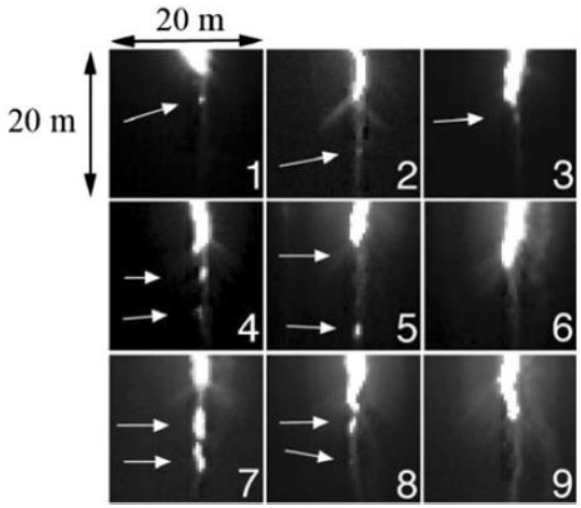

The bottom 20 m of the downward-extending leader channel of a triggered-lightning flash (Camp Blanding, Florida) in the nine high-speed video frames (240 kfps, 4.17 μs per frame). Each image shows about 20 m × 20 m. The *white arrows* point to the luminous segments (space stems or leaders), 1–4 m in length, that formed separately from and 1–10 m below the downward-extending leader channel. The leader traveled about 100 m from frame 1 to frame 9 where it was about 30 m above its termination point. The return stroke began during frame 10. Adapted from Biagi et al. (2010)

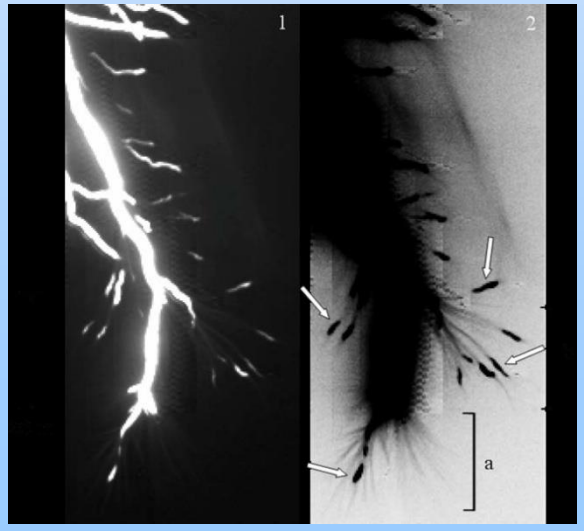

Лавины, стримеры, стемы…

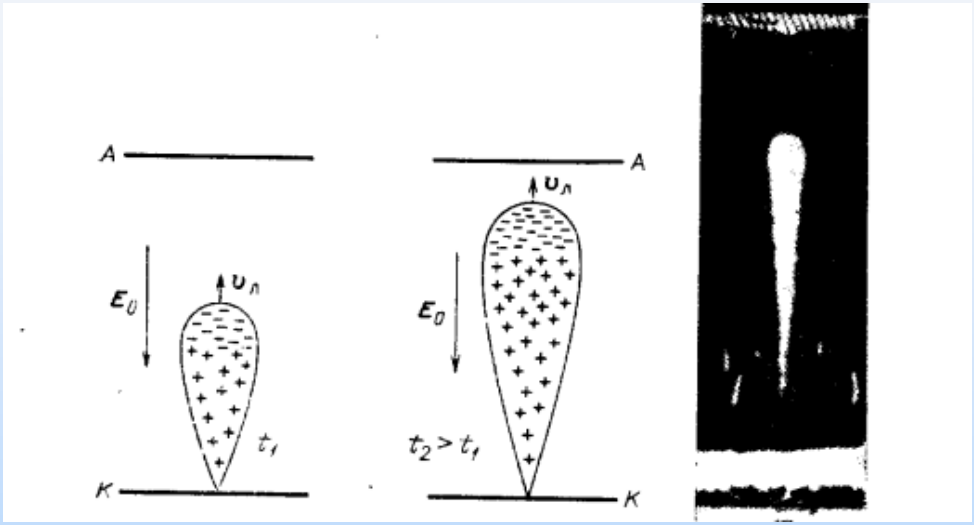

- Avalanches
- Streamers
- Stems, Stalkers
- Leaders:
  - positive/negative
  - first/subsequent
  - direct/recoil
- Return stroke (spark)

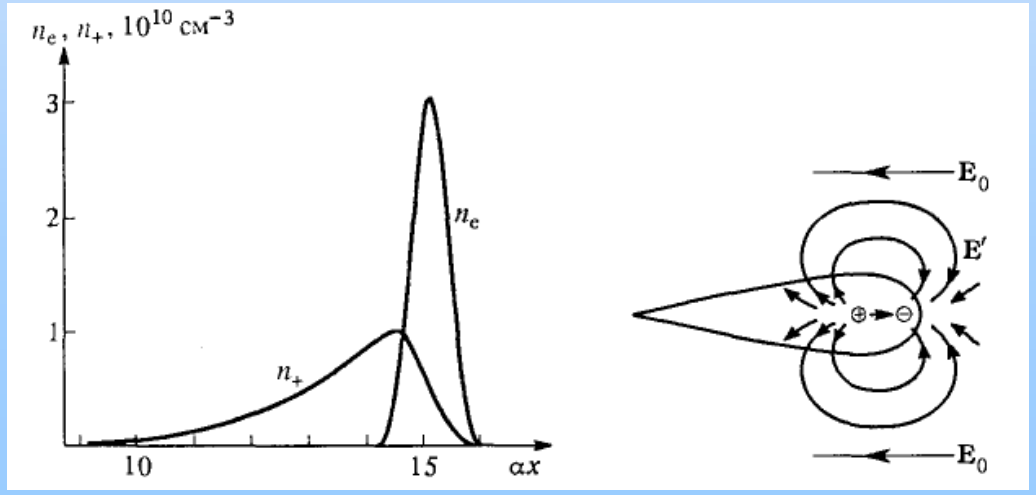

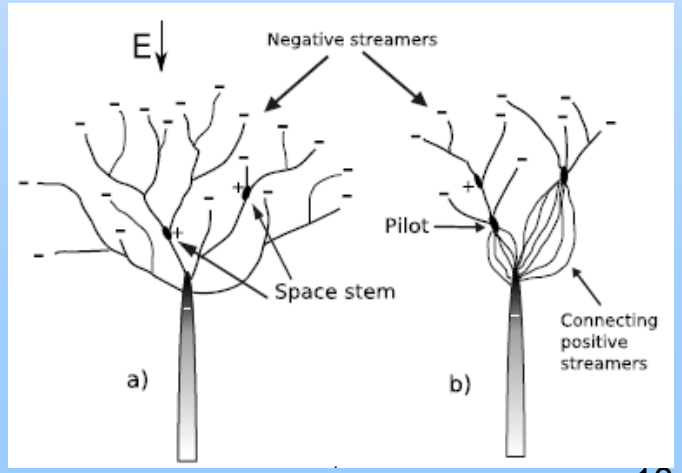

Return stroke current

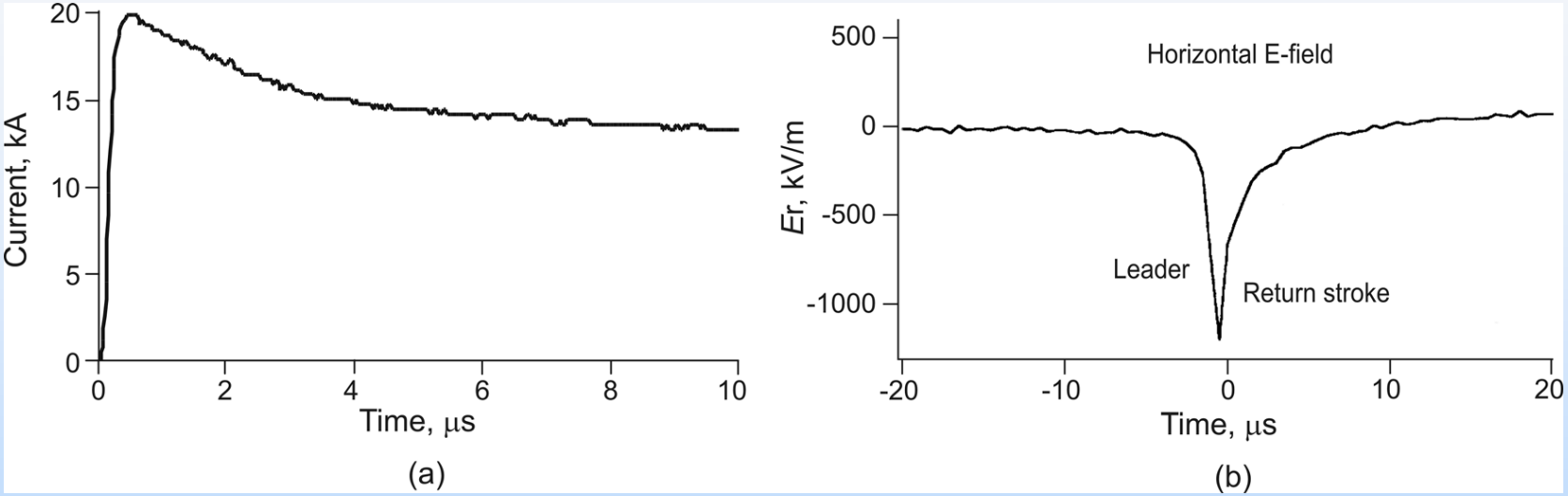

Miki et al. (2002)

Return stroke current at the channel base and (b) corresponding horizontal (radial) electric field 0.1 m from the triggered lightning channel core

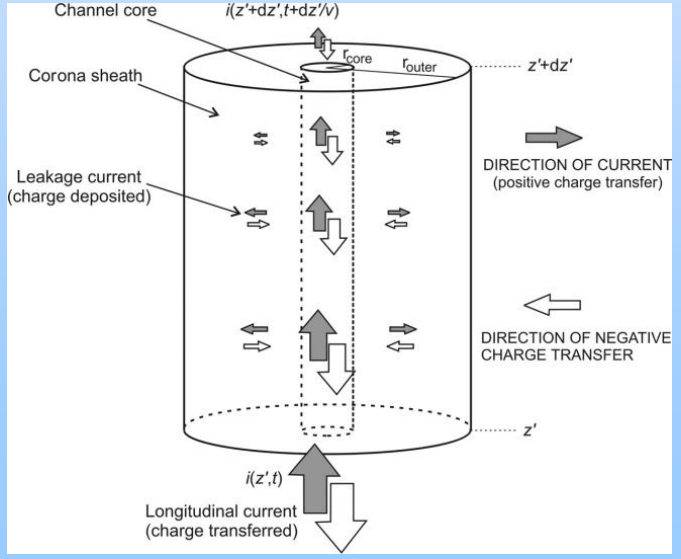

Maslowsky and Rakov (2006)

Газодинамика канала молнии

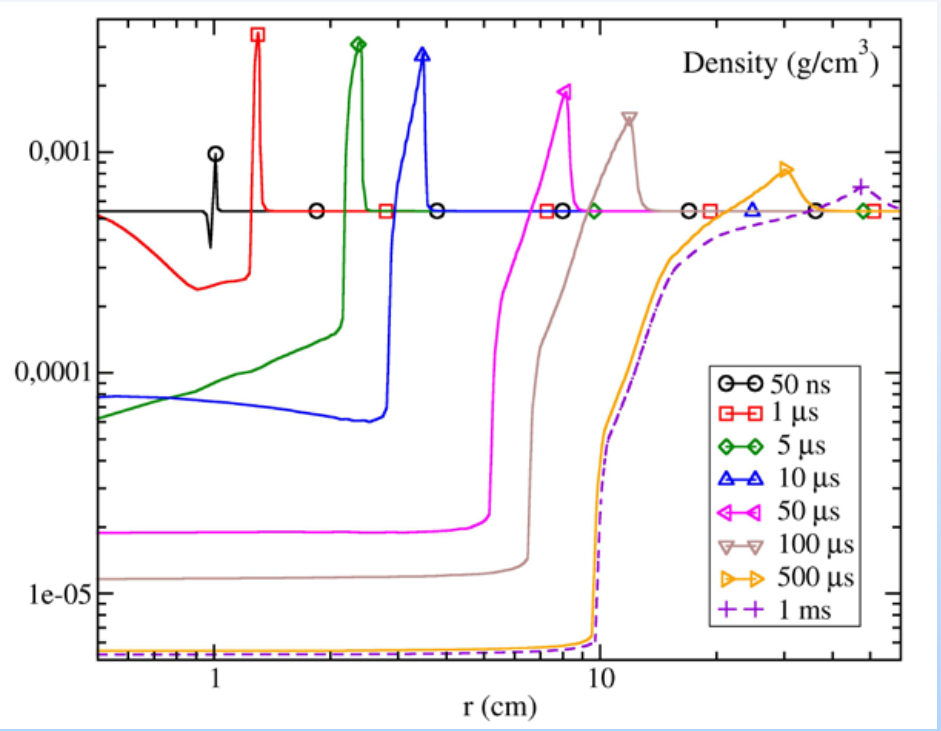

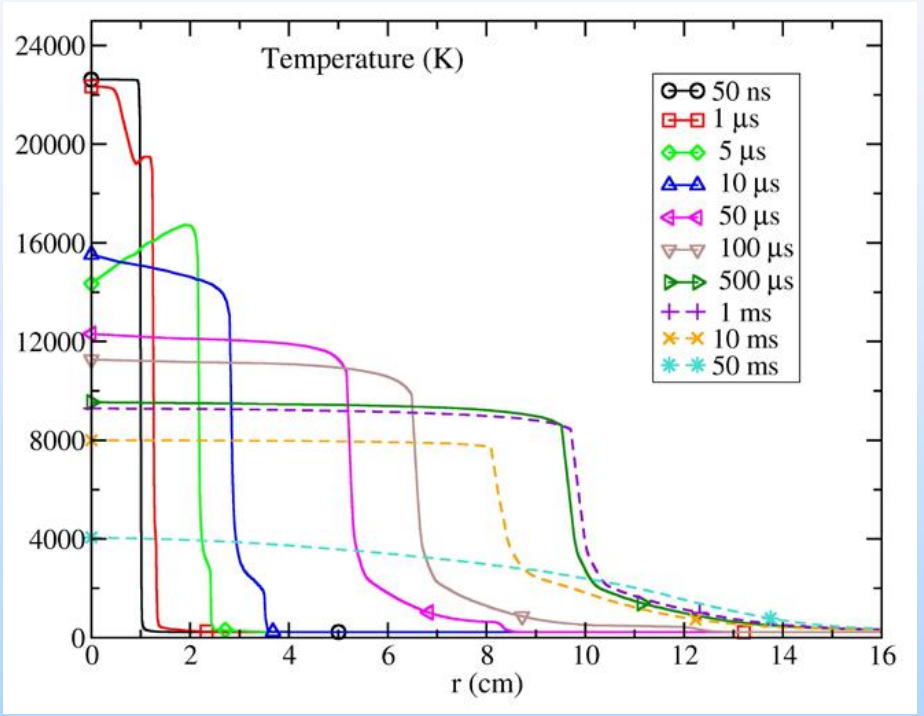

Ripoll et al., 2014.

$$-\frac{\partial V(z',t)}{\partial z'} = L\frac{\partial I(z',t)}{\partial t} + RI(z',t)$$

$$-\frac{\partial I(z',t)}{\partial z'} = C\frac{\partial V(z',t)}{\partial t}$$

Berger et al. (1975) data for peak current

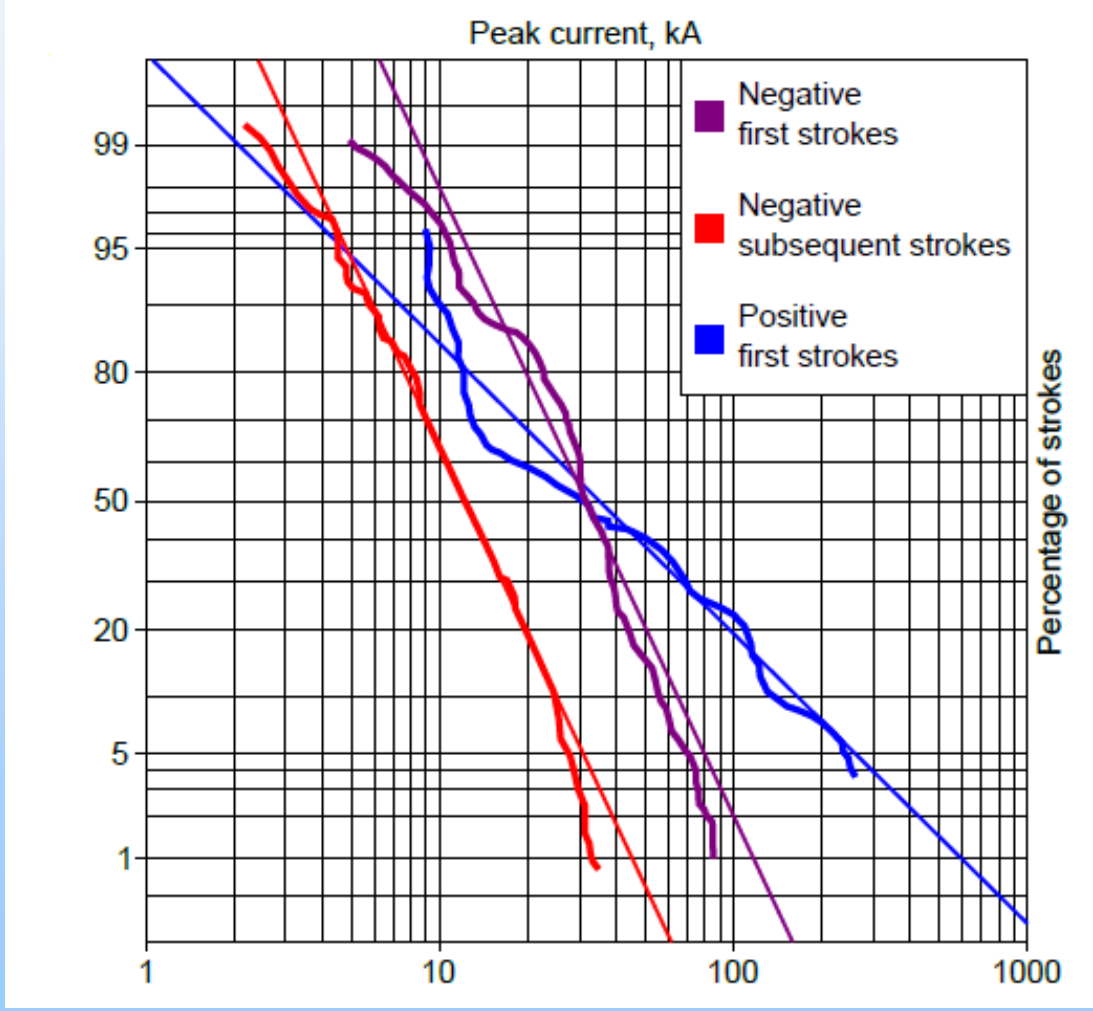

Histograms derived from Berger et al. (1975)

Negative first strokes

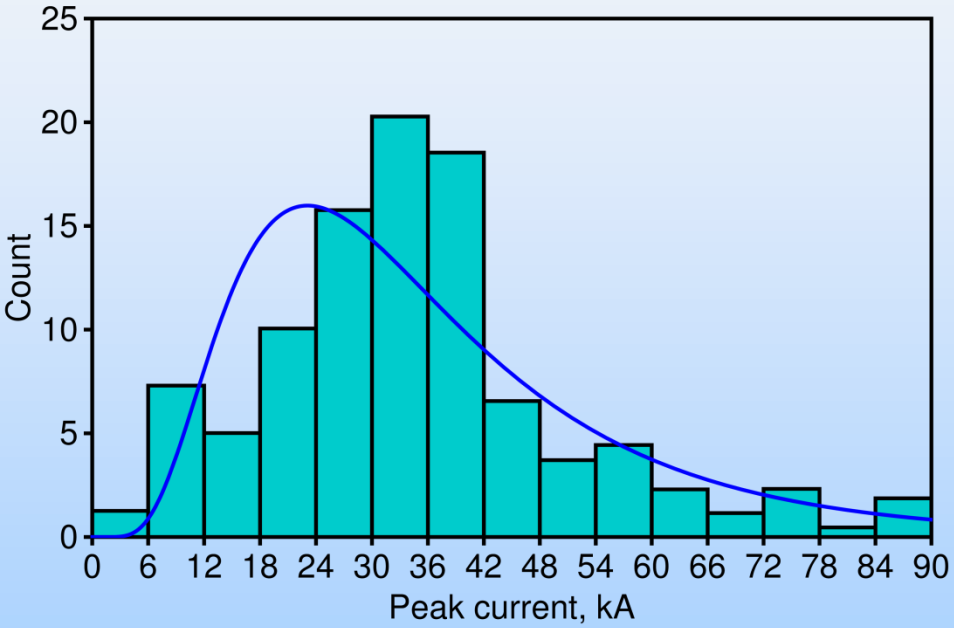

Negative subsequent strokes

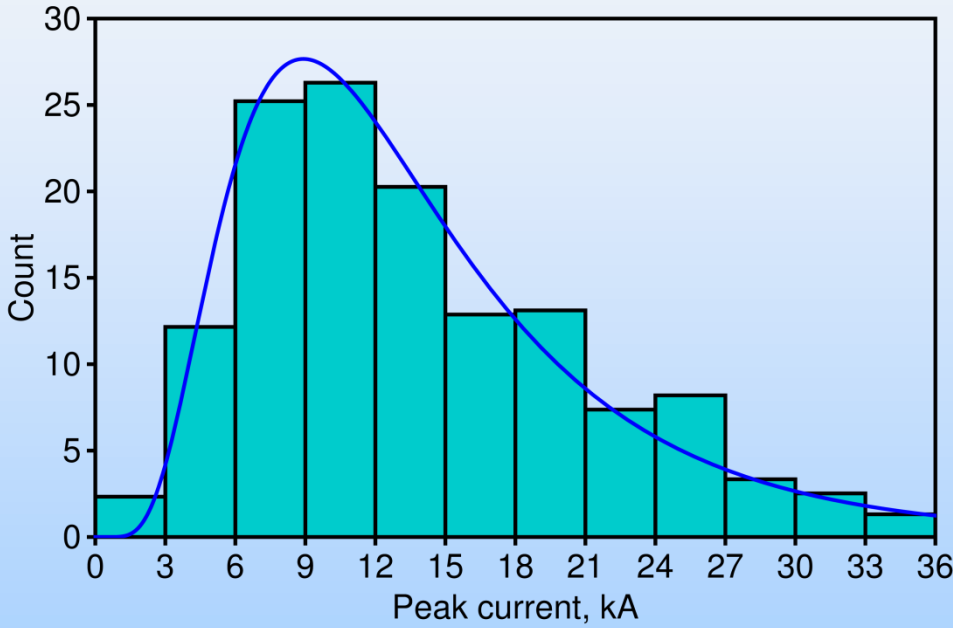

Сравнение с данными NLDN и триг. молнии

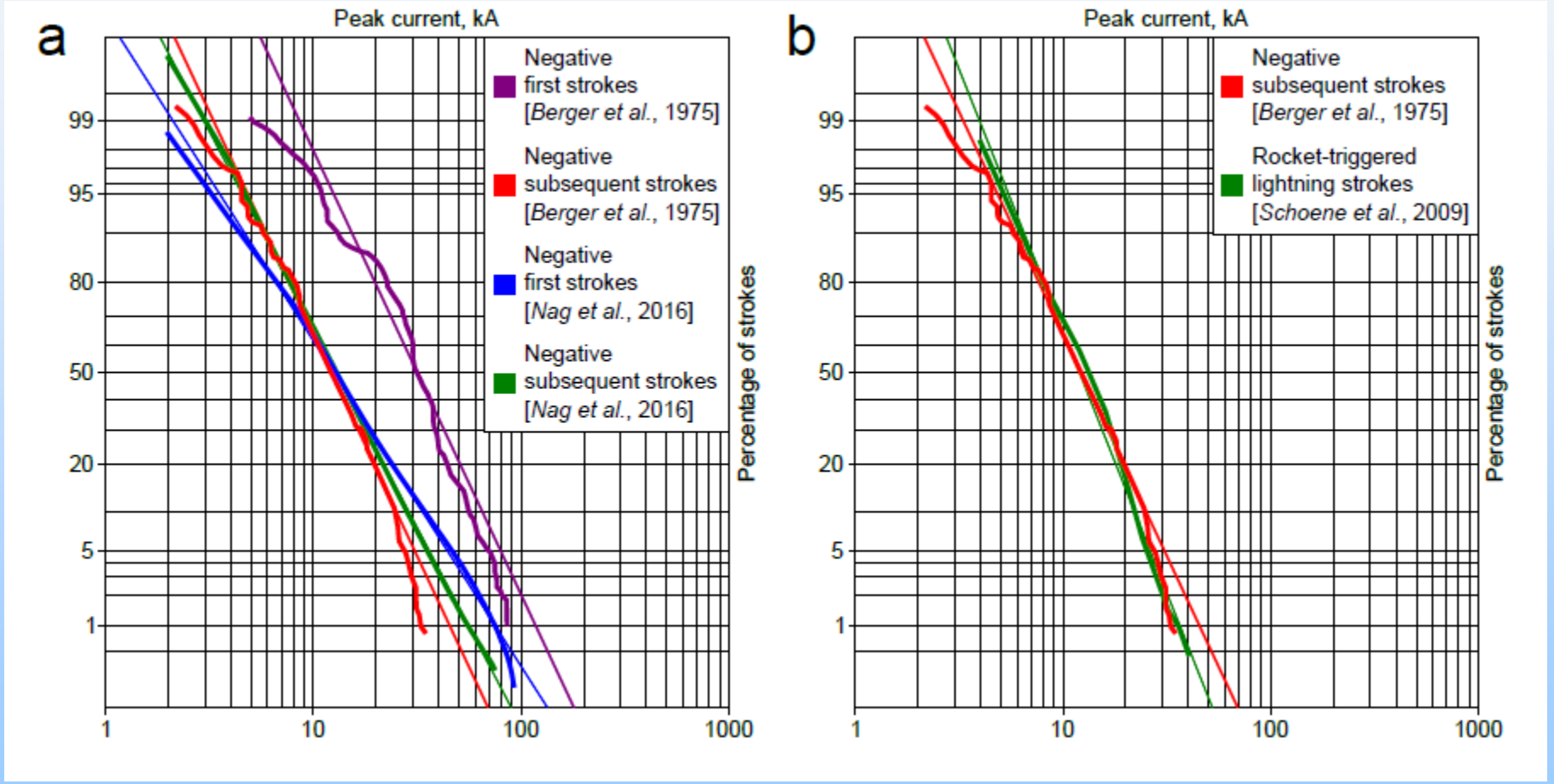

Lightning PC – Berger's Distributions

Lightning peak currents for first strokes vary by a factor of 50 or more, from about 5 to 250 kA.

The probability of occurrence of a given value rapidly increases up to 25 kA or so and then slowly decreases.
Statistical distributions of this type are often assumed to be lognormal.

$$P(I) = \frac{1}{\sqrt{2\pi}\sigma I} \exp\left\{-\frac{(\ln I - \ln I_0)^2}{2\sigma^2}\right\} \qquad I\,(\mathrm{kA}) = 10.6\,Q^{0.7}.$$

Cumulative statistical distributions of lightning peak currents, giving percent of cases exceeding abscissa value, from direct measurements in Switzerland (Berger et al. 1975). The distributions are assumed to be lognormal and given for (1) negative first strokes (N=101), (2) positive first strokes (N=26), and (3) negative subsequent strokes (N=135).

Lightning current characteristics

	Measured Values		Modeled Values	
	50%	1%	50%	1%
RETURN STROKE PARAMETERS				
NEGATIVE FIRST STROKES				
(a) Peak current (kA)	30	150	32	160
(b) Time from zero to current peak (μs)	5	30	6	6
(c) Maximum rate of current rise (kA/μs)	100	400	100	500
(d) Time to decay from peak to half-peak value (μs)	70-80	300	75	80
(e) Charge Transfer (C)	5	40	5.5	27
POSITIVE FIRST STROKES				
(a) Peak current (kA)	35	500	35	350
(b) Time to current peak (μs)	10-20	150	11	11
(c) Maximum rate of current rise (kA/μs)	100	400	100	500
(d) Time to decay to half-peak value (μs)	†	†	30	40
NEGATIVE SUBSEQUENT STROKES				
(a) Peak current (kA)	10-15	50	11	56
(b) Time to current peak (10-90 percent) (μs)	0.3-0.6	9	0.6	0.6

The median (50%) and severe (1%) lightning currents at ground appear to be:
30 kA and 150 kA for negative first strokes,
10-15 kA and 50 kA for negative subsequent strokes, 35 kA and 500 kA for positive first strokes (as follows from lognormal distributions)

Gamerota et al., IEEE Trans. Electrom. Compat., 2012

The largest directly measured lightning currents (positive lightning, probably of upward type, in winter storms in Japan)

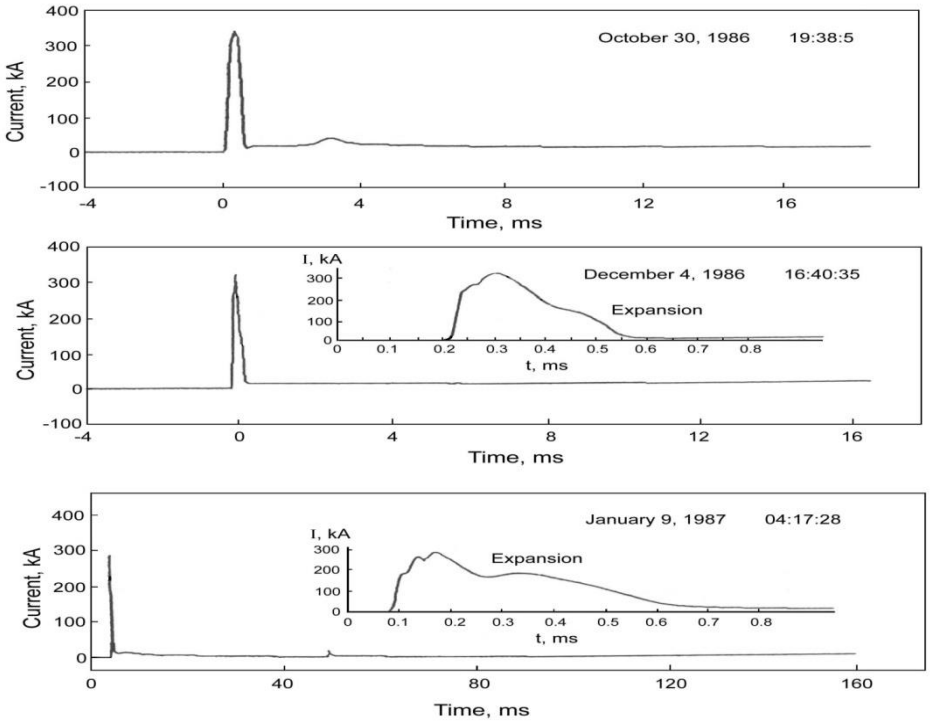

Directly measured currents in three positive lightning discharges in Japan. The insets in the middle and bottom diagrams show the current on an expanded scale. The transferred charges, from top to bottom, are 330,180, and 400 C. Adapted from Goto and Narita (1995).

Model of lightning channel. Electrodynamics

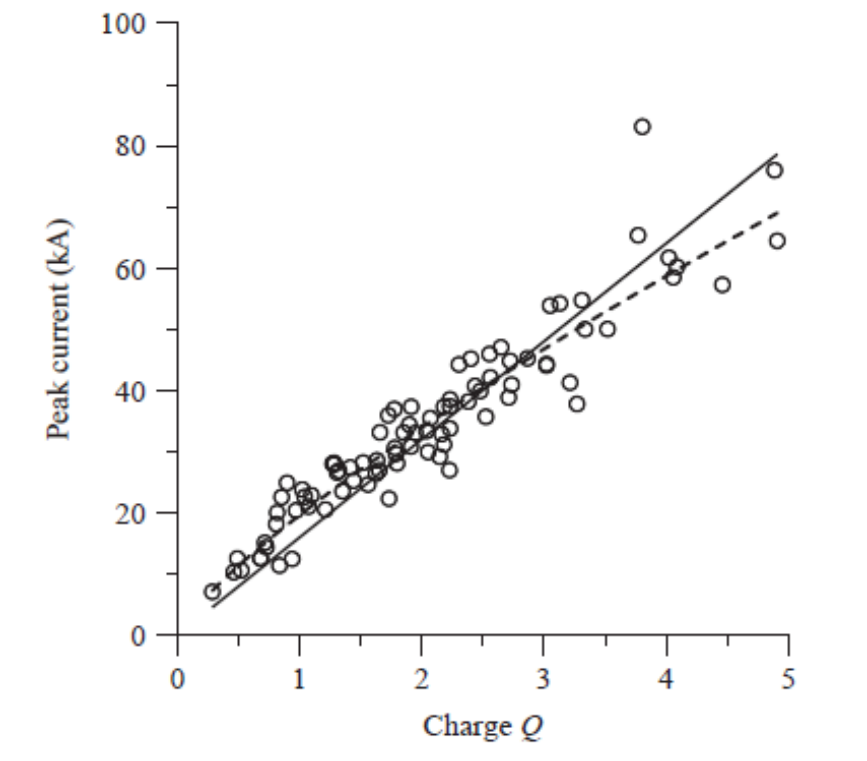

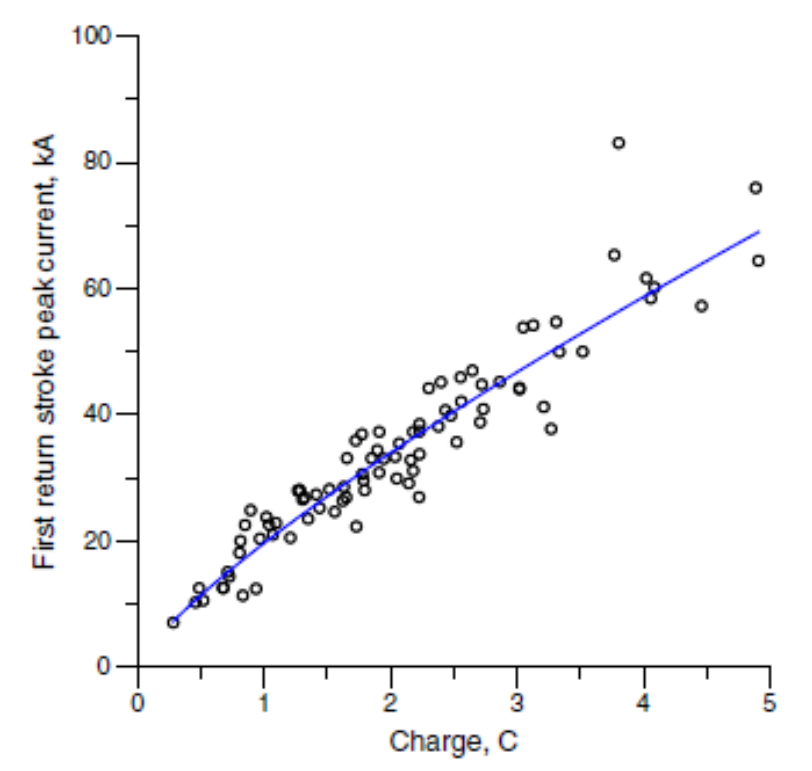

$$I\ peak = 19.6\ Q^{0.78}$$

Cooray and Rakov, 2012

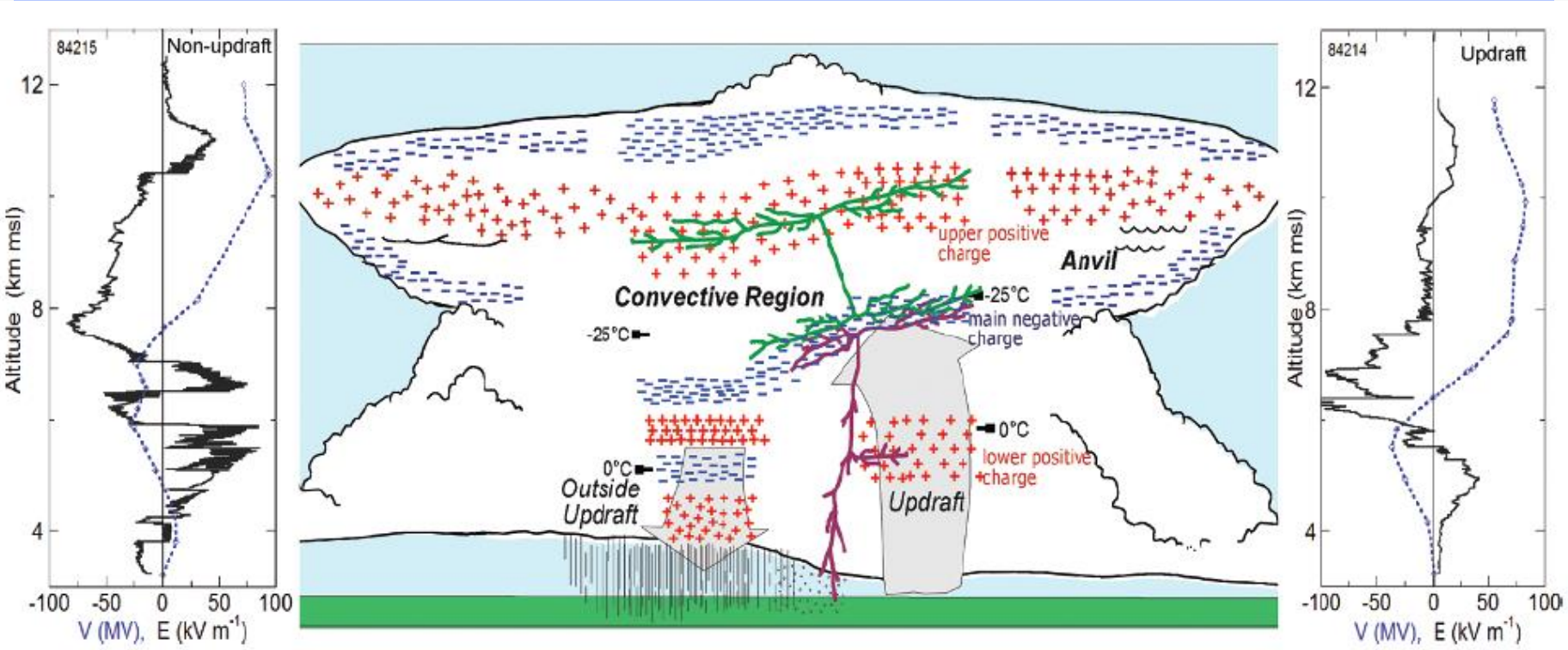

Conceptual model of the electrical structure in mature, mid-latitude convection. Four main charge regions (with red + for positive charge, blue – for negative charge) are typically found in soundings through updrafts, while soundings outside updrafts have at least six charge regions in common. Representative electric field (E) and electrostatic potential (V) profiles in the nonupdraft (left) and updraft (right) of the convective region are also shown; the altitudes in these soundings do not correspond exactly to the conceptual model. Schematic representations of an intracloud flash (in green) and a cloud-to-ground flash (in purple) are shown as they might appear in lightning mapping data (**Stolzenburg and Marshall, 2009**)

A sketch of the stepped leader approaching ground; charge distribution along the leader

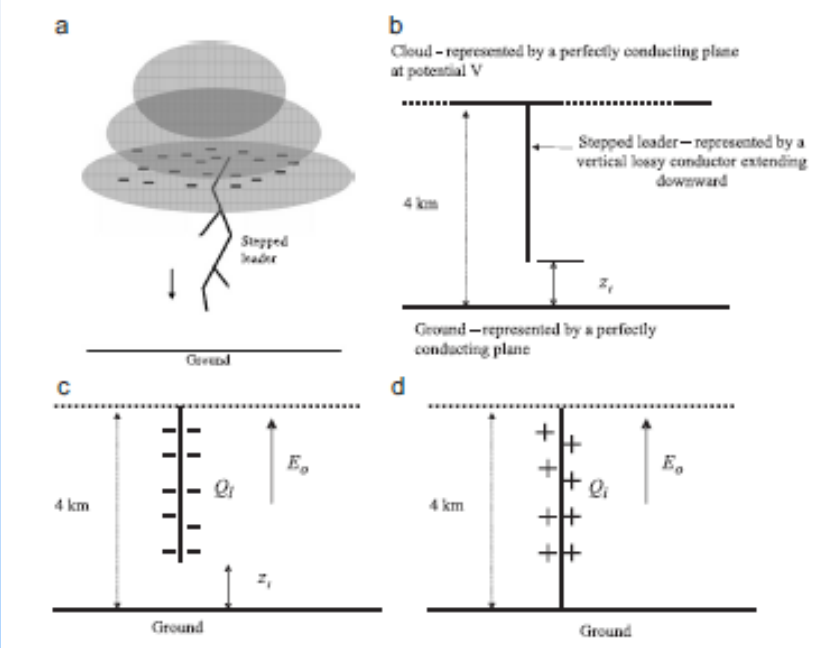

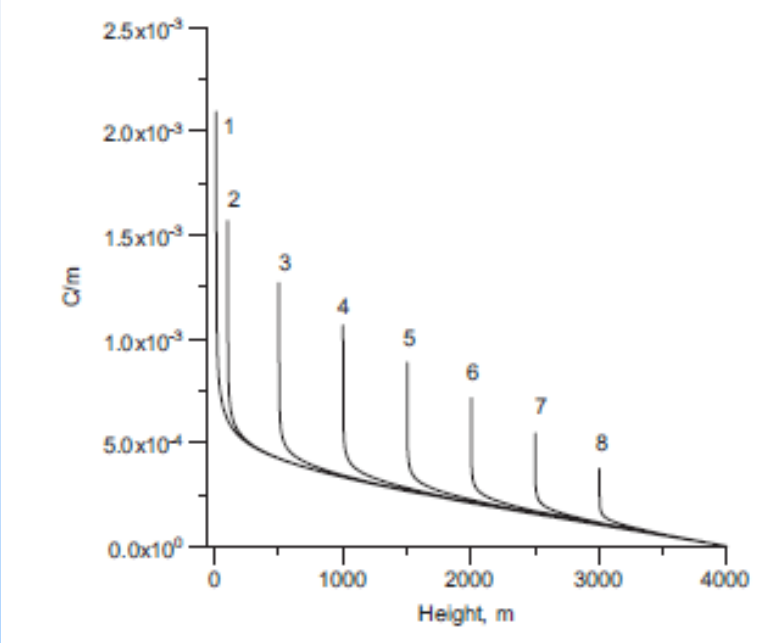

Cooray et al., J. Electrost., 2007

Peak current vs large-scale electric field and cloud potential

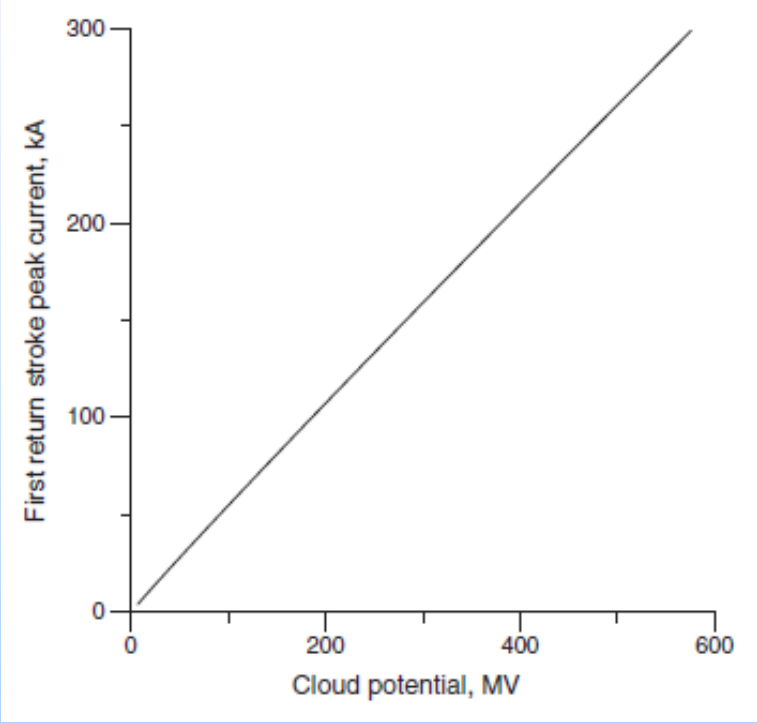

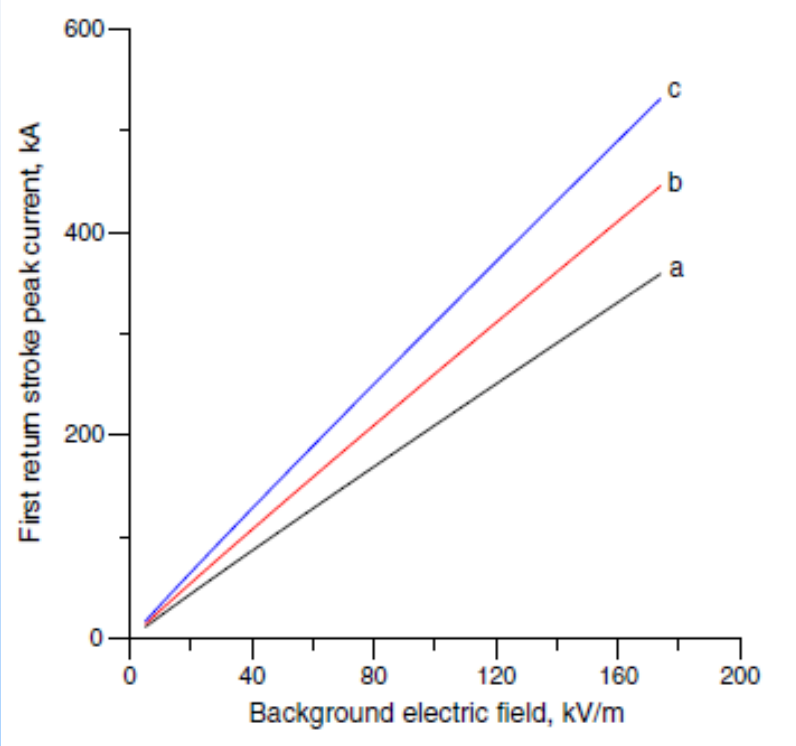

$$I\,peak = 2.44\,E^{0.967}$$

$$I\,peak = 10^{-6}\,V^{0.967}$$

Cooray and Rakov, 2012

Electric field in thunderclouds

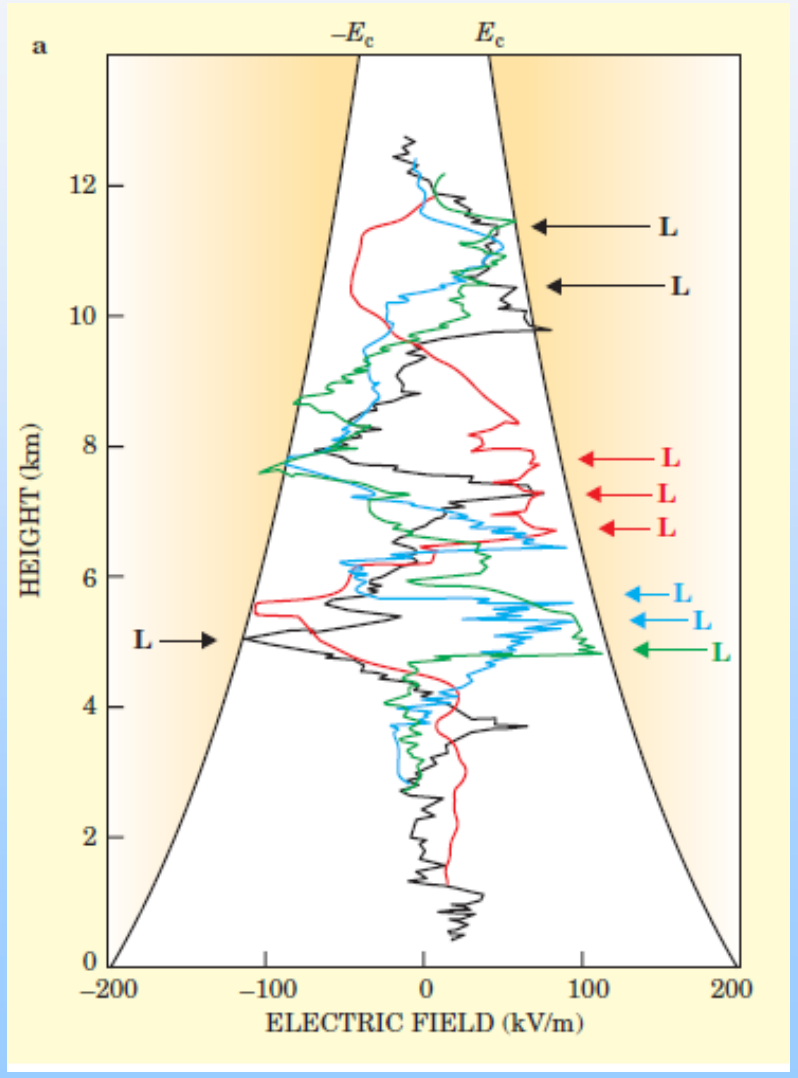

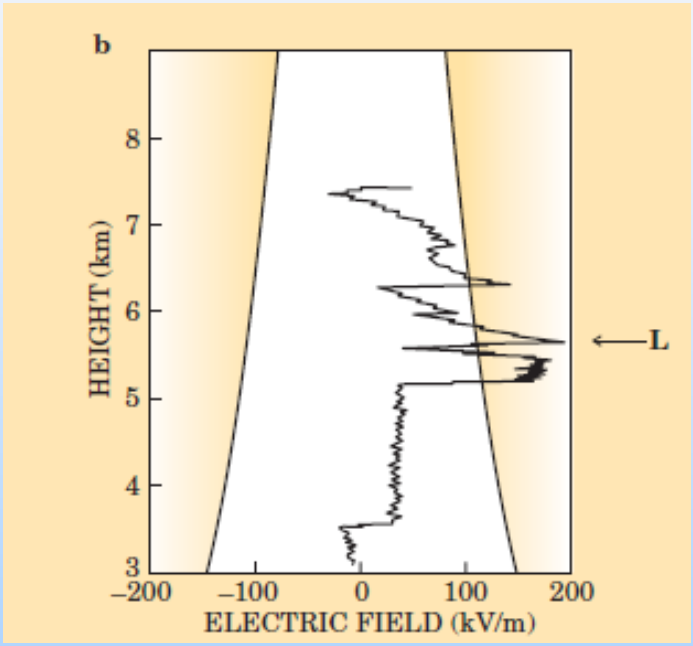

Marshall et al., JGR, 1995

Выводы по экстремальным токам

- The CIGRE Broshure #549 (2013) recommends the use of direct current measurements.
- The median (50%) and severe (1%) lightning currents at ground appear to be:
  - 30 kA and 150 kA for negative first strokes,
  - 10-15 kA and 50 kA for negative subsequent strokes,
  - 35 kA and 500 kA for positive first strokes (as follows from lognormal distributions)
- The maximum directly measured peak current to date is about 300 kA, and it is for positive lightning.
- For negative lightning, the maximum directly measured peak current is about 200 kA.
- Theory: Maximum peak current is about 300 kA in temperate regions and about 450 kA–500 kA in the tropics

Peak current distribution and its genesis

$$P(E,\tau_0)=\begin{cases}0, & 0\le E\le E_0,\\ \dfrac{E-E_0}{E_1-E_0}, & E_0<E\le E_1,\\ 1, & E>E_1;\end{cases}$$

$$\mathrm{P(I)}=\frac{1}{\sqrt{2\pi}\sigma \mathrm{I}}\exp\left\{-\frac{(\ln I-\ln I_0)^2}{2\sigma^2}\right\}$$

$$\begin{aligned}F_E(\epsilon)&=1-\lim_{\eta\to\epsilon+0}\exp\left(\int_0^{t(\eta)}\ln\left(1-P(E(\tau),\tau_0)\right)\frac{d\tau}{\tau_0}\right)\\&=1-\lim_{\eta\to\epsilon+0}\exp\left(\frac{1}{\tau_0}\int_{E(0)}^{\eta}\ln\left(1-P(E',\tau_0)\right)\frac{dt}{dE}(E')\,dE'\right)\end{aligned}$$

$$F_E(\epsilon)=\begin{cases}1-\exp\left(\dfrac{1}{k\tau_0}\left(\epsilon-E_0+(E_1-\epsilon)\ln\dfrac{E_1-\epsilon}{E_1-E_0}\right)\right), & E_0\le\epsilon<E_1,\\ 1, & \epsilon\ge E_1.\end{cases}$$

Statistical distributions of lightning peak currents: Why do they appear to be lognormal?

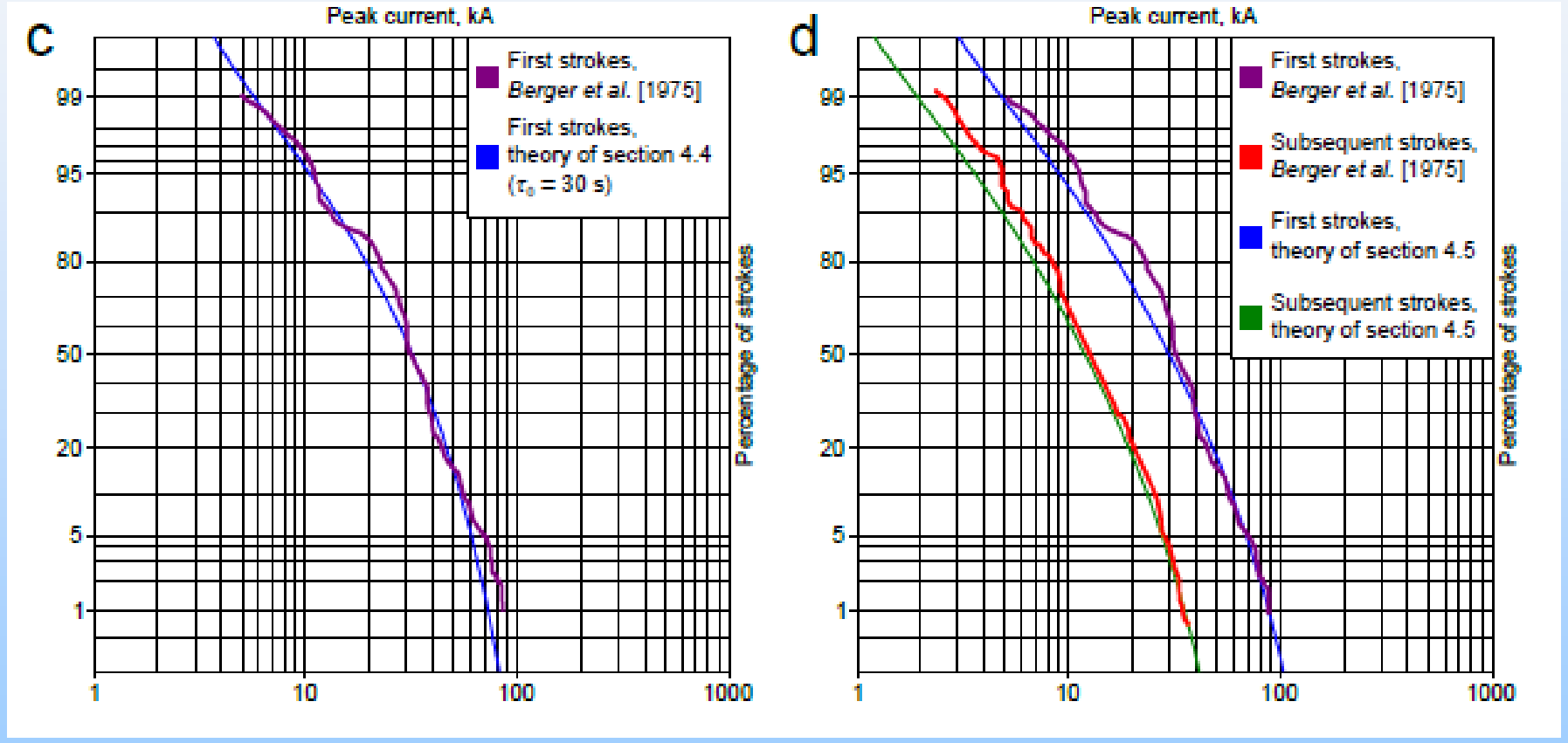

N. Slyunyaev, E. Mareev, V. Rakov, and G.Golitsin, 2017

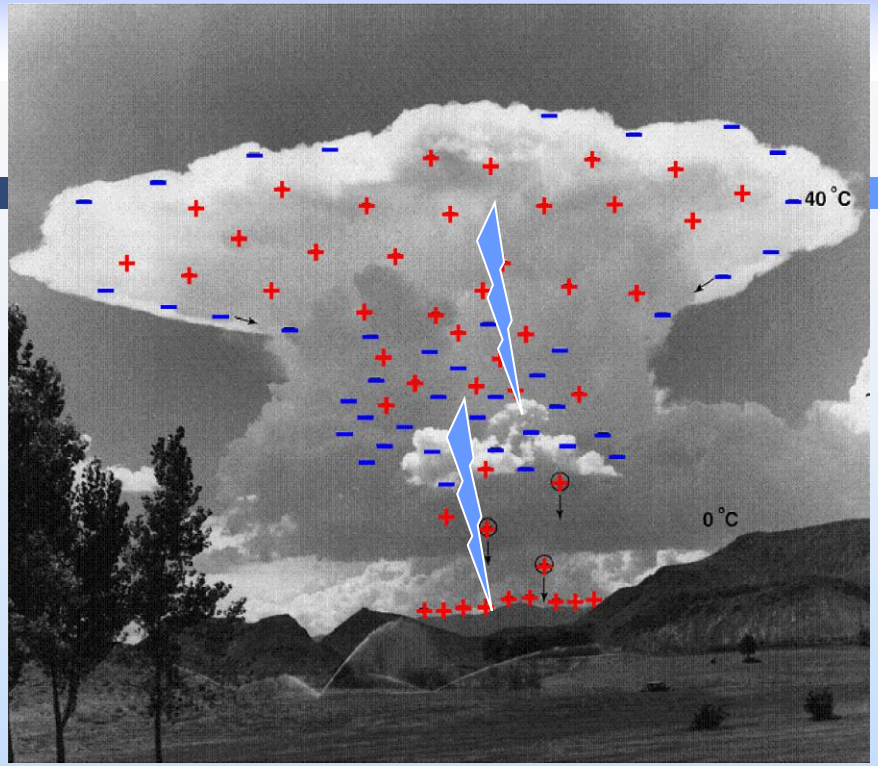

Пространственно-временная структура разрядного тока:

$$\mathbf{j}_{\text{ext}}(\mathbf{r},t) = \mathbf{z}_0 j_0 \exp[-(r/r_0)^{\beta} - (|z - z_{\max}|/z_0)^{\gamma}]F(t),$$

$$\frac{\partial \rho_{\text{ext}}}{\partial t} = -\nabla \cdot \mathbf{j}_{\text{ext}}(\mathbf{r},t).$$

$$F(t) = j_{\text{RS0}}\left[\exp\left(-\frac{t}{t_{\text{rs}}}\right) - \exp\left(-\frac{t}{t_{\text{fs}}}\right)\right] +$$

$$+ j_{\text{CC0}}\left[\exp\left(-\frac{t^2}{t_{\text{CC}}^2}\right) - \exp\left(-\frac{t}{t_{\text{rs}}}\right)\right] +$$

$$+ j_{\text{M0}} \exp\left(-\frac{(t - t_{\text{M0}})^2}{t_{\text{M}}^2}\right).$$

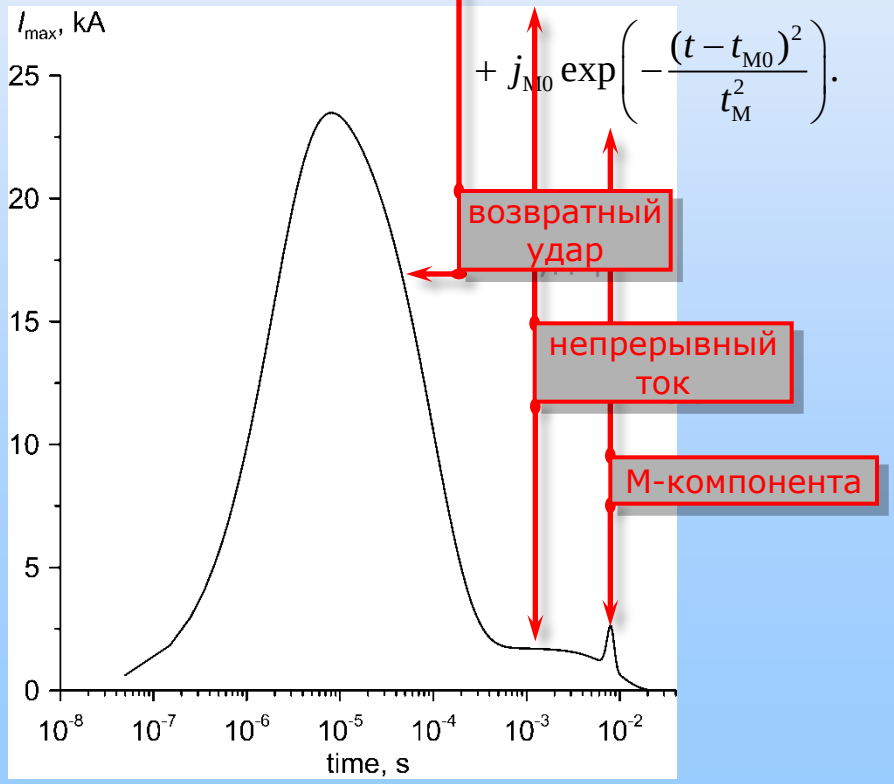

Распределение удельной электрической проводимости атмосферы:

$$\sigma(r,z) = \sigma_0 \exp\left(\frac{z}{H}\right) \times$$

$$\times \left\{1 - \alpha \exp\left[-\left(\frac{r}{R_0}\right)^{\eta} - \left(\frac{|z - Z_{\max}|}{Z_0}\right)^{\chi}\right]\right\}$$

Электромагнитный импульс разряда облако-земля:

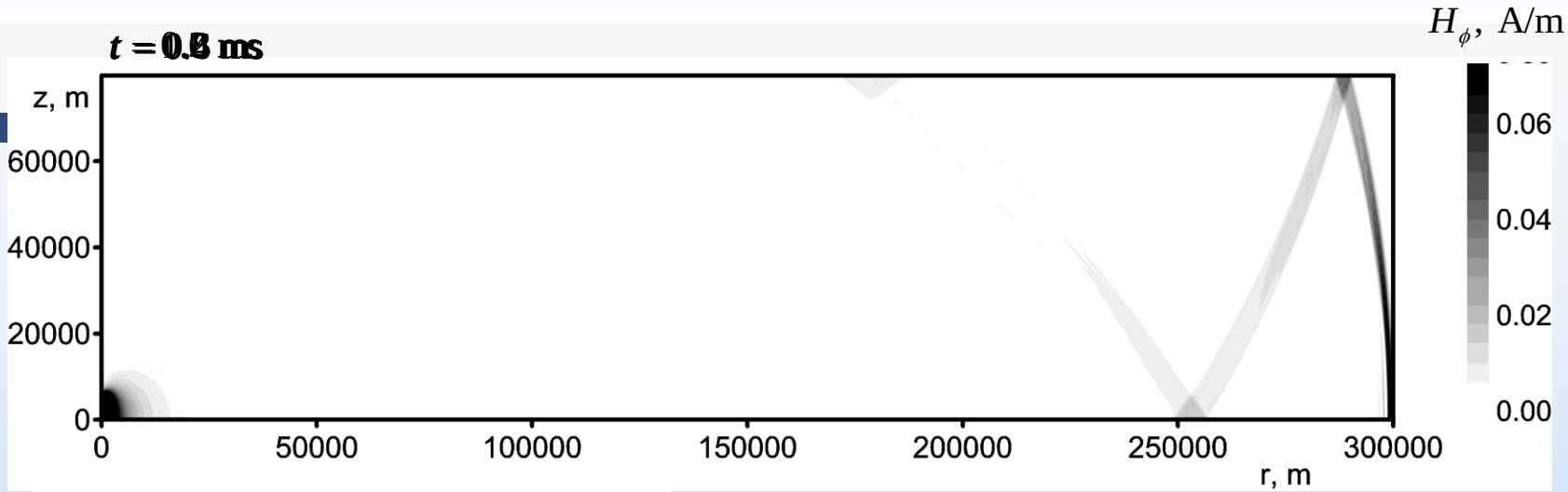

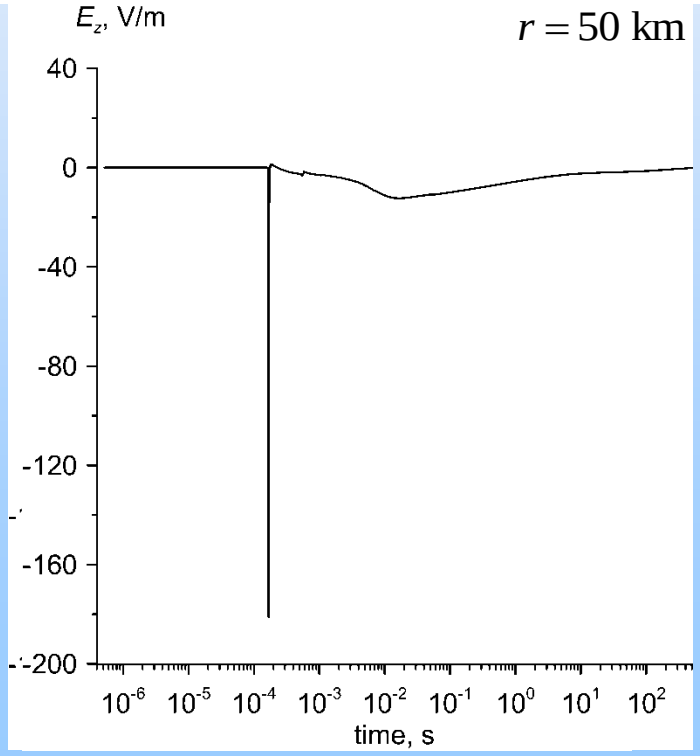

Перенос заряда к ионосфере:

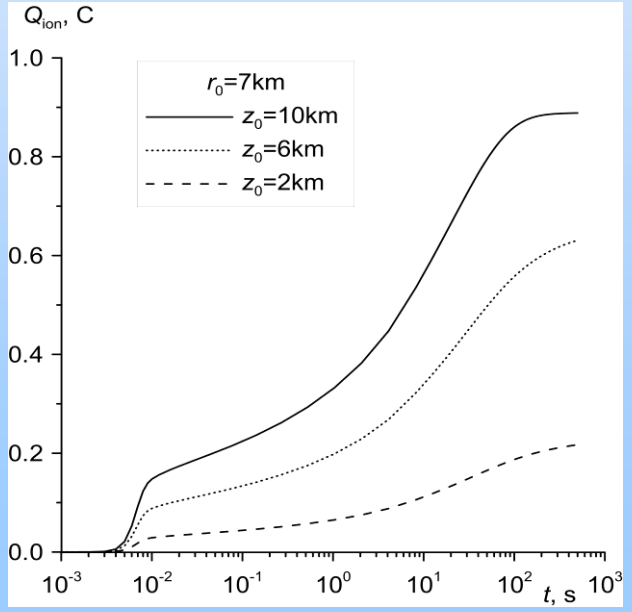

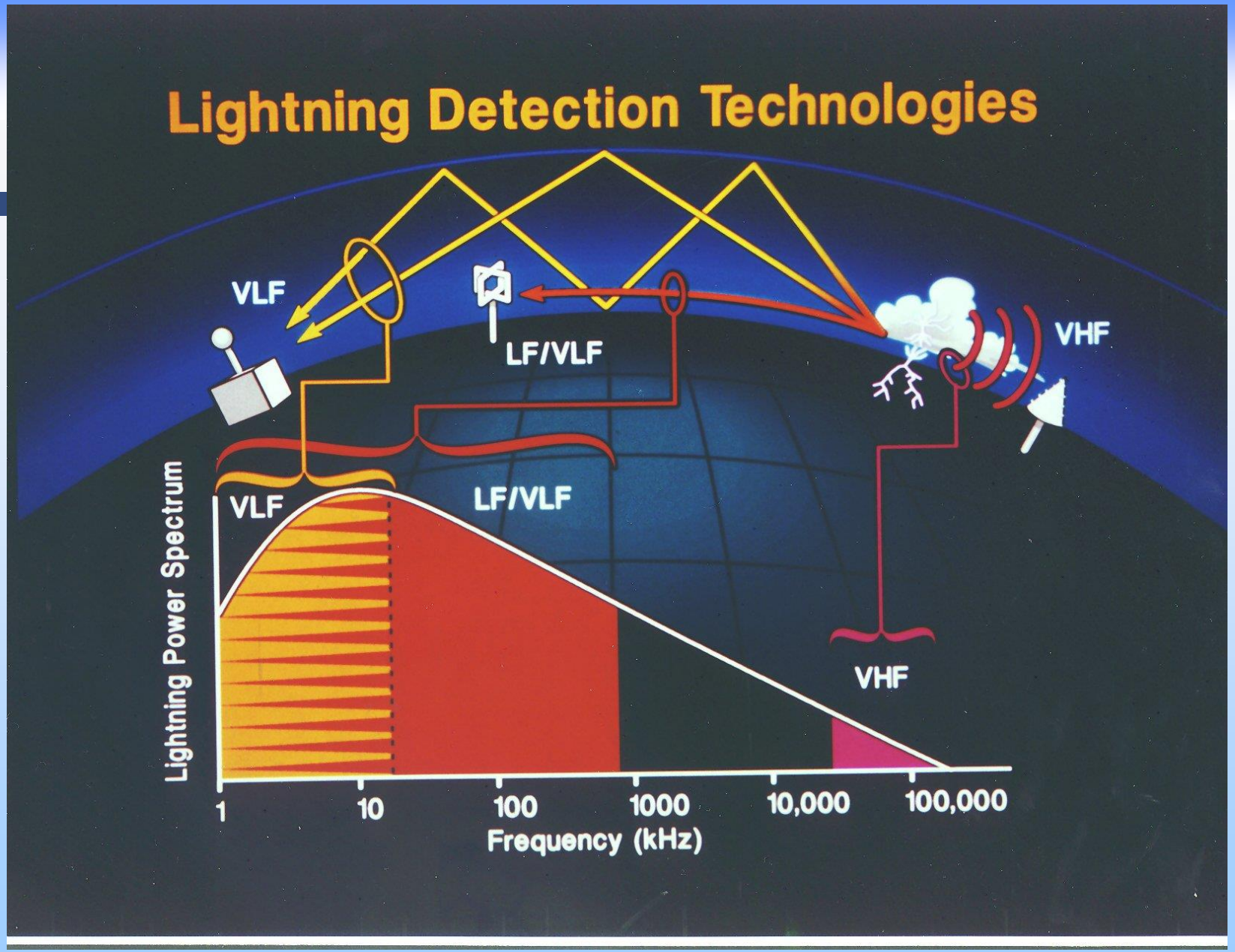

Courtesy of Dr. K.L.Cummins and Vaisala

VLF: 3-30 kHz; LF: 30-300 kHz; VHF: 30-300 MHz

Modern multiple-station regional and global lightning detection (locating) systems

REGIONAL:

U.S. National Lightning Detection Network (NLDN), 400 Hz-400 kHz, combination of time-of-arrival (TOA) and magnetic direction finding (MDF) techniques.

Earth Networks (formerly WeatherBug) Total Lightning Network (ENTLN), 1 Hz-12 MHz, TOA

GLOBAL:

World Wide Lightning Location Network (WWLLN), 6-18 kHz, time-of-group-arrival (TOGA) technique (based on the fact that lightning VLF signals propagating in the Earth-ionosphere waveguide experience dispersion, in that the higher-frequency components arrive earlier than the lower-frequency components).

Global Lightning Dataset (GLD360), 300 Hz – 48 kHz, combination of TOA, MDF, and waveform recognition algorithm (relies on the bank of "canonical" field waveforms for different ranges).

Map showing the locations of WWLLN sensors (blue circles) as of 2013. The number of sensors has grown from 18 in 2004 to 70 in 2013. Since April 15, 2009, stroke radiated energy is reported. The approximate location of Camp Blanding (red star) is also shown. Evaluation was performed in 2008-2013.

WWLLN performance characteristics (RS, SIP)

	2008–2013
Flash Detection Efficiency	8.8% (N = 80)
Stroke Detection Efficiency	2.5% (N = 360)
Stroke Detection Efficiency (for I_p >25 kA)	29% (N = 21)
Median Location Error	2.1 km (N = 10)
Median Absolute Event-Time Mismatch	15.3 μs (N = 7)
Median Absolute Peak Current Estimation Error	30% (N = 7)

Adapted from Mallick et al. (2014)

Характеристики систем локации молнии

Regional LLSs allow one to achieve location errors as low as a few hundreds of meters and flash detection efficiencies exceeding 90%.
Global LLSs presently cannot distinguish between ICs and CGs. Detection efficiency of WWLLN is low.

Rocket-triggered lightning can be used for calibrating LLSs, although the results are applicable only to subsequent strokes in negative lightning.
Natural-lightning data can be used for estimating DE and CA for both CG and IC events, but generally cannot be used for estimating LA and peak-current errors.

VHF mapping: LMA

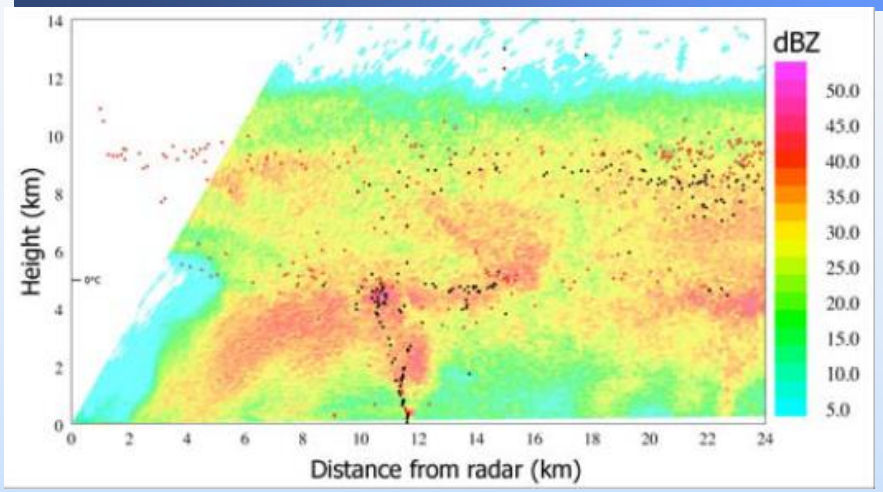

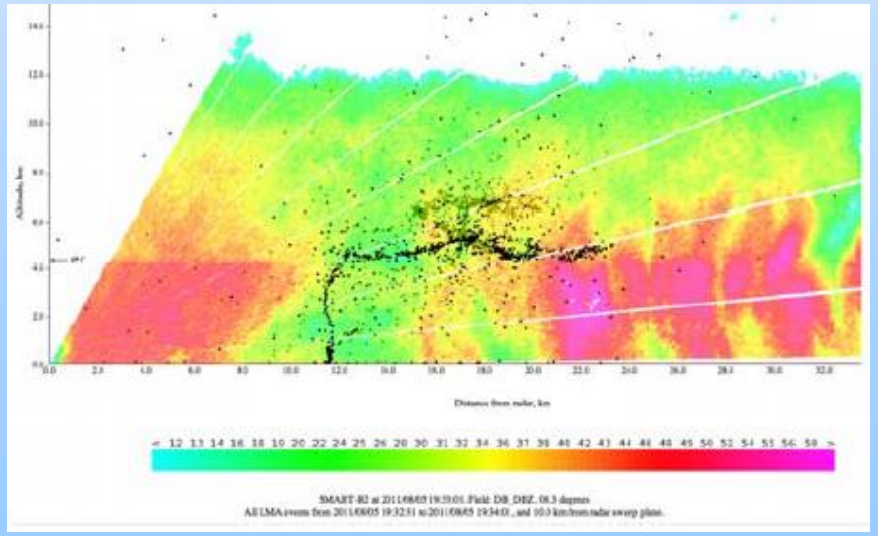

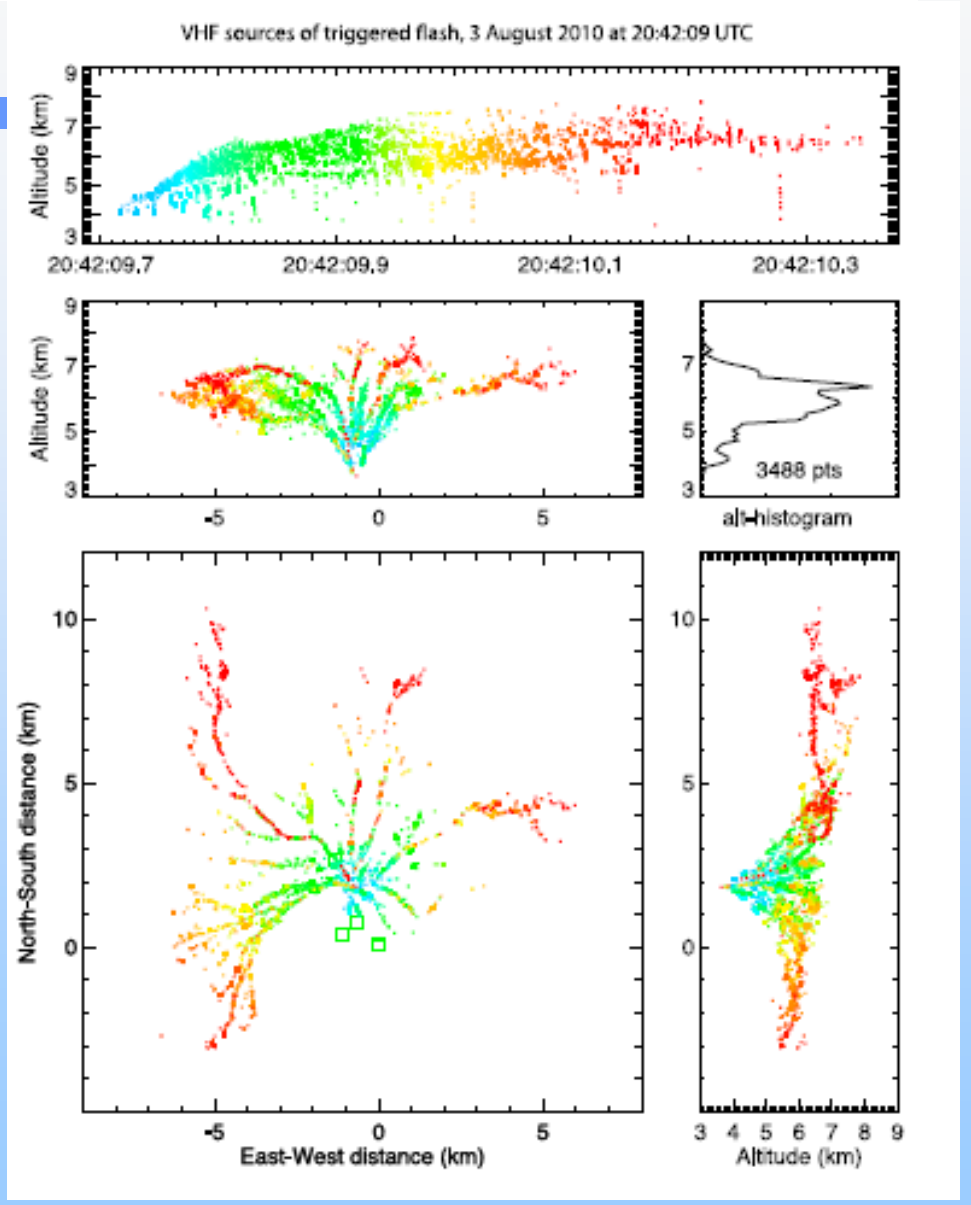

Наблюдательная сеть в Верхне-Волжском регионе

Расположение пунктов наблюдательной сети

Региональная система оперативного прогноза опасных атмосферных явлений

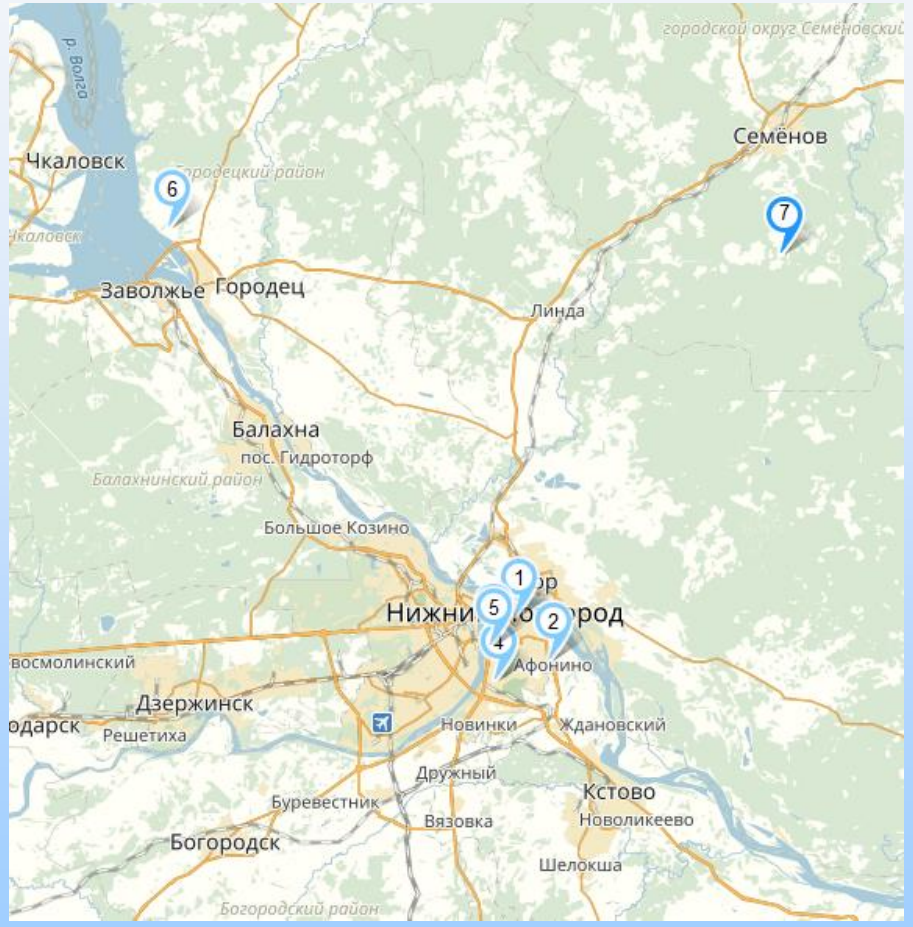

Объекты на карте

(1) Флюксметр и грозопеленгатор ИПФ РАН

(2) Флюксметр ИФМ РАН

(3) Флюксметр ННГУ

(4) Аэрологическая станция "Нижний Новг...

(5) Метеорадар

(6) Волжская ГМО, грозопеленгатор

(7) Грозопеленгатор

http://nowcasting.lightninglab.ru/

http://diogen.lightninglab.ru/

Инструментарий

- Multi-station regional lightning detection system (Boltek Stormtracker devices)
- Quasi-static electric field measuring network
- Meteorological and radar data

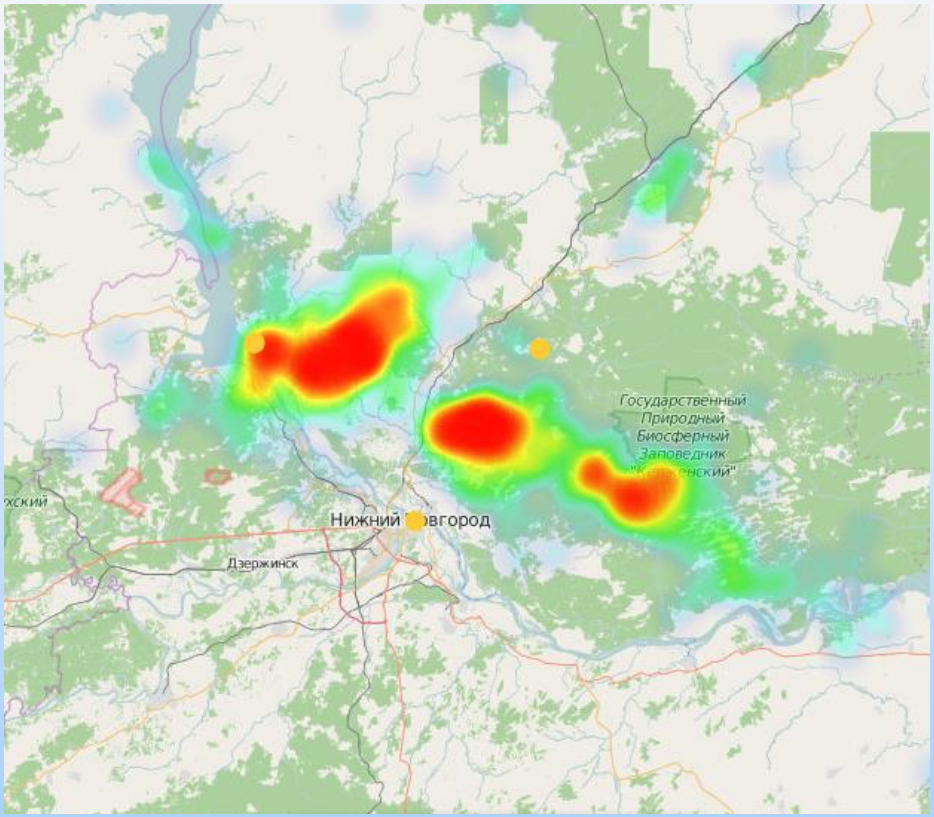

Lightning location system data for a thunderstorm on July 5, 2016 from 8.20 to 8.30 UTC. Nizhny Novgorod is in the center. Three yellow dots represent observation points The scale of the map is 150x150 km.

Kuterin et al., 2014

Мезомасштабная негидростатическая модель WRF

We have chosen the strategy of two embedded grids: the external grid covered the European part of Russia (the area of 1200*1200 km size with a step of 3 km), and the internal one of 210*210 km size with a step of 1 km.

Global Forecasting Model (GFS) data with a resolution of 0.25 degrees are used for WRF model initialization.

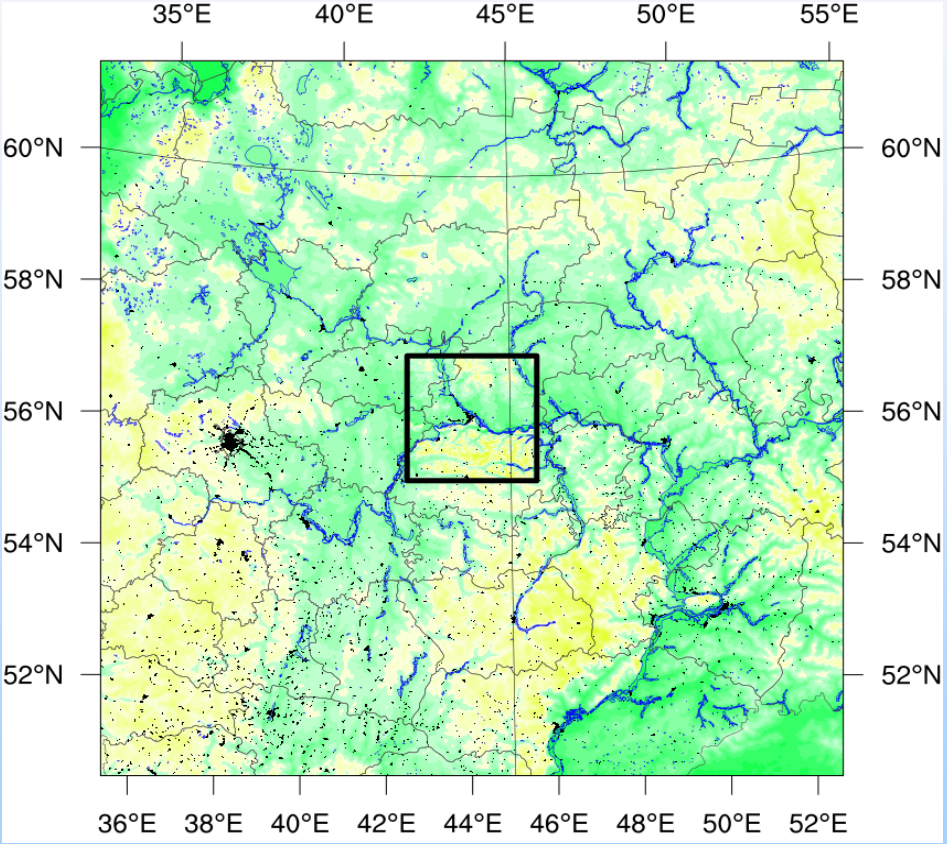

A set of embedded grids of the forecast.

Dementyeva et al., 2014a; Dementyeva et al., 2014b; https://www.ncdc.noaa.gov/data-access/model-data/model-datasets/global-forcast-system-gfs

Thunderstorm 1 June 2015 14:30 – 21:30 (UTC)

Earliness of forecast: 6 h

Initial conditions: GFS 0.5°

Calculations area:
1200 x 1200 x 20 km
210 x 210 x 20 km

Grid:
3 x 3 x 0.5 km
1 x 1 x 0.5 km

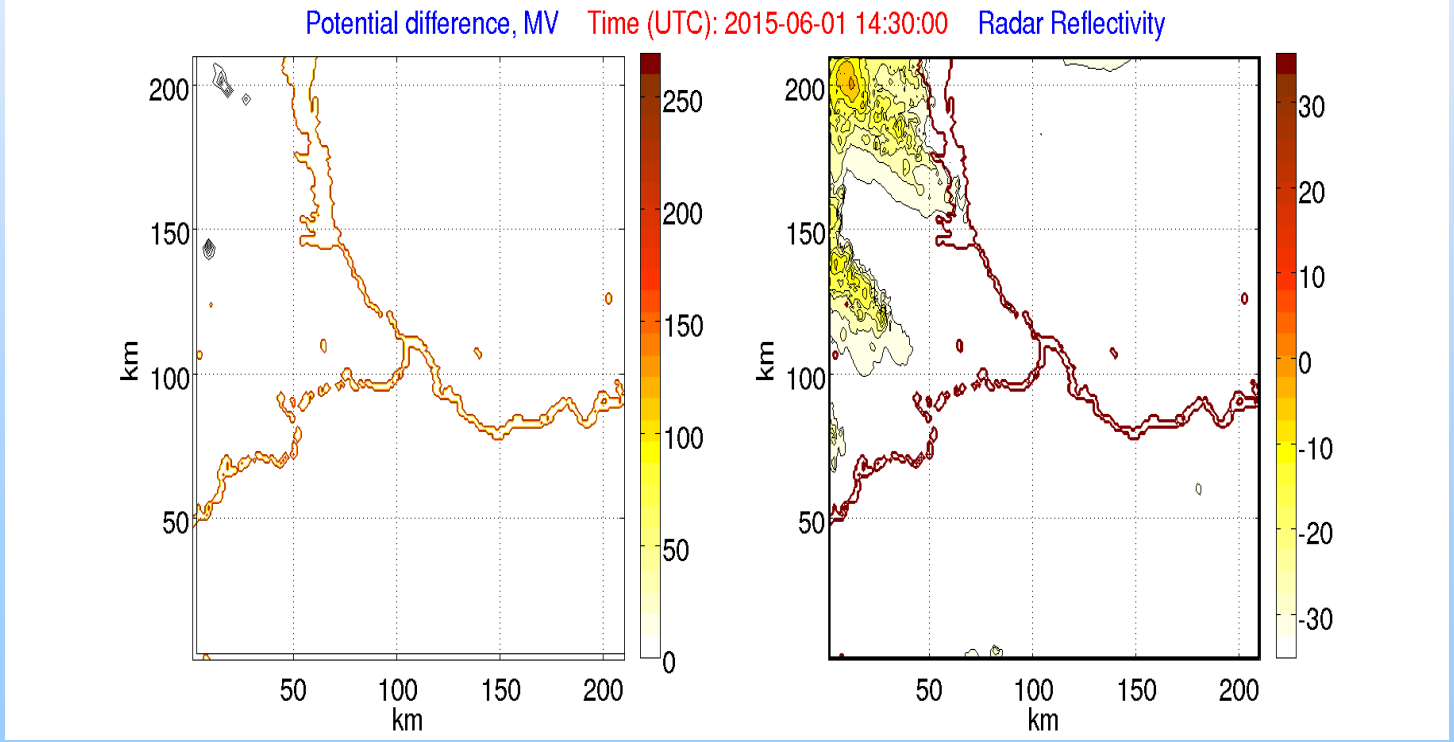

Global lightning integrations from VLF/ELF: Vaisala GLD360 versus WWLLN and satellite data

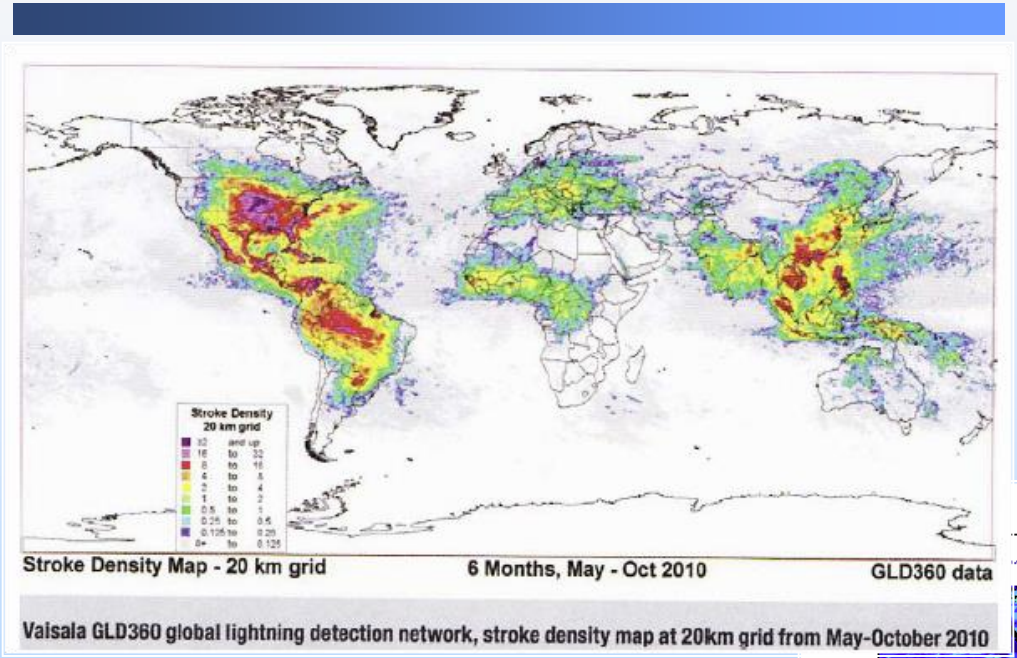

Vaisala GLD360 global lightning detection network, stroke density map at 20km grid from May-October 2010

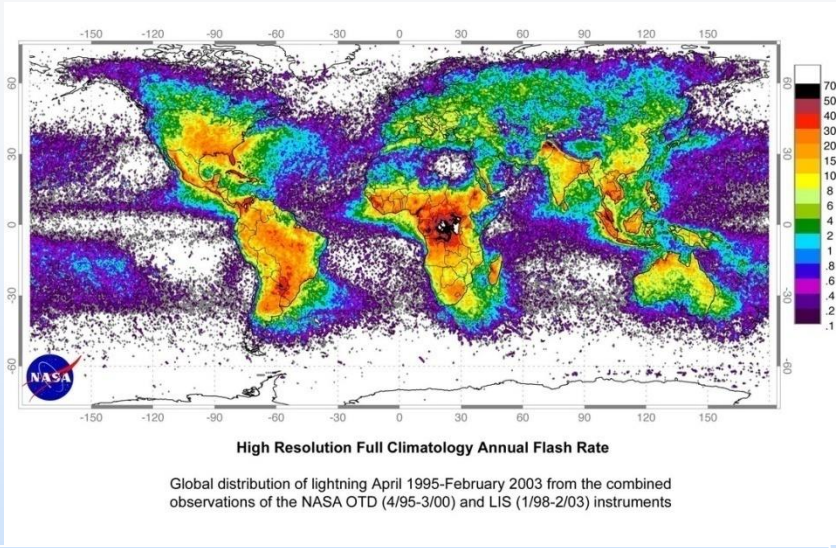

High Resolution Full Climatology Annual Flash Rate

Global distribution of lightning April 1995-February 2003 from the combined observations of the NASA OTD (4/95-3/00) and LIS (1/98-2/03) instruments

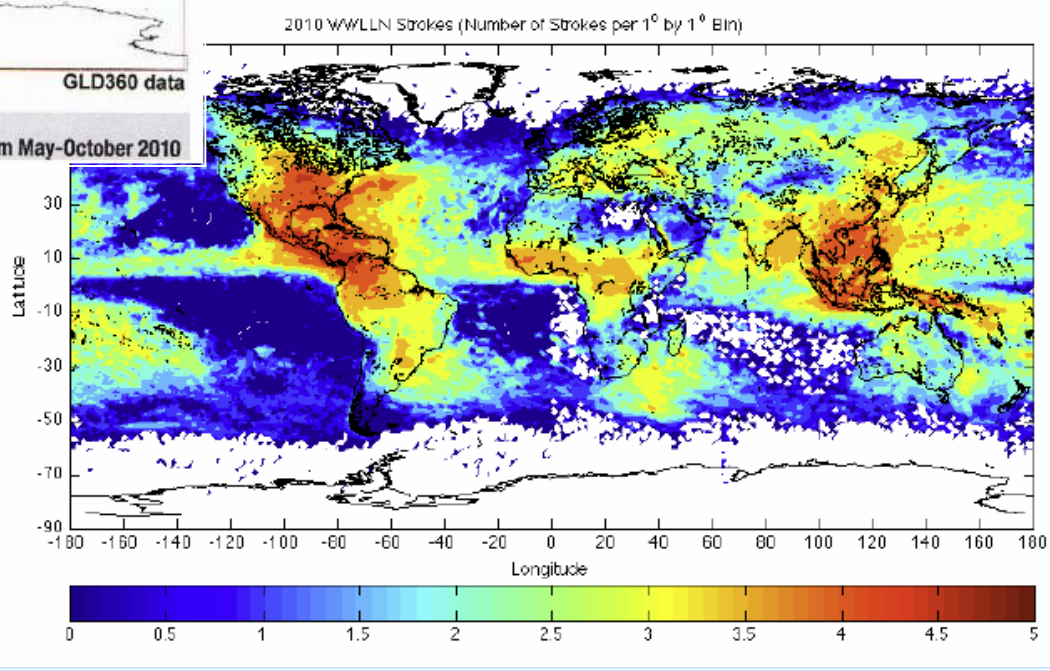

From R. Holzworth, 2011,

R.Said et al., 2013,

Williams and Mareev, 2014

Mean annual flash density per km squared in INMCM4.0 model for the modern climate

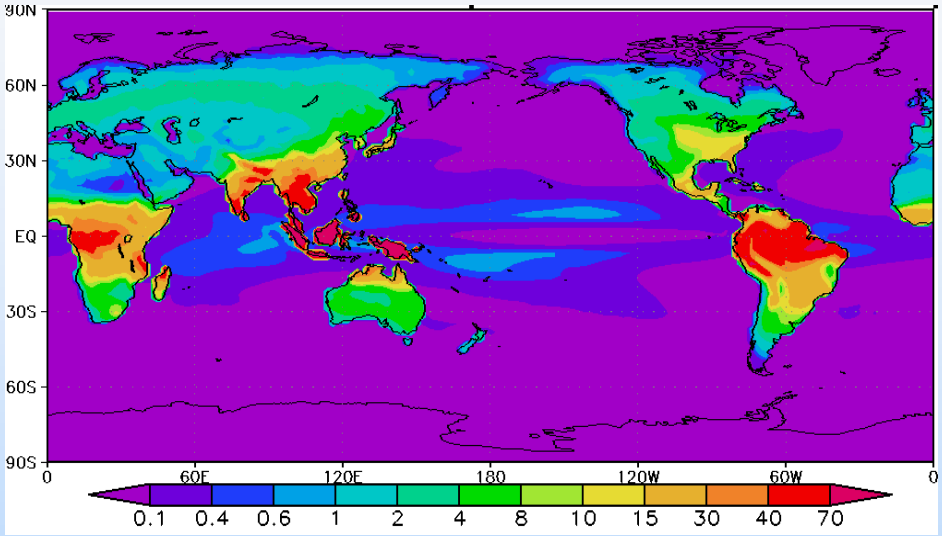

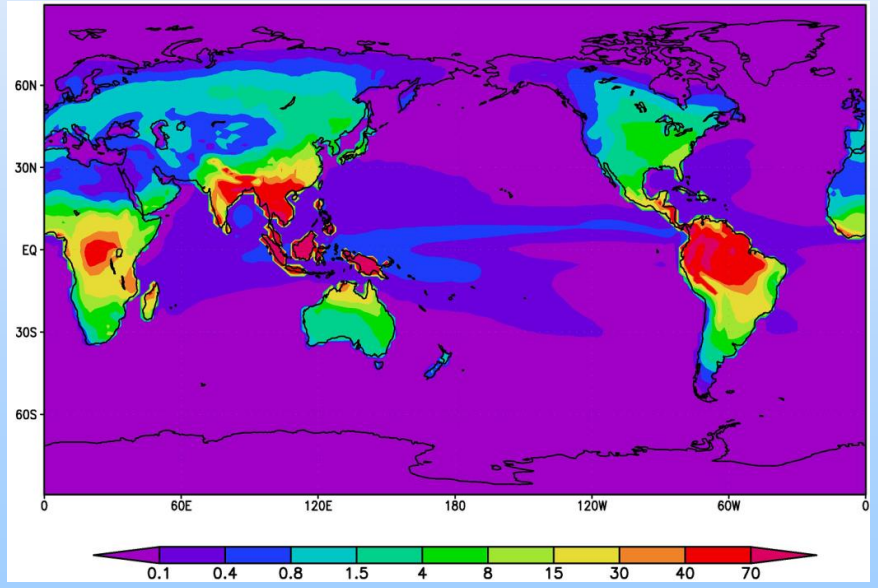

$$F_c = 3.44\times10^{-5} H^{4.9} \qquad F_m = 6.40\times10^{-4} H^{1.73}$$

C.Price & D.Rind, 1992

Эль-Ниньо

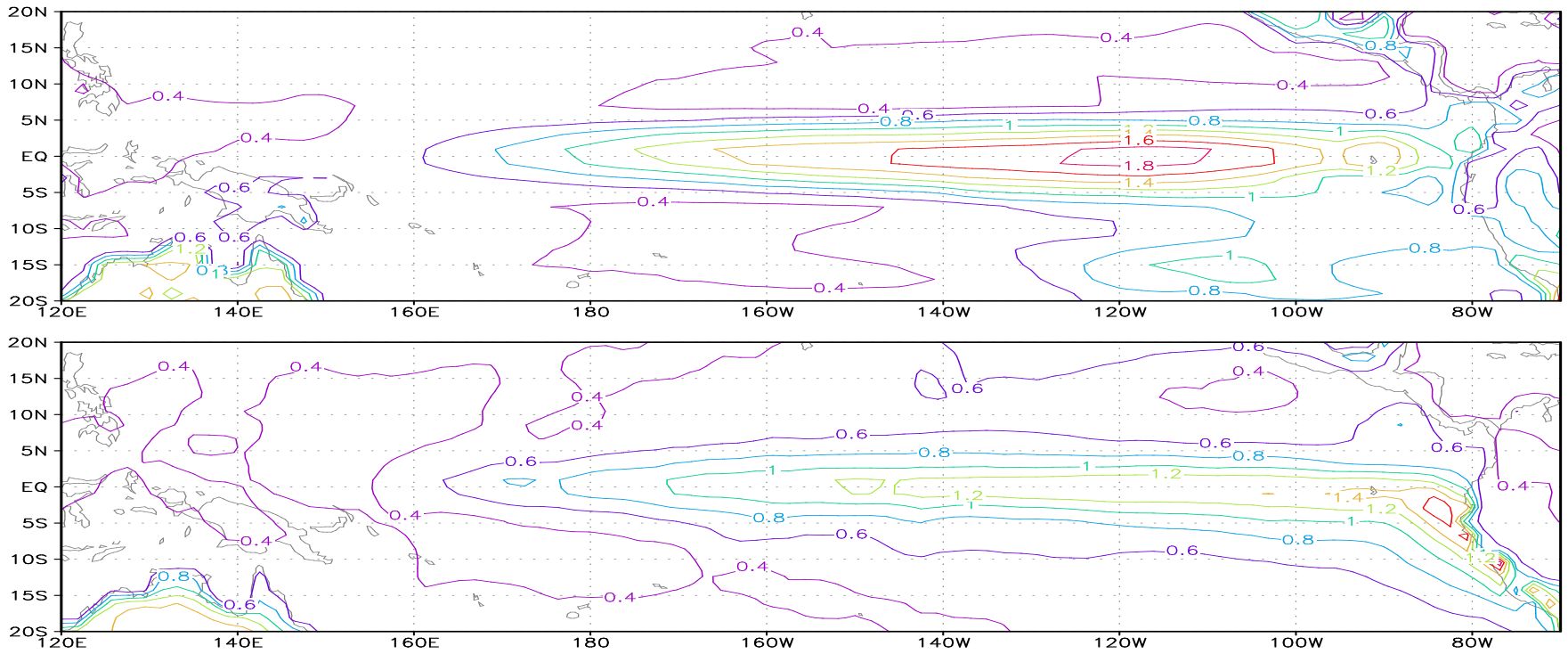

Среднеквадратичное отклонение ТПО в районе Эль-Ниньо по данным модели (вверху) и наблюдений (внизу)

Chronis et al., 2008

NINO3.4>1.08(red)NINO3.4<-1.22(blue) (a)

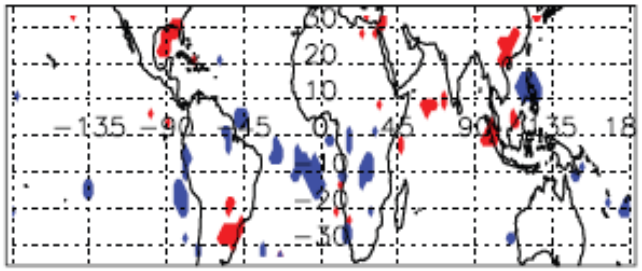

ENSO temporal evolution from 1998-2006 (b)

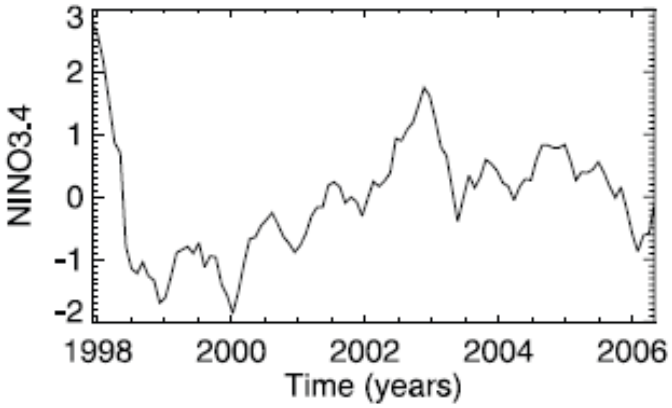

CMAP (PA) vs.NINO3.4 Correlation Map (a)

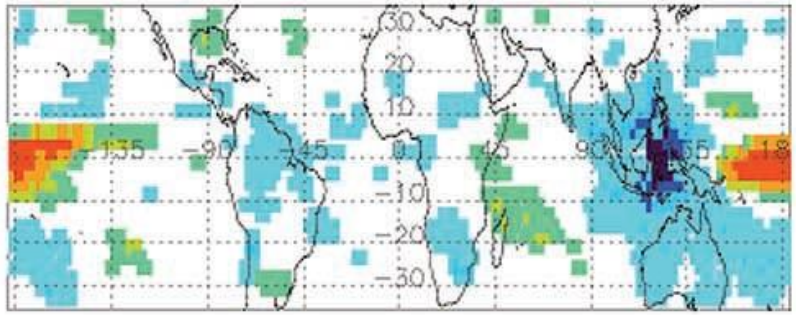

OTD/LIS (LA) vs.NINO3.4 Correlation Map (b)

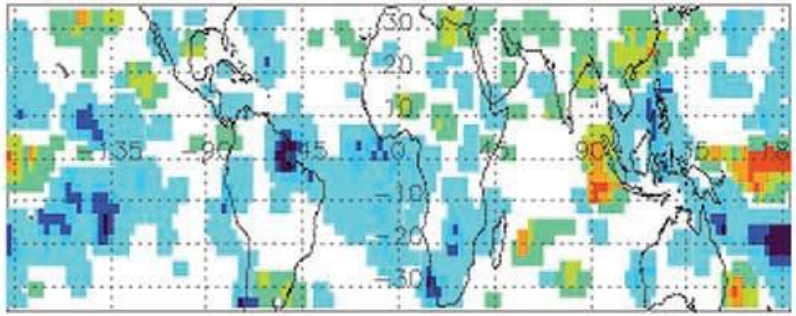

W.Shear(WA) vs.NINO3.4 Correlation Map (c)

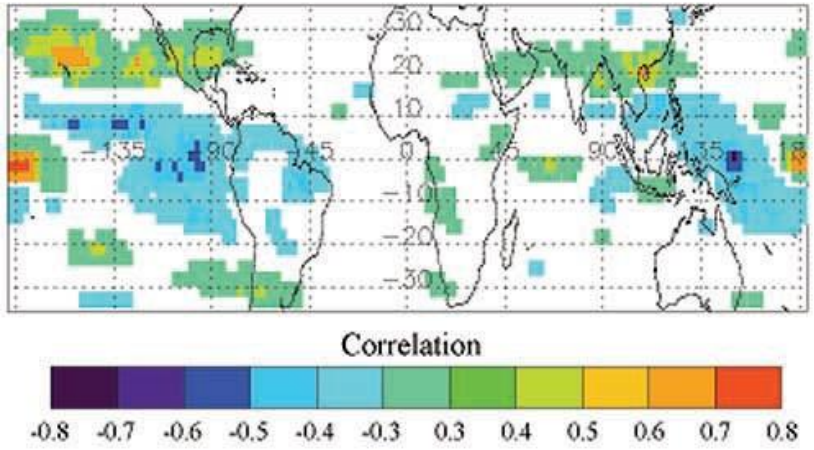

Mean diurnal SR intensity variations at NCK, Hungary in two warm and two cold episodes in NH winter months

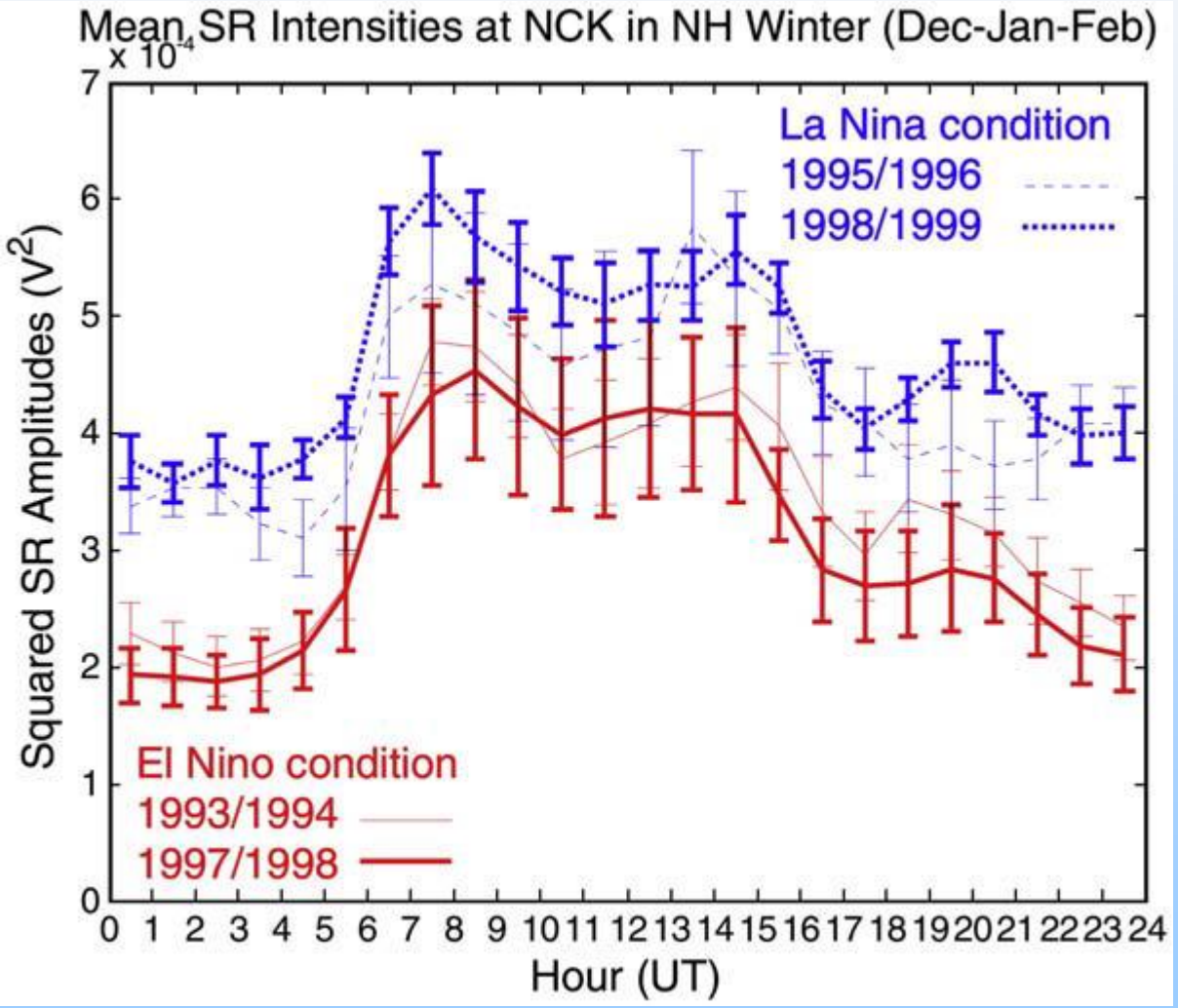

Variability of global lightning activity on the ENSO time scale by G.Satori et al., 2009

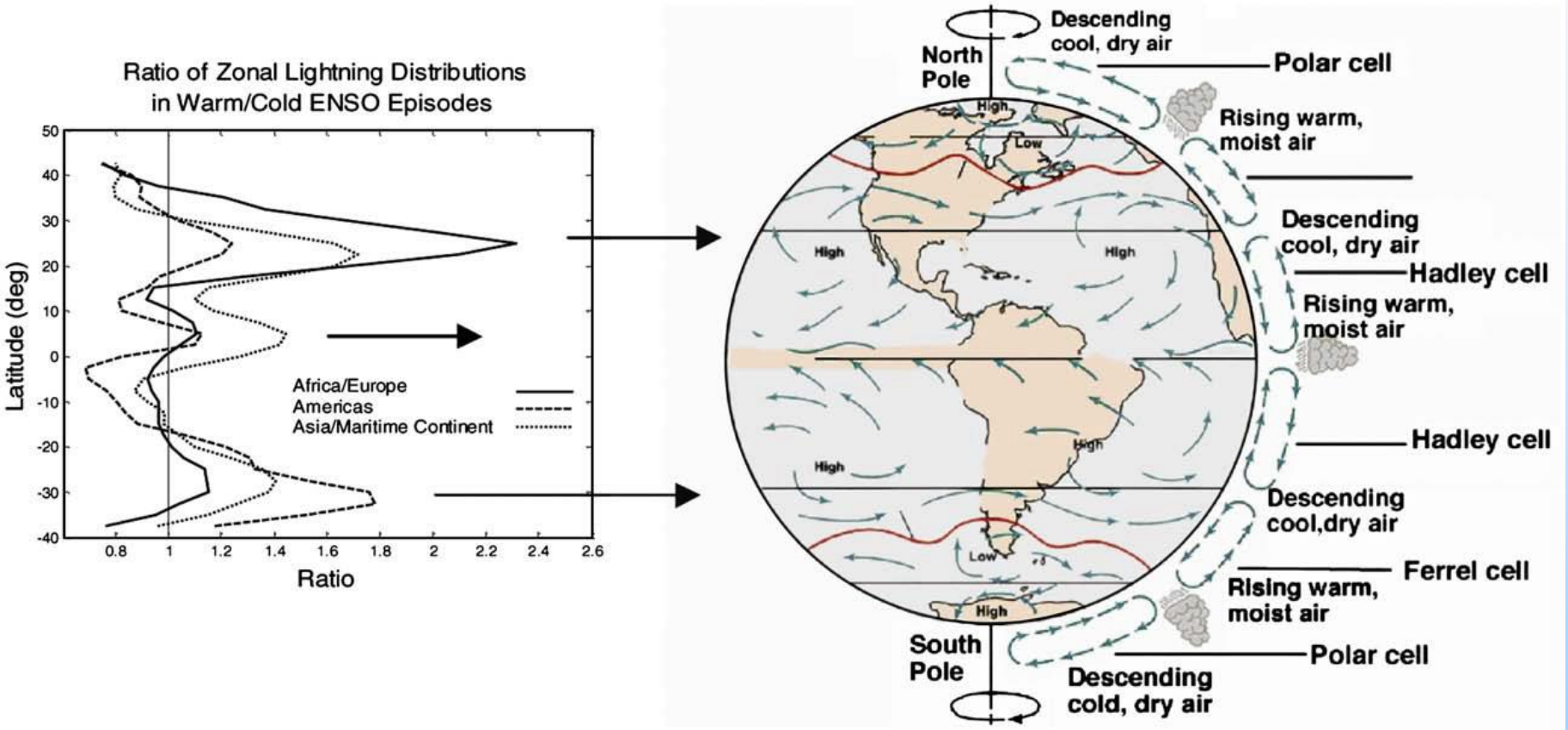

Lightning shows strong regional preference during different ENSO phases. Most of the areas appearing during the warm ENSO phase are located away from the equator and coincide with regions of anomalous jet stream circulation enhanced by the meridional heat transport

Схемы зональной и меридиональной циркуляции в Тихом океане

Зональная циркуляция

Меридиональная циркуляция

Распределение вспышек по широте

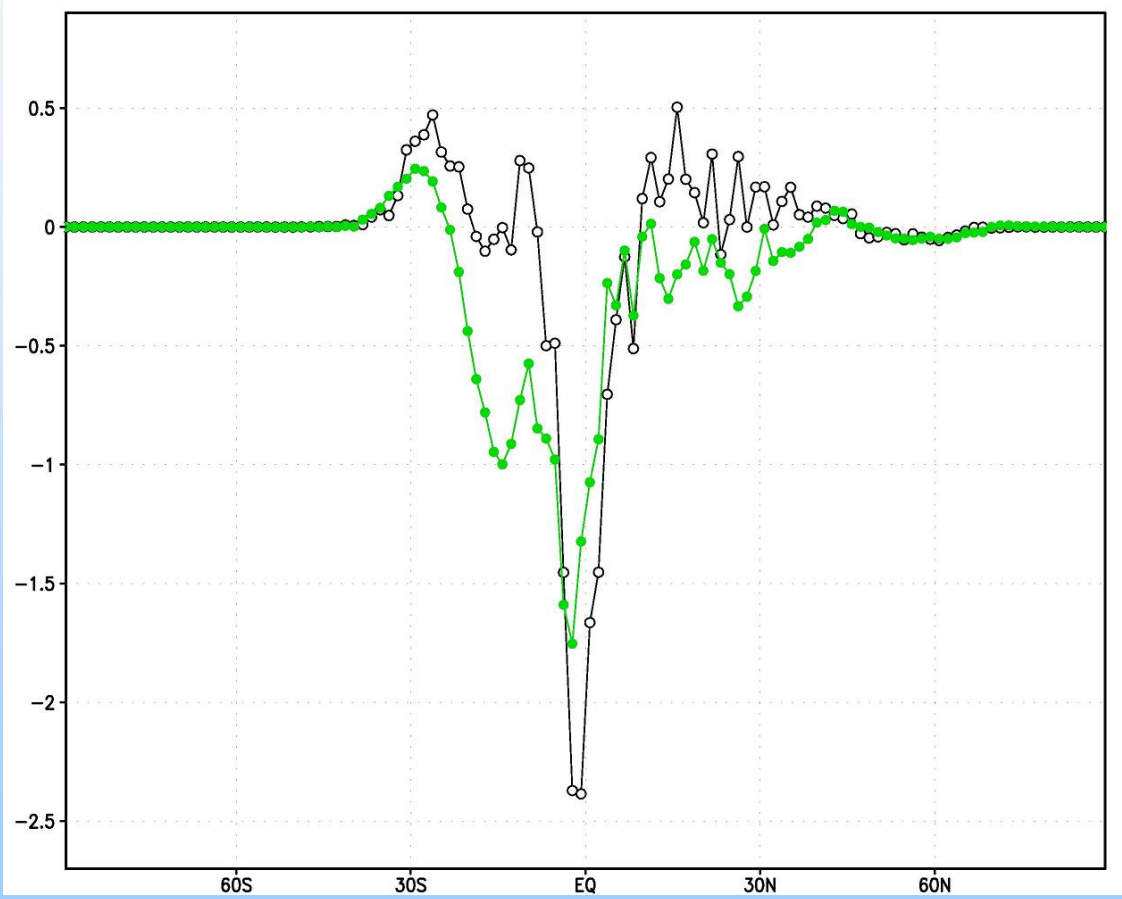

Разность количества вспышек (с-1) средняя вдоль долготы в годы Эль-Ниньо и Ла-Нинья в модели с учетом вертикального сдвига ветра (черный) и без учета (зеленый)

Учет сдвига скорости ветра

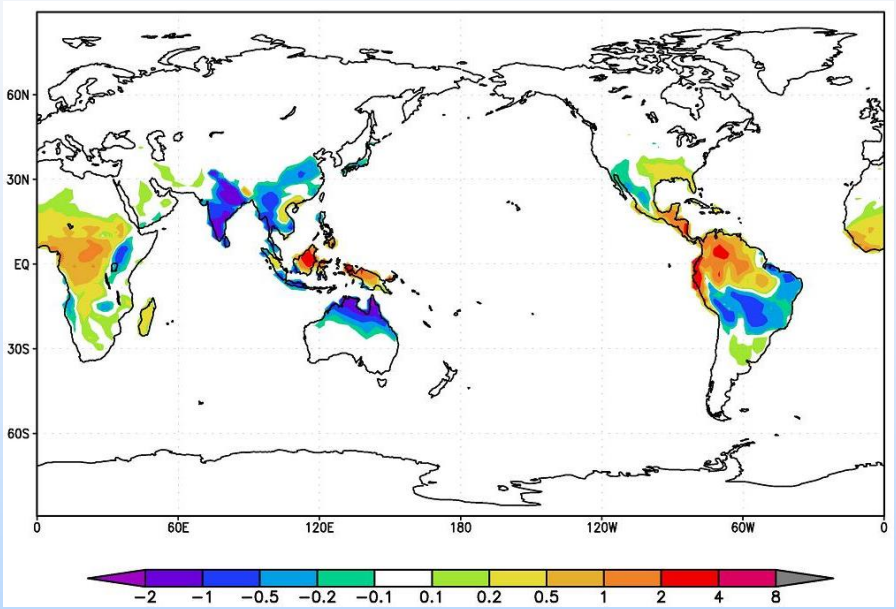

Разность композитов количества вспышек (1/(км2 год)) для положительной и отрицательной фаз Эль-Ниньо. Данные модели, 500 лет предындустриального эксперимента.

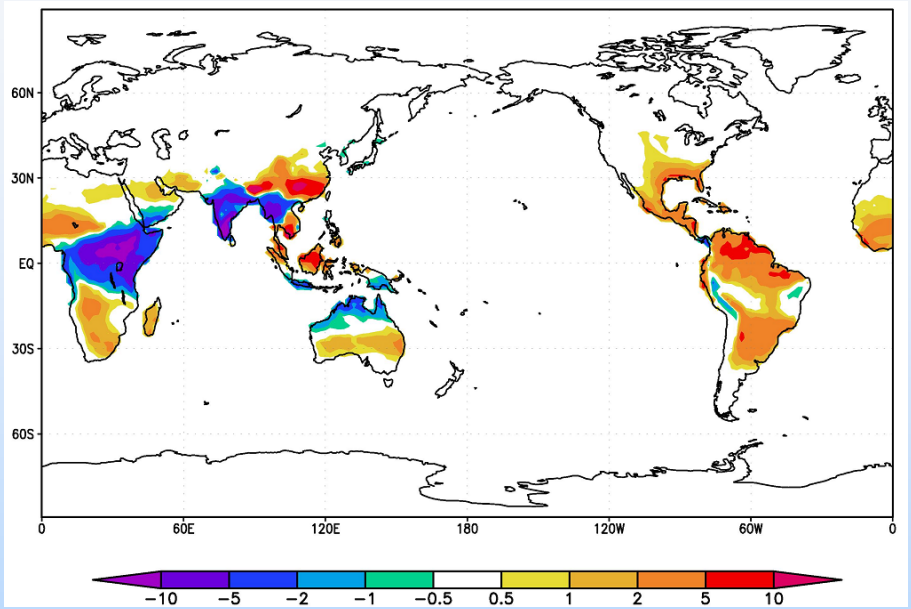

Разность количества вспышек (штук/(км2 год)) во время Эль-Ниньо и Ла-Нинья в модели. Количество вспышек корректировалось с учетом сдвига скорости ветра.

$$FL1 = FL *(SQRT(SH**2 +SH0**2)/SH0)**6$$

The *Galilee* and *Carnegie*

The Galilee and Carnegie became the Carnegie Institution's survey ships. The Carnegie was constructed specially, built from wood, copper and bronze, with an observing deck

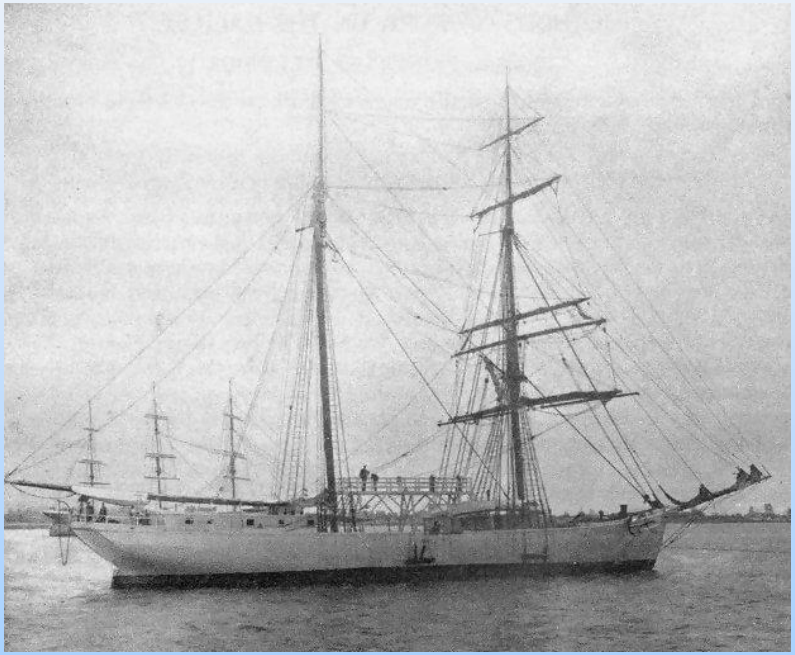

Galilee – brigantine built in 1925, as a fast packet between San Francisco and Tahiti. Chartered by CIW in 1905.

Carnegie under full sail in 1909 at launch. From 1909 to 1929 she covered 500,000 km, and made the fastest circumnavigation of Antarctica.

Global Atmospheric Electric Circuit and Ionospheric Potential

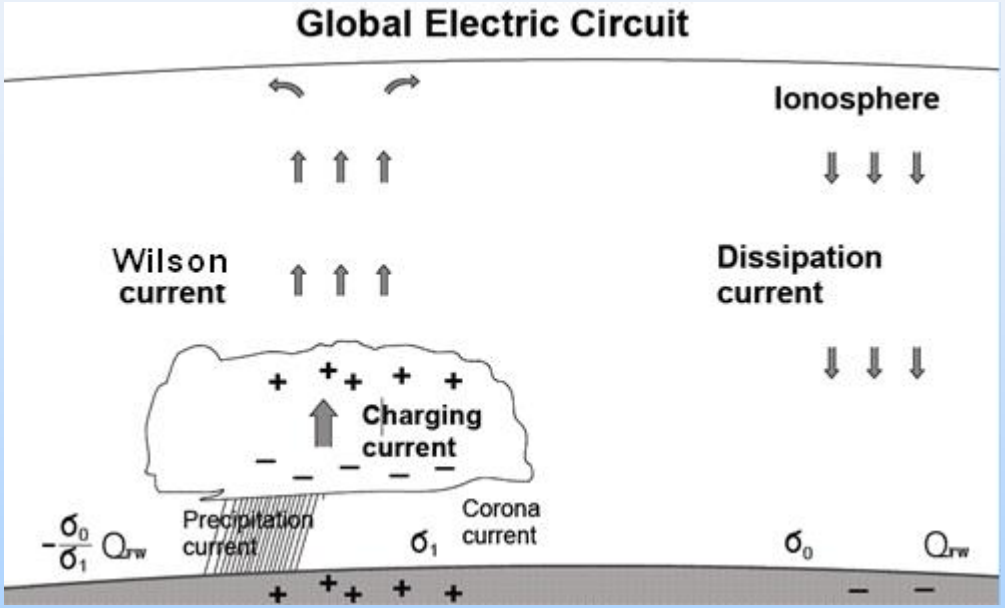

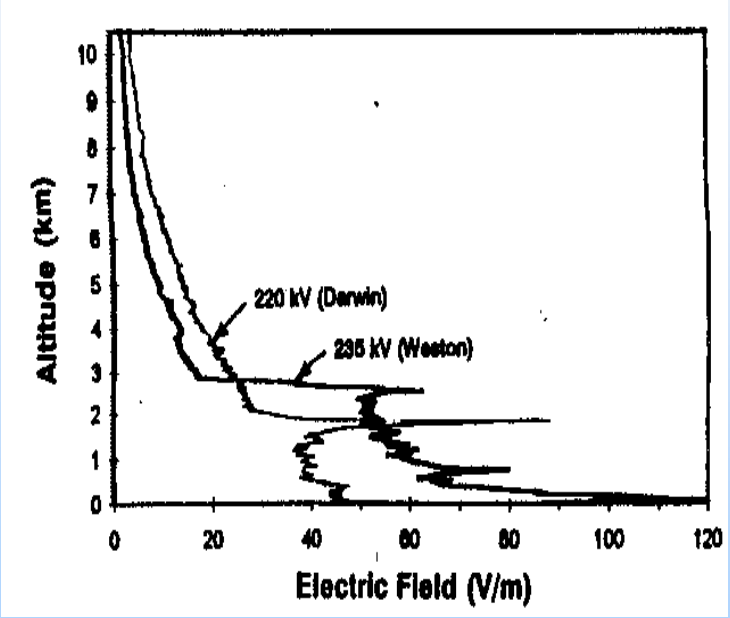

S.Anisimov , S.Davydenko, E.Mareev, 2011

Distant points: Darwin, Australia – 220 kV
Weston, USA – 235 kV
R.Markson, L.Ruhnke, E.Williams, 1996

Recent progress on the global electrical circuit (E.Williams and E.Mareev, Atm.Res., 2014)

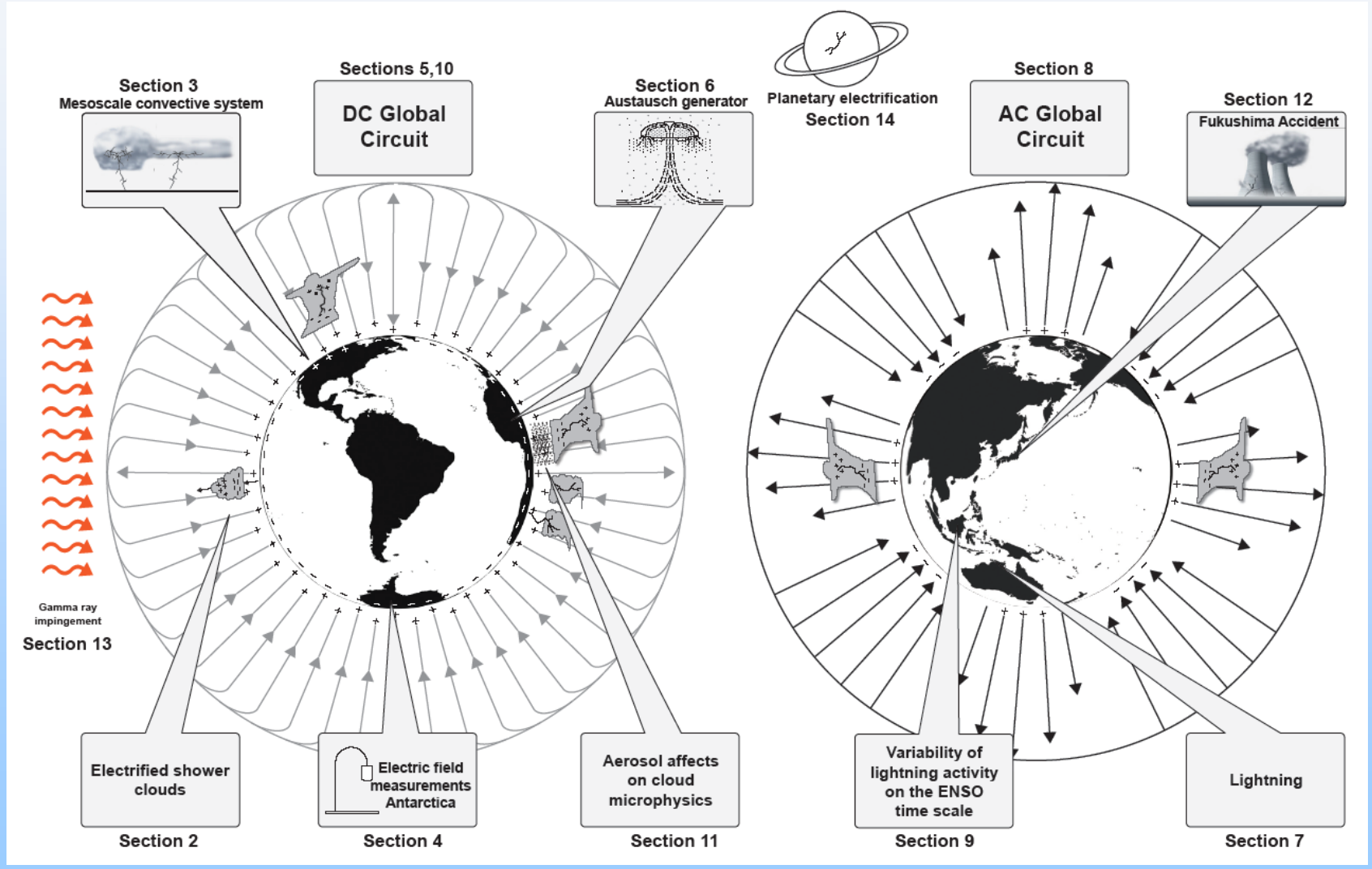

Electric generators in the atmosphere: problems of parameterization

$$\varphi_i = \tilde{\varphi}(R_i) = \frac{1}{4\pi} \int_{V_c} \frac{j_r \, dV}{\sigma(r) r^2}$$

$$\Delta V_i = \frac{j_0 S H_0}{\sigma_0 S_E} \exp\left(-\frac{z_b}{H_0}\right)\left(1 - \exp\left(-\frac{\Delta z}{H_0}\right)\right)$$

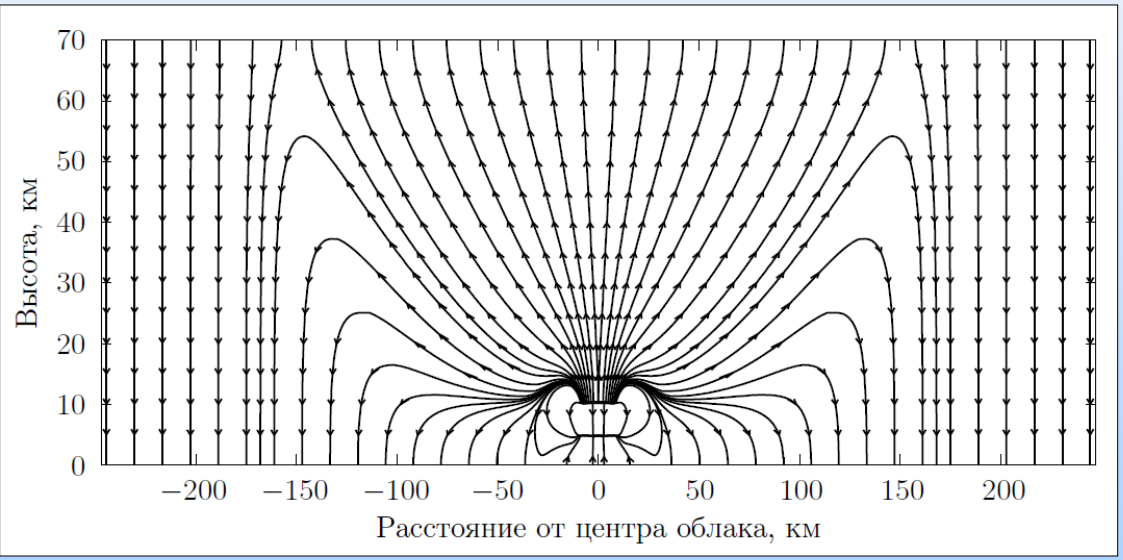

$$\operatorname{div}(\sigma \operatorname{grad} \varphi) = \operatorname{div} \mathbf{J}^{\text{ext}}$$

$$\oint_{\Sigma_1} \sigma \operatorname{grad} \varphi \, d\mathbf{S} = \oint_{\Sigma_1} \mathbf{J}^{\text{ext}} \, d\mathbf{S}$$

$$\varphi|_{\Sigma_1} = 0$$

$$\varphi|_{\Sigma_2} = V_i$$

Kalinin A.V. et al., 2011; P8;
Mareeva et al., 2011; P58

$$\Delta V_i = \frac{j_0 S H_0}{\sigma_0 S_E} \frac{\exp\left(-\frac{z_b}{H_0}\right)\left(1 - \exp\left(-\frac{\Delta z}{H_0}\right)\right)\left(1 - \exp\left(-\frac{z_{max}}{H_0}\right)\right)}{k\left(1 - \exp\left(-\frac{z_{max}}{H_0}\right)\right) + (1-k)\left(1 - \frac{S}{S_E}\right)\exp\left(-\frac{z_b}{H_0}\right)\left(1 - \exp\left(-\frac{\Delta z}{H_0}\right)\right)}$$

Diurnal Vi variation averaged over each day of 1986-2005. (right) Annual Vi variation averaged over all the hours of 1986-2005

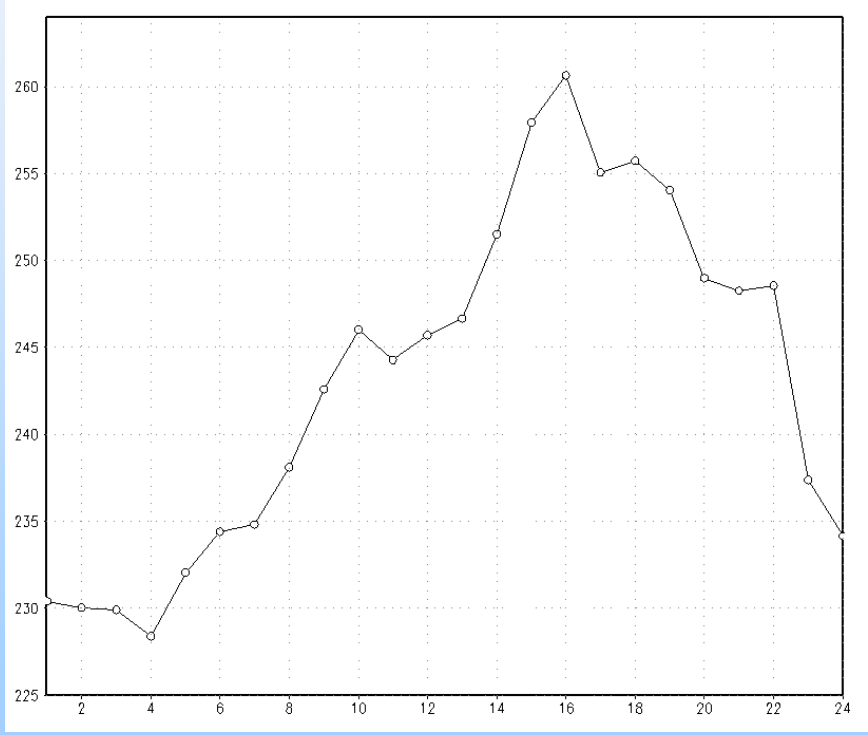

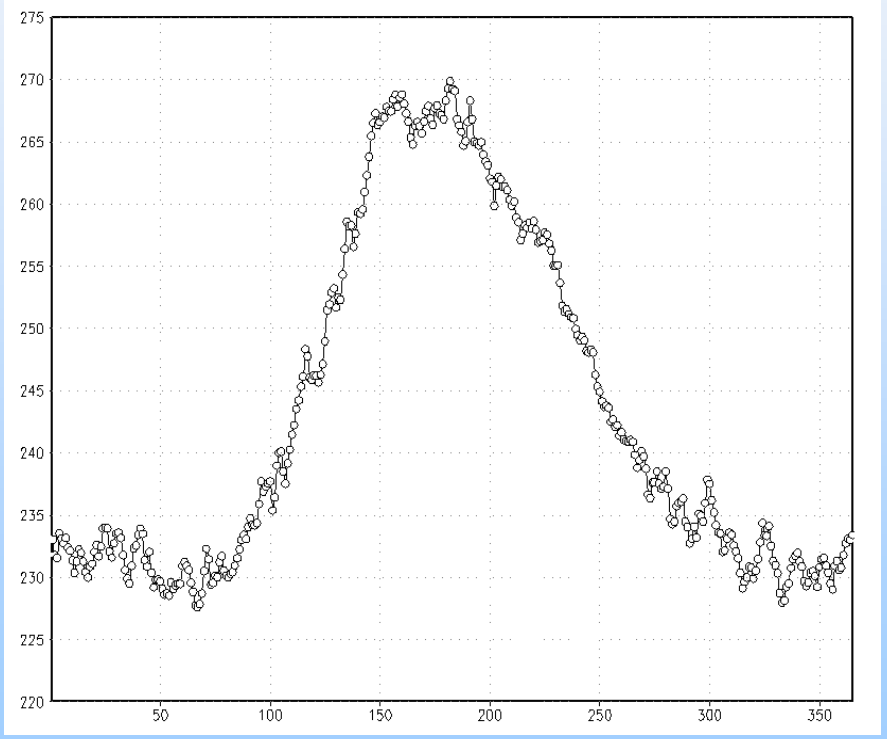

Mareev E.A., Volodin E.M., 2011

Ionospheric potential variation in XX century

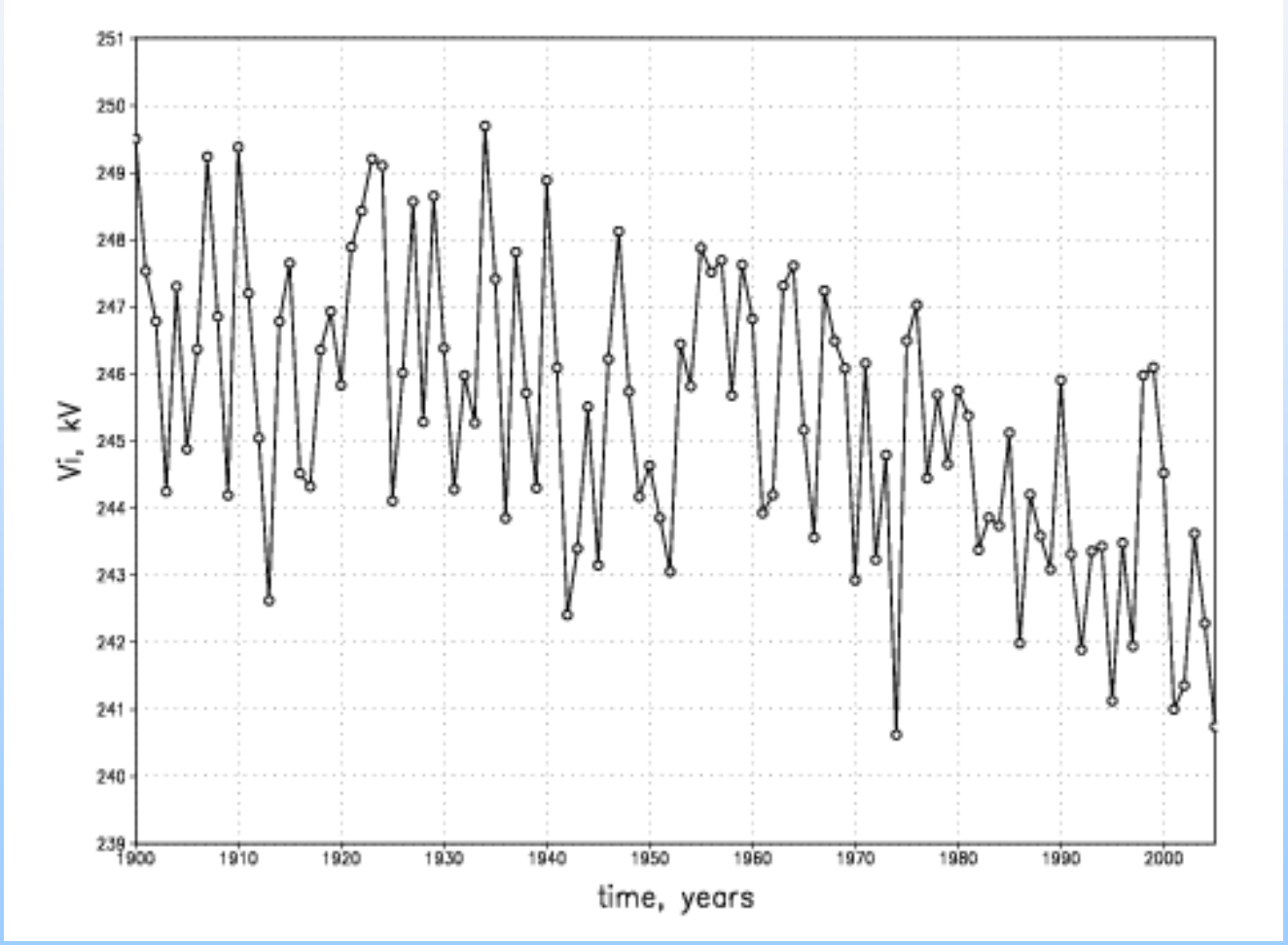

Mareev E.A., Volodin E.M., GRL, 2014

Mean-annual V_i and mean-annual square of convection in the model (XXI century); RCP8.5

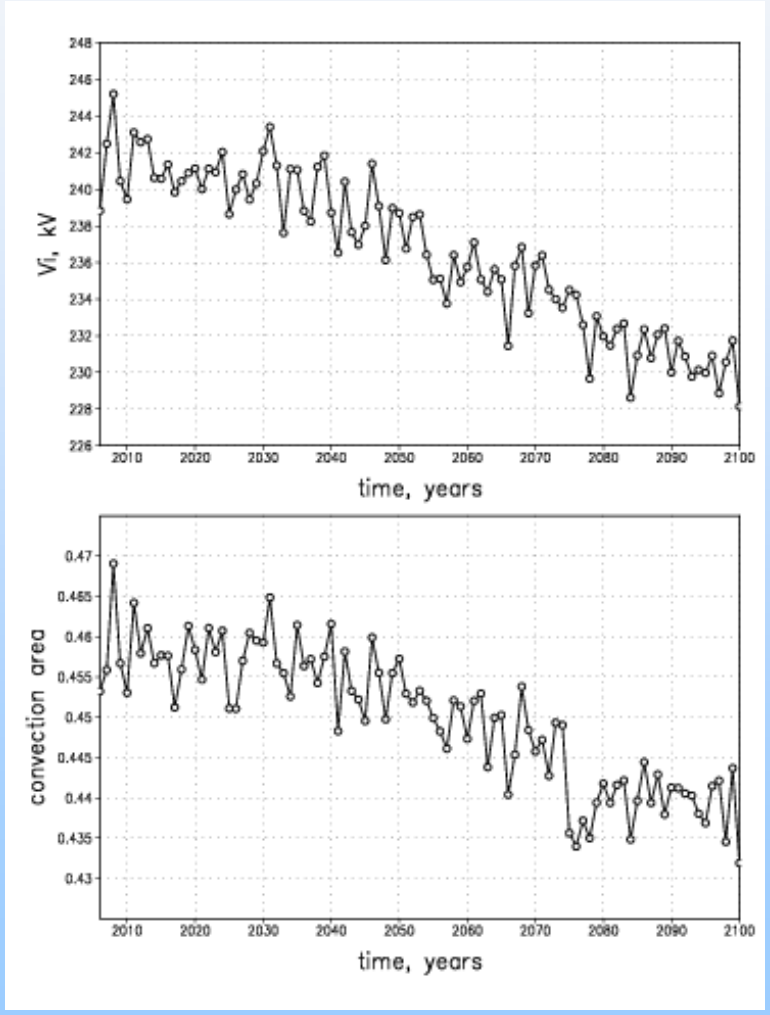

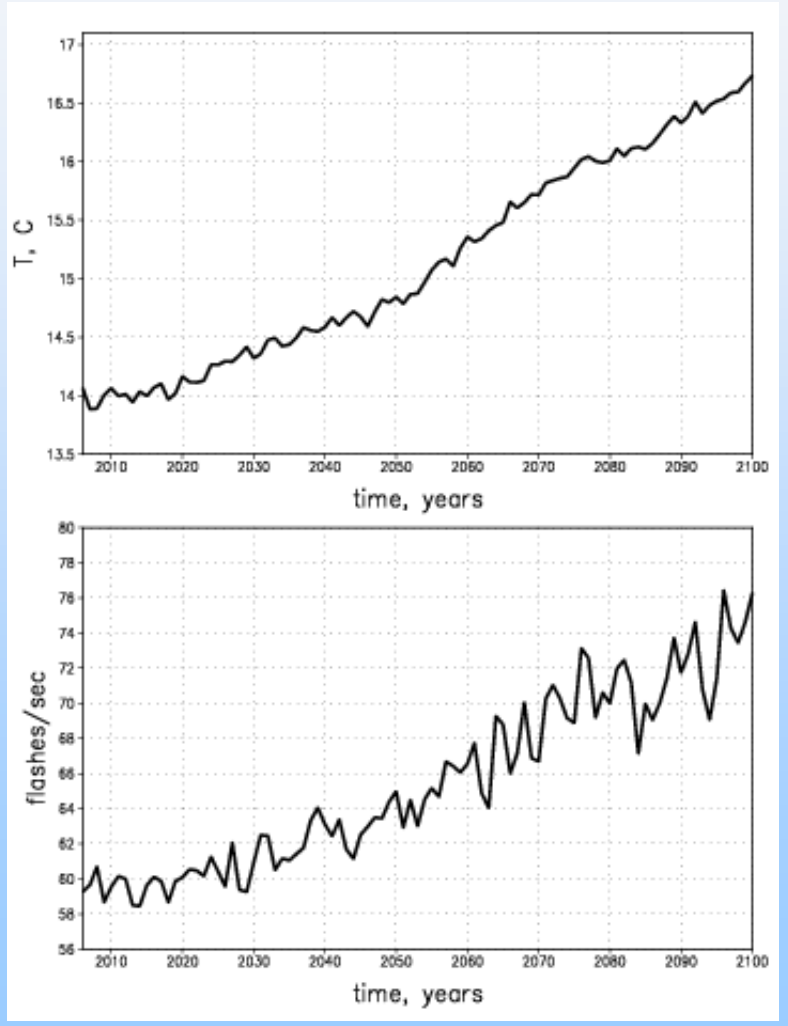

Aerosol influence on lightning activity

Direct effect

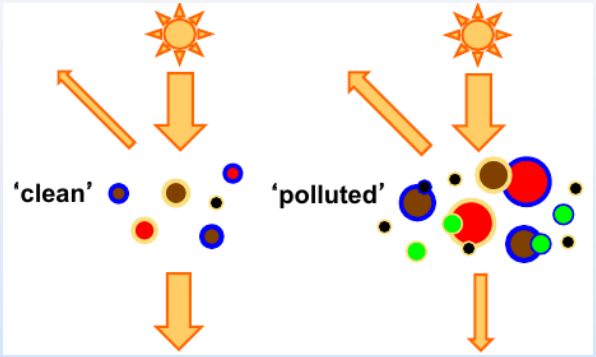

Second indirect effect

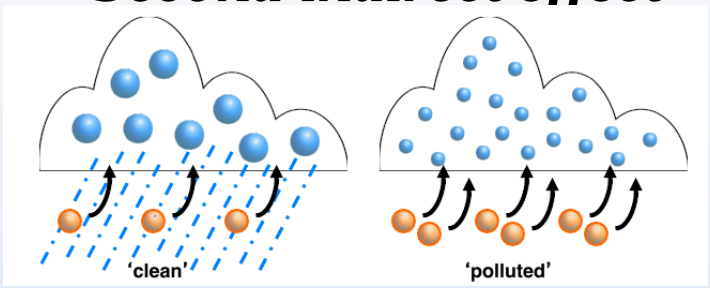

First indirect effect

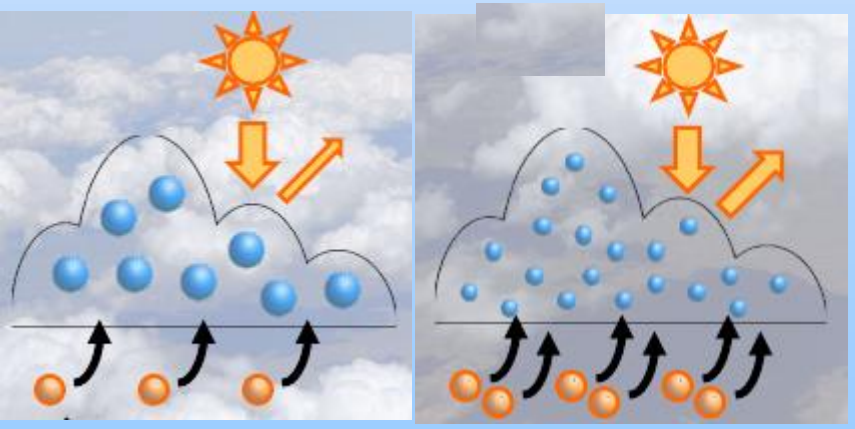

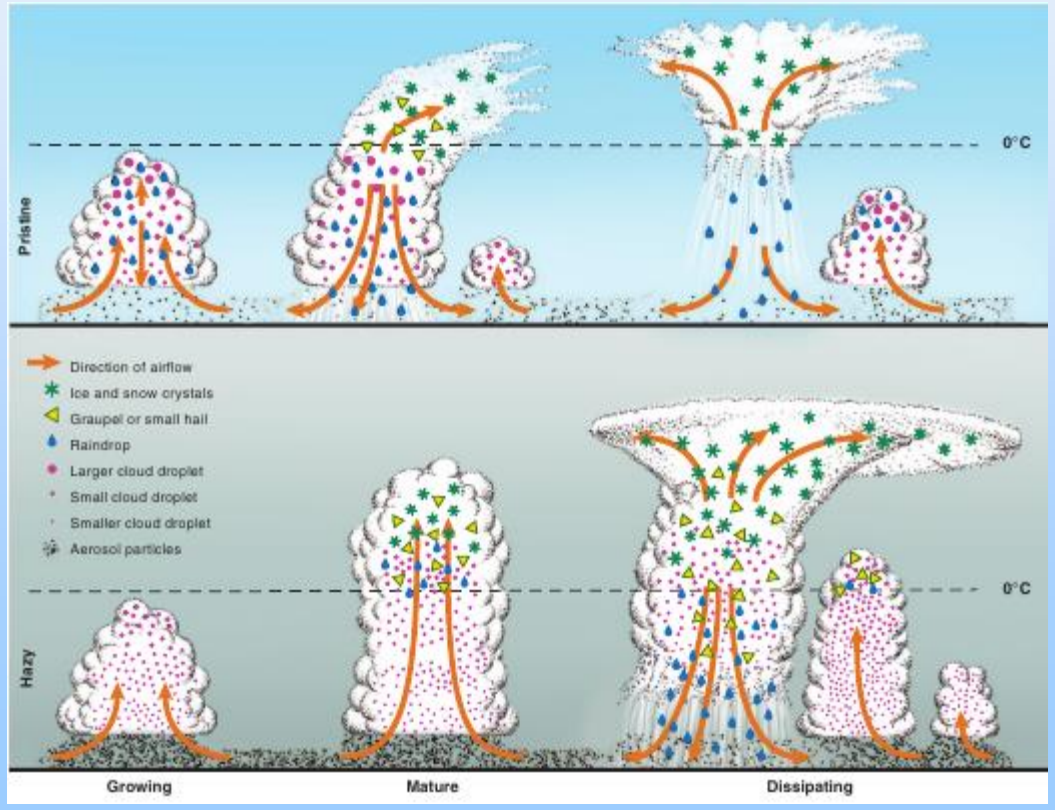

D. Rosenfeld et al., Science, V.301, p.1309, 2008

Aerosol impact on clouds

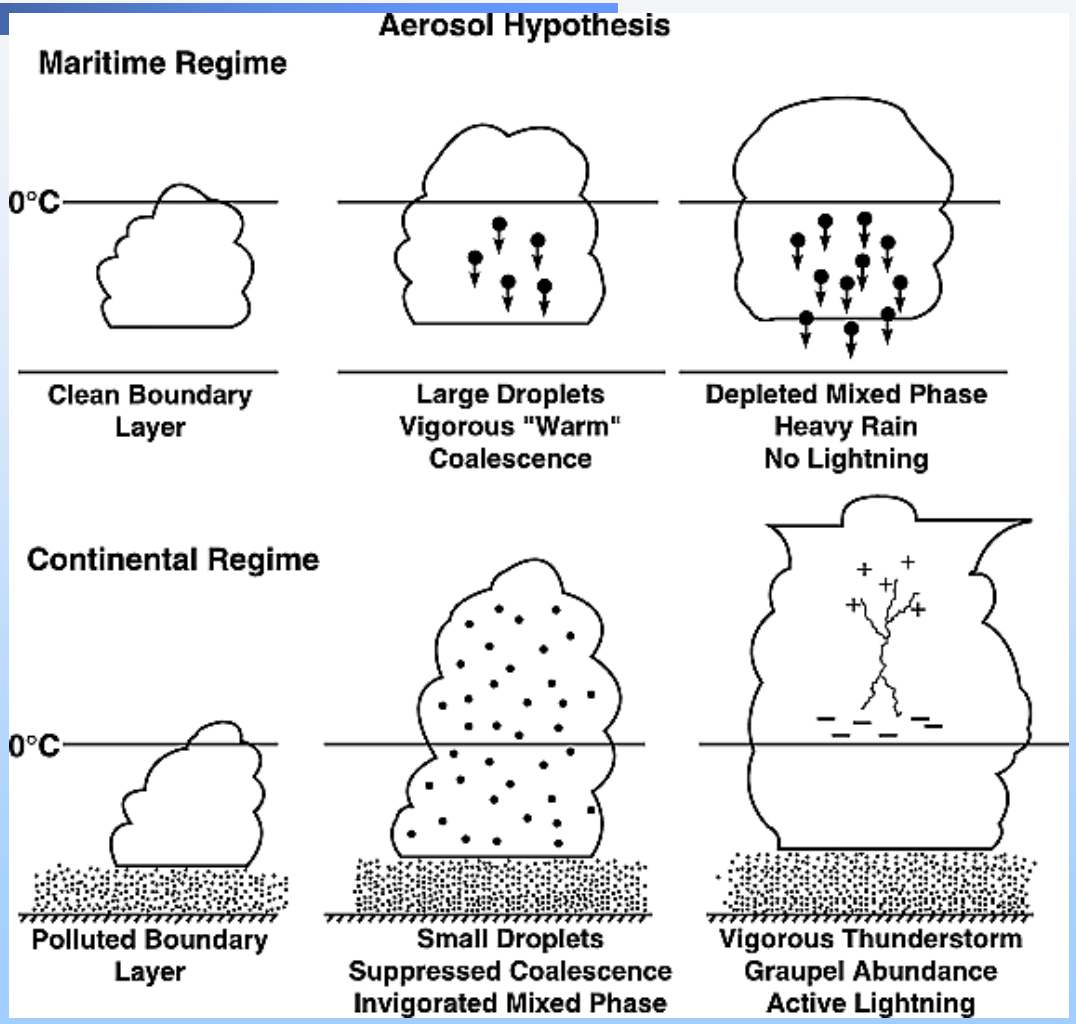

Illustration of the aerosol hypothesis for control of cloud precipitation and electrification. Williams et al., JGR, 2002

Lightning and smoke from Amazonian fires

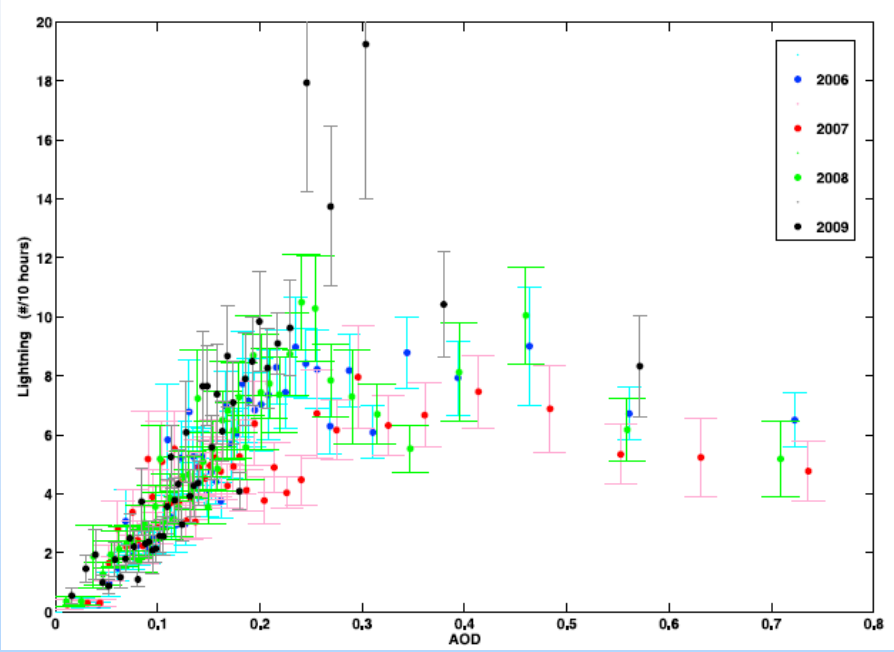

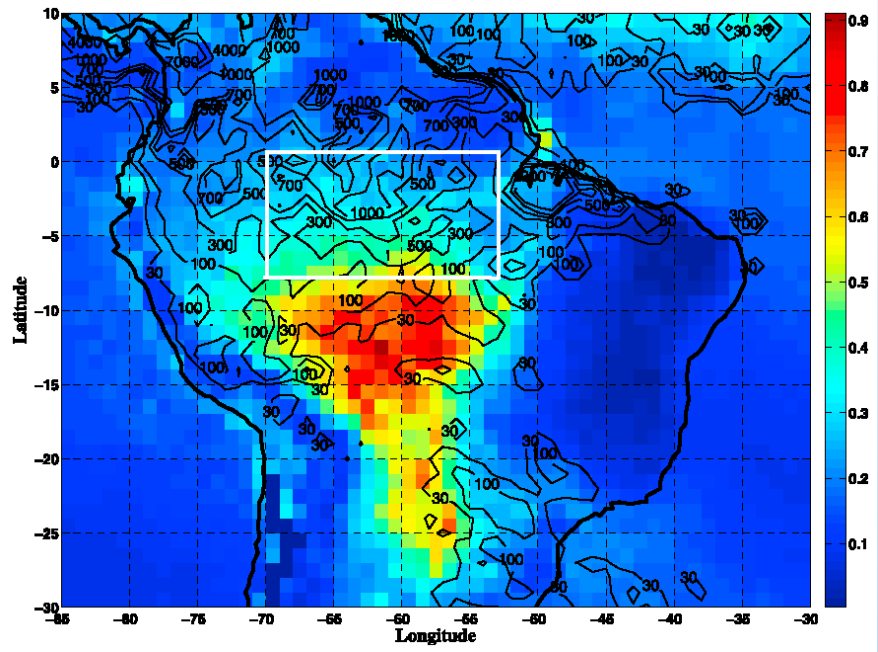

Altaratz et al., 2010. Relationship between number of lightning strokes between 12–22 local time (#/10 hours) and AOD. 2006 data are marked in blue, 2007 in red, 2008 in green and 2009 in black.

Положительные вспышки - пожары

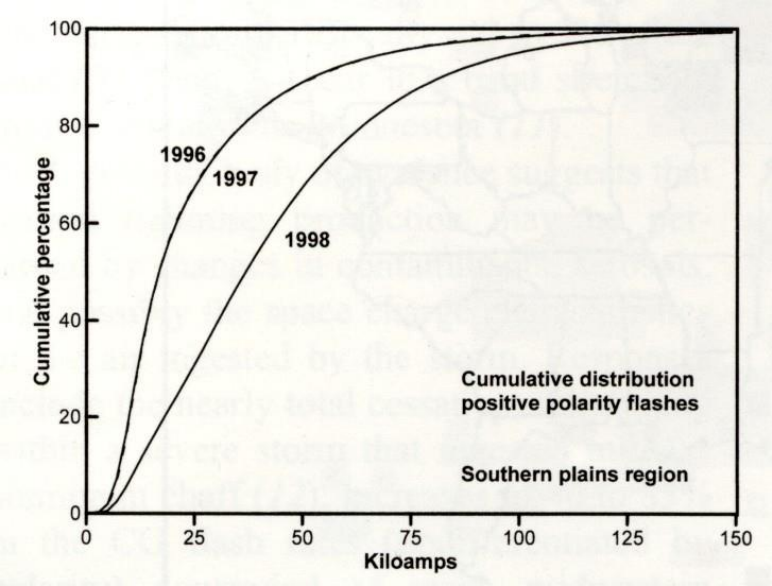

Вероятность возгорания: 1-5% вспышек

Минимальное значение потока энергии (импульс длительностью 500 мс): $8 \cdot 10^4$ Дж/м^2

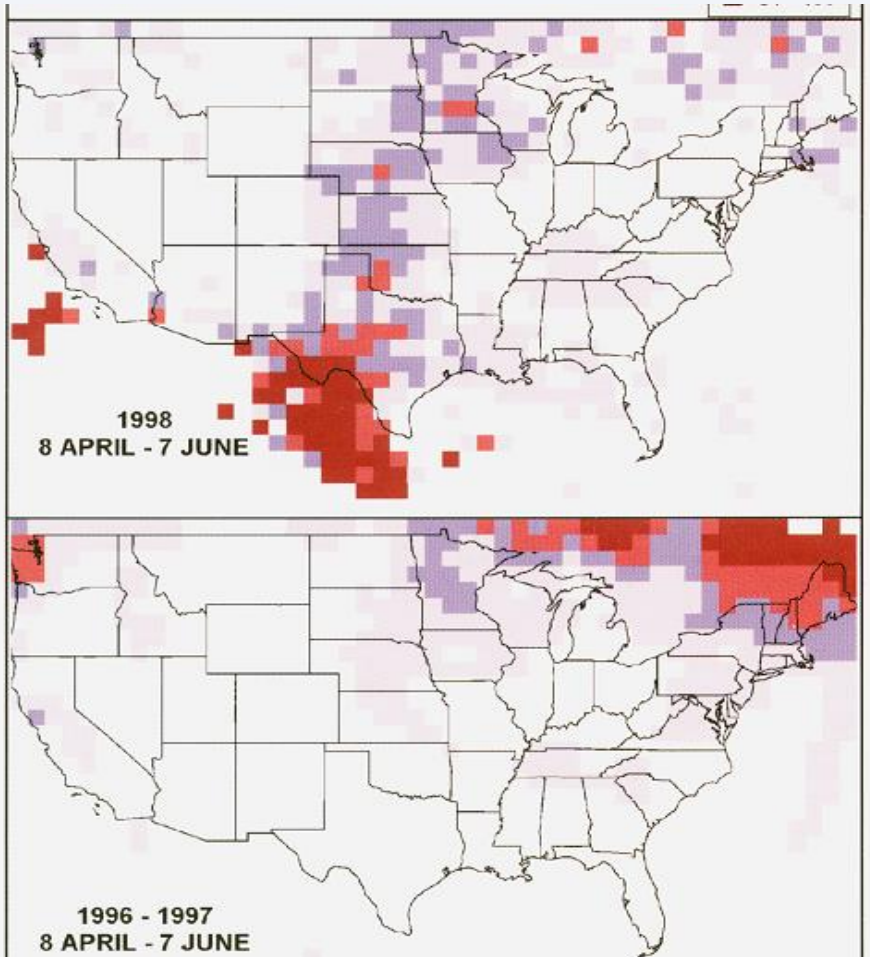

W.A.Lyons et al, 1998

Количество вспышек (LIS data) и содержание NO_2 в столбе (GOME data)

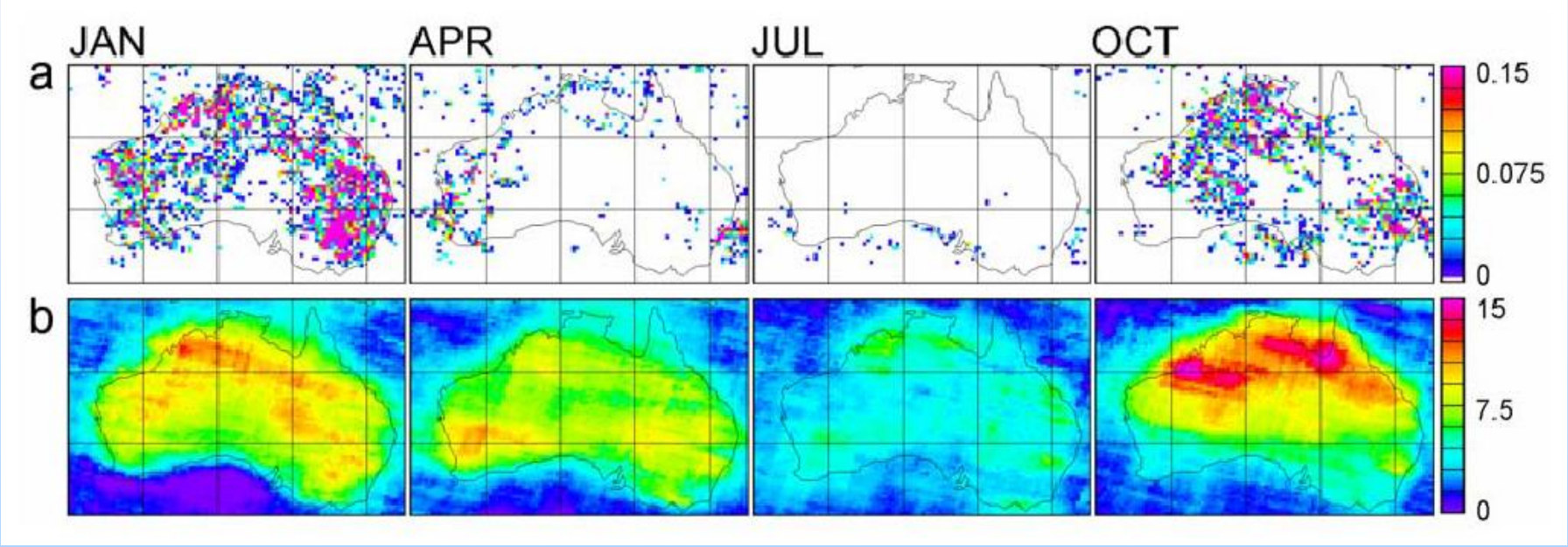

Beirle, 2004

«Все лучшие произведения мои писаны мною для какого-нибудь сильного таланта и под влиянием этого таланта…»

Кулигин. Вот хоть бы теперь то возьмем: у нас грозы частые, а не заведем мы громовых отводов.

Дикой. Да гроза-то что такое по-твоему, а? Ну, говори!

Кулигин. Электричество.

Дикой (топнув ногой). Какое еще там елестричество! Ну, как же ты не разбойник! Гроза-то нам в наказание посылается, чтобы мы чувствовали...

Кулигин. Ну чего вы боитесь, скажите на милость! Каждая теперь травка, каждый цветок радуется, а мы прячемся, боимся, точно напасти какой! Гроза убьет! Не гроза это, а благодать! Да, благодать! … ну смотрел бы да любовался! А вы боитесь и взглянуть-то на небо, дрожь вас берет! Изо всего-то вы себе пугал наделали. Эх, народ! Я вот не боюсь.

Выводы

- ГЭЦ и частота молний – показатели состояния климатической системы
- Необходим мониторинг климатологии ГЭЦ
- Существует ряд механизмов влияния атмосферного электричества на климат. Особый интерес представляет изучение роли ионов в образовании мелкодисперсных аэрозолей и облачных частиц, связи молниевых разрядов с пожароопасностью и малыми атмосферными составляющими, моделирование ГЭЦ и влияния на нее солнечной активности в различных сценариях развития климата.
- В ближайшие годы следует ожидать расширения исследований взаимосвязи атмосферного электричества, погоды и климата. Развитие этих исследований невозможно без совершенствования системы мониторинга гроз и молниевых разрядов.

Спасибо за внимание!

Sources of the secondary cosmic rays detected on the Earth's surface (Chilingarian, JASTP, 2014)

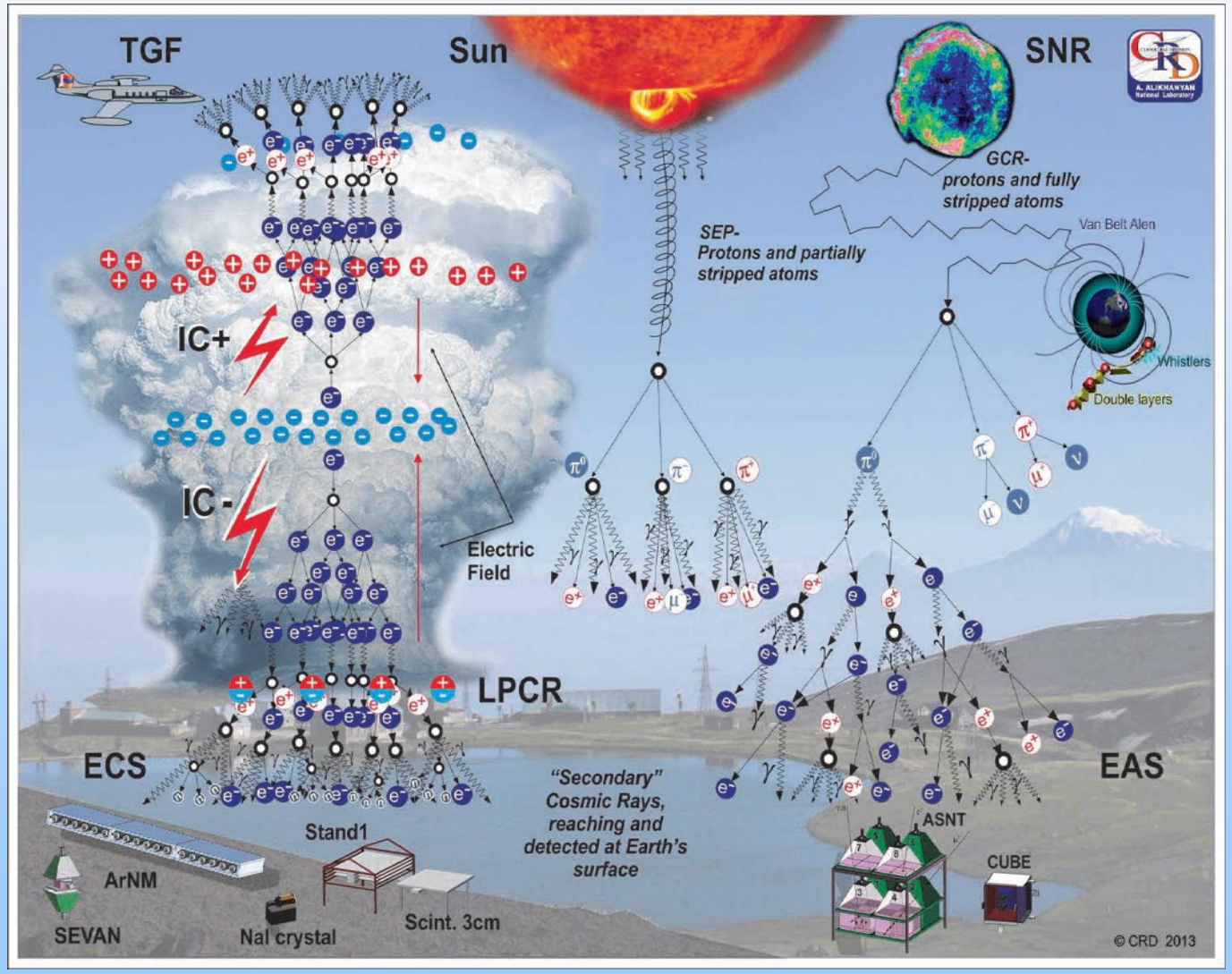

Ionisation in the atmosphere

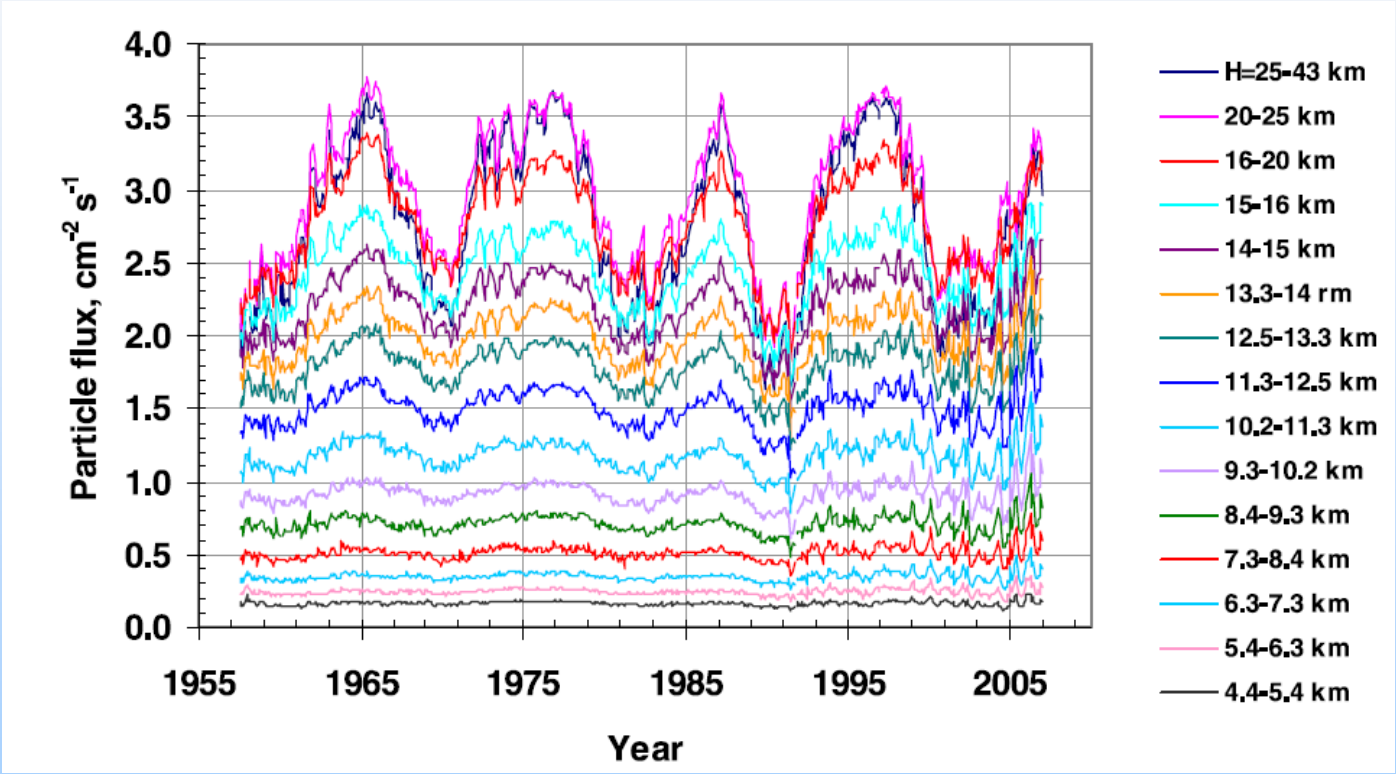

(G.A. Bazilevskaya, I.G. Usoskin, E.O. Flückiger, R.G. Harrison, L. Desorgher, R. Bütikofer, M.B. Krainev, V.S. Makhmutov, Y.I. Stozhkov, A.K. Svirzhevskaya, N.S. Svirzhevsky, G.A. Kovaltsov, 2008)

Monthly averaged fluxes of ionising particles in the atmosphere over Murmansk region

Vertical profiles of the ion-pair production rate at solar minimum and solar maximum

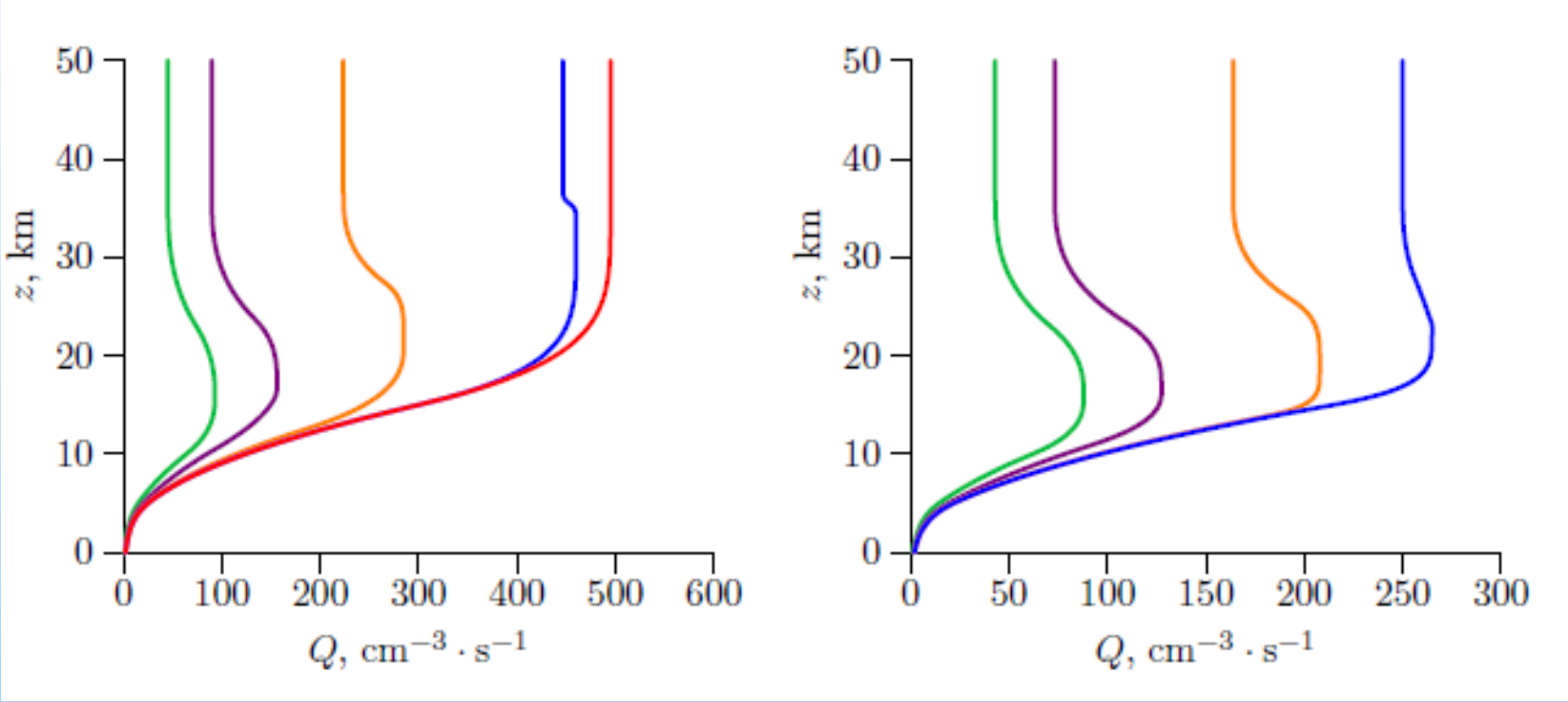

Geomagnetic latitude: 0 (green line), 30 (purple line), 45 (orange line), 60 (blue line), and 90 (red line). At solar maximum, the cosmic-ray knee moves to lower latitudes and the profiles at 60 and 90 coinside

Slyunyaev et al., JGR, 2014

Modelling the influence of conductivity enhancement in the stratosphere

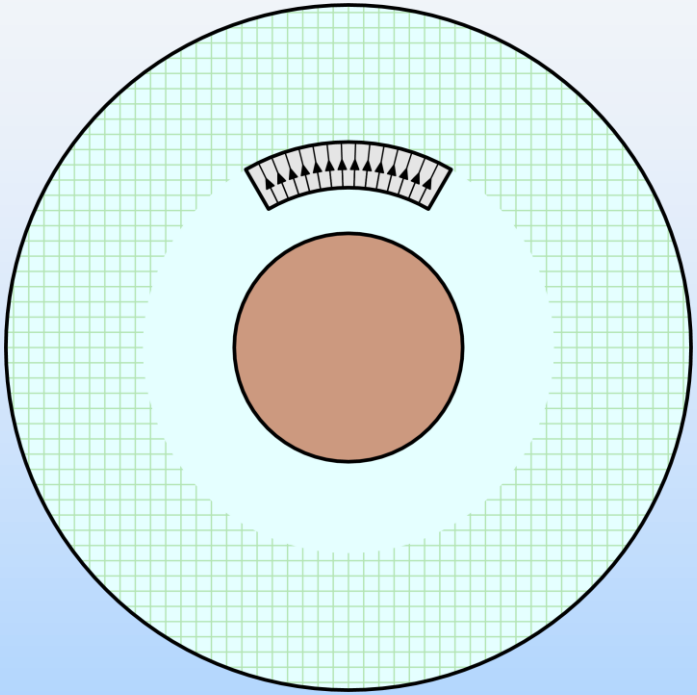

If the conductivity in the cross-hatched region above the clouds is increased by a factor of 2, the sign of the change in the cloud contribution to the ionospheric potential **depends on the source type**

- Current source, no conductivity reduction $\Delta V_i/V_i = 0\%$
- Current source, reduced conductivity $\Delta V_i/V_i = -4.7\%$
- Voltage source $\Delta V_i/V_i = +8.6\%$

Modelling the ionospheric potential variation over the solar cycle

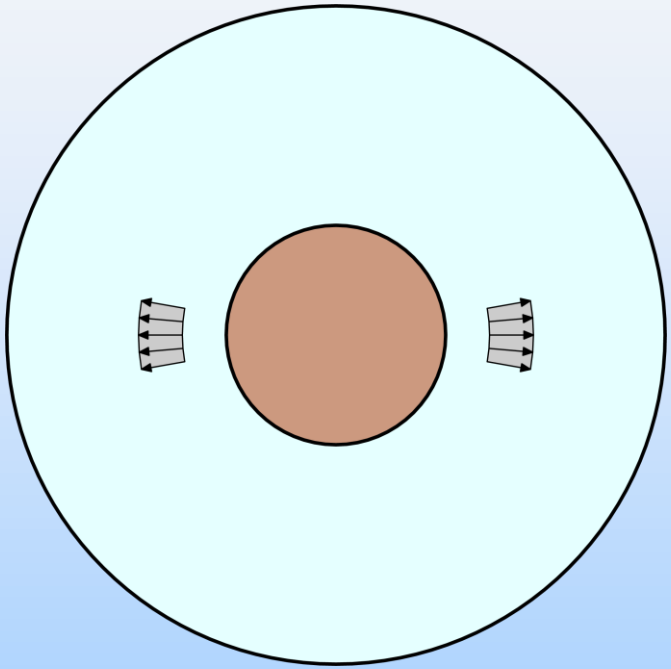

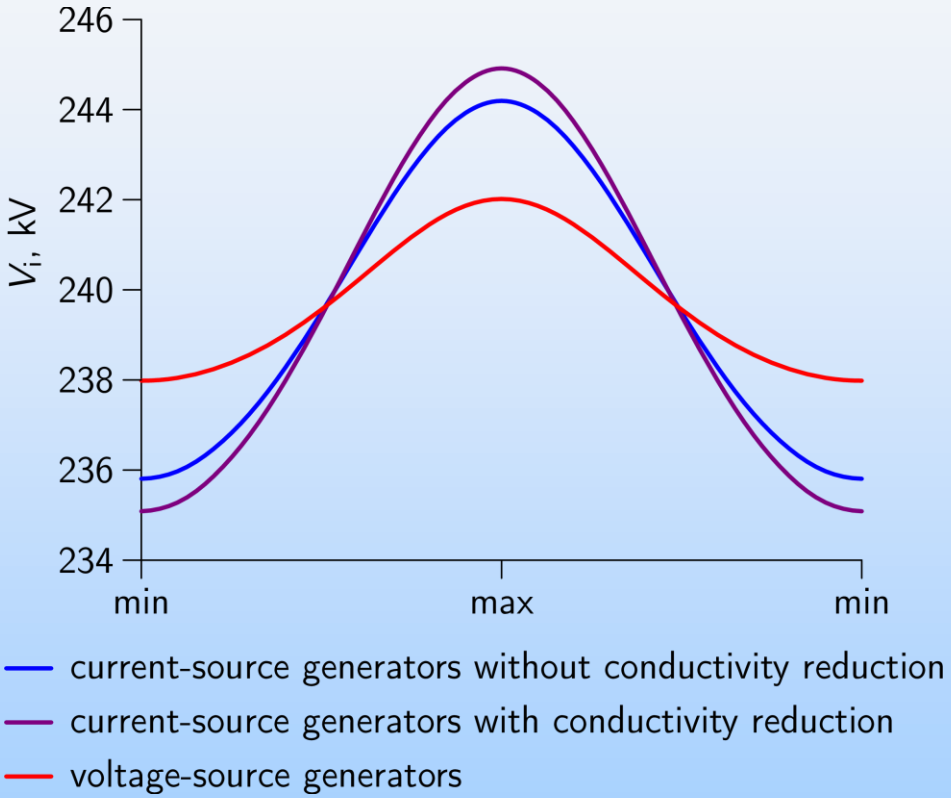

The conductivity variation is determined primarily by the variation in atmospheric ionisation; in this model problem generators are assumed to occupy low latitudes, whereas the conductivity distribution is most perturbed at high latitudes, which eventually results in similar trends of V_i

A more general view on the GEC sources in network models

We suppose that a thunderstorm is represented by a current-source generator whose **source current $I^s(E)$ depends on the electric field intensity**

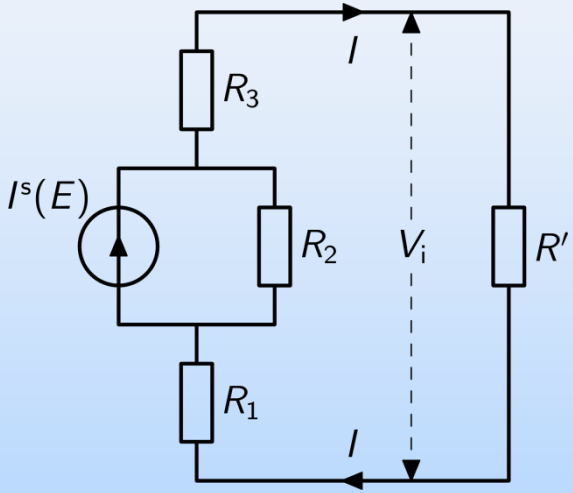

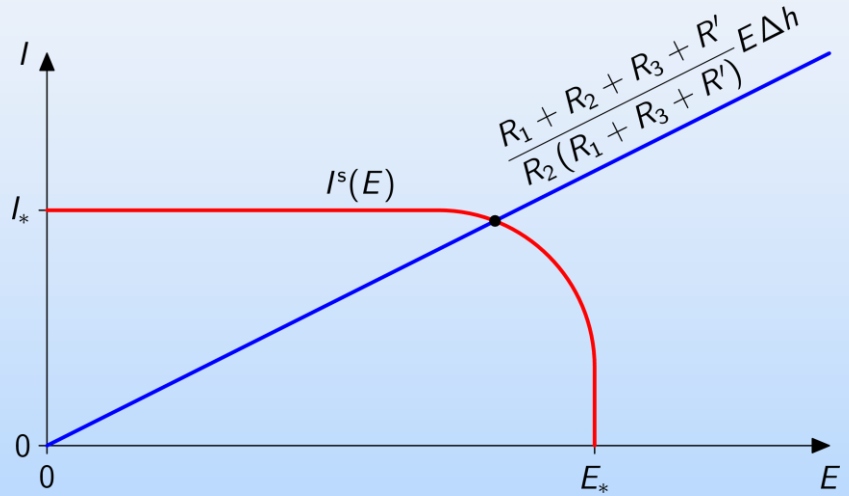

$$I = \frac{I^s(E)R_2}{R_1 + R_2 + R_3 + R'} = \frac{E\Delta h}{R_1 + R_3 + R'} \quad \Rightarrow \quad I^s(E) = \frac{R_1 + R_2 + R_3 + R'}{R_2\,(R_1 + R_3 + R')}E\Delta h$$

The generator can operate in different regimes depending on the relationships between the resistances

$$\frac{1}{R_2} + \frac{1}{R_1 + R_3 + R'} \gg \frac{I_*}{E_*\Delta h} \quad \Rightarrow \quad \textbf{a current source}$$

$$\frac{1}{R_2} + \frac{1}{R_1 + R_3 + R'} \ll \frac{I_*}{E_*\Delta h} \quad \Rightarrow \quad \textbf{a voltage source}$$

Conclusions

- The traditional source current density description of GEC generators (corresponding to current sources in network models) in some cases is insufficiently accurate and fails to account for the existing observations (in particular, the enhancement of the ionospheric potential due to nuclear weapons testing in the 1950s and 1960s)
- Voltage-source generators, which have been occasionally used in network models of the GEC, can be consistently implemented in more realistic continuous GEC models
- Actual GEC generators probably can operate in different regimes depending on the parameters of the system; a more general approach within which the source current depends on the electric field intensity contains current-source and voltage-source regimes as two limiting cases (at least for network models of the GEC)
- The variability of the regime of operation must be taken into consideration in order to faithfully represent GEC generators in numerical models

Многопунктовые системы грозопеленгации в России

Россия

- Система «Алвес»
  - Разработка ООО «Алвес» и Главная Геофизическая Обсерваторя
  - Покрытие — Европейская часть и Урал, 70 пунктов пеленгации
- Северо-кавказская грозопеленгационная система
  - Развернуто при Высокогорном геофизическом институте, оборудование и ПО — LS8000, Vaisala ltd.
  - Покрытие — Северный Кавказ, 2 пункта пеленгации
- Система авиалесоохраны
  - Нет данных
- WWLLN — международная система
  - На территории России несколько пунктов пеленгации

Методы многопунктовой пеленгации молний

- Разностно-дальномерный метод
  - Используется информация о точном времени прибытия переднего фронта импульса на пункт пеленгации
- Триангуляционный метод
  - Используются записи горизонтальных компонент магнитного поля

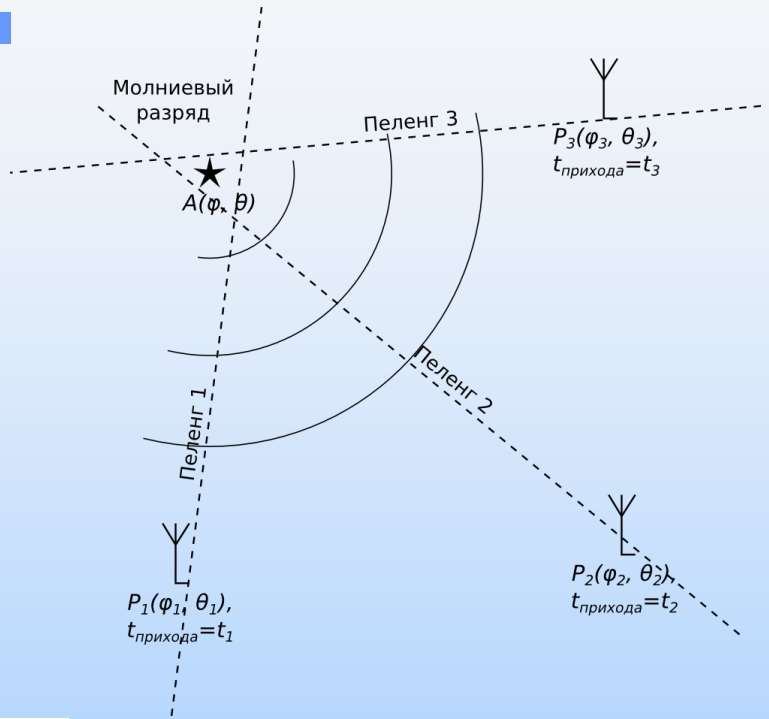

$$\mathbf{E}(P_t) = \sum_{\substack{i,j=1..N \\ i \neq j}} \left[(T_i - T_j) - \frac{\rho(P_t, P_i) - \rho(P_t, P_j)}{c} \right]^2 + \xi \sum_{i=1..N} \gamma_i (\varphi(P_i, P_t) - \varphi_i)^2 ,$$

$$\mathrm{tg}(\varphi_B) = \frac{2\sum B_i^N B_i^W}{\sum (B_i^W)^2 - \sum (B_i^N)^2}$$

- Построение комбинированной функции ошибки
- Решение вариационной задачи минимизации функции ошибки

Организация разработанной системы

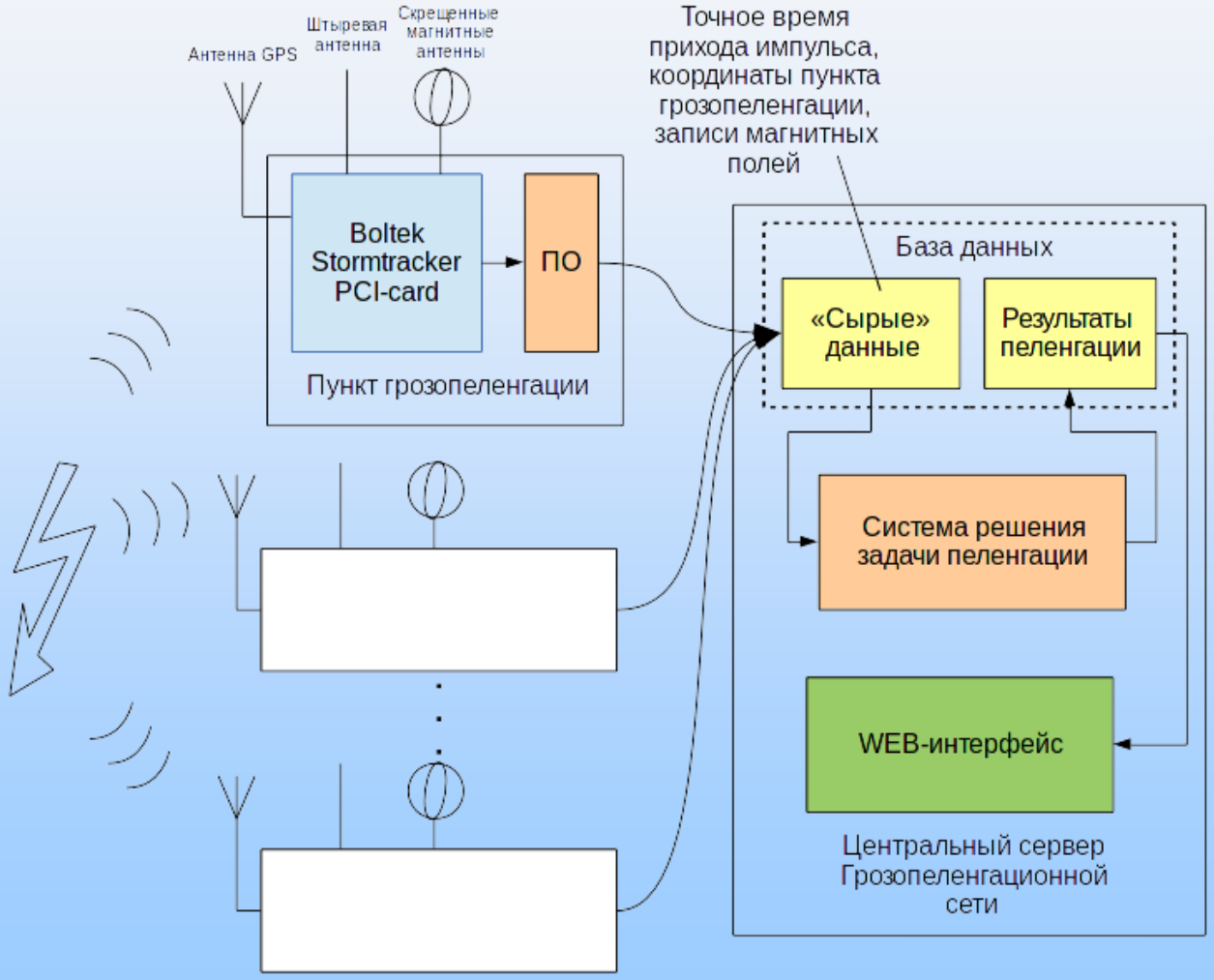

Устройство пункта пеленгации

- Компьютер
- Устройство Boltek Stormtracker с платой расширения LTS-2
- Программное обеспечение, работающее под управлением ОС Linux

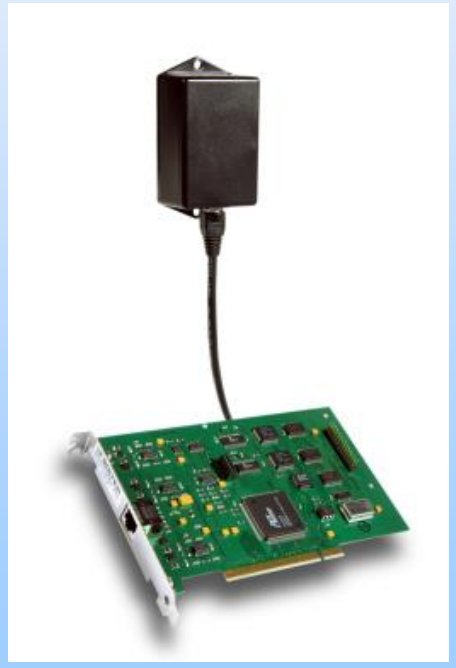

Boltek Stormtracker

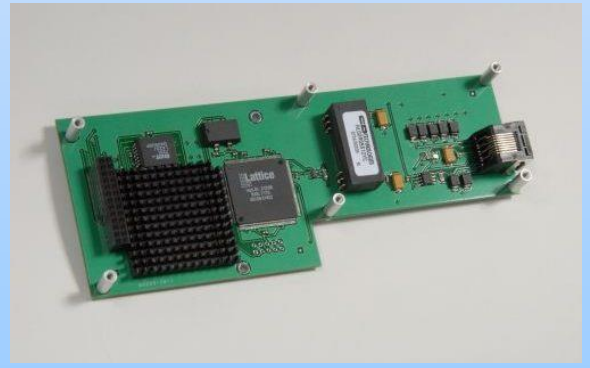

LTS-2

Антенна в защитном корпусе

Наземные измерения: evidence for diurnal variation and large-scale correlated events

Evidence for Diurnal Variations of the Local/Regional Convective Generator

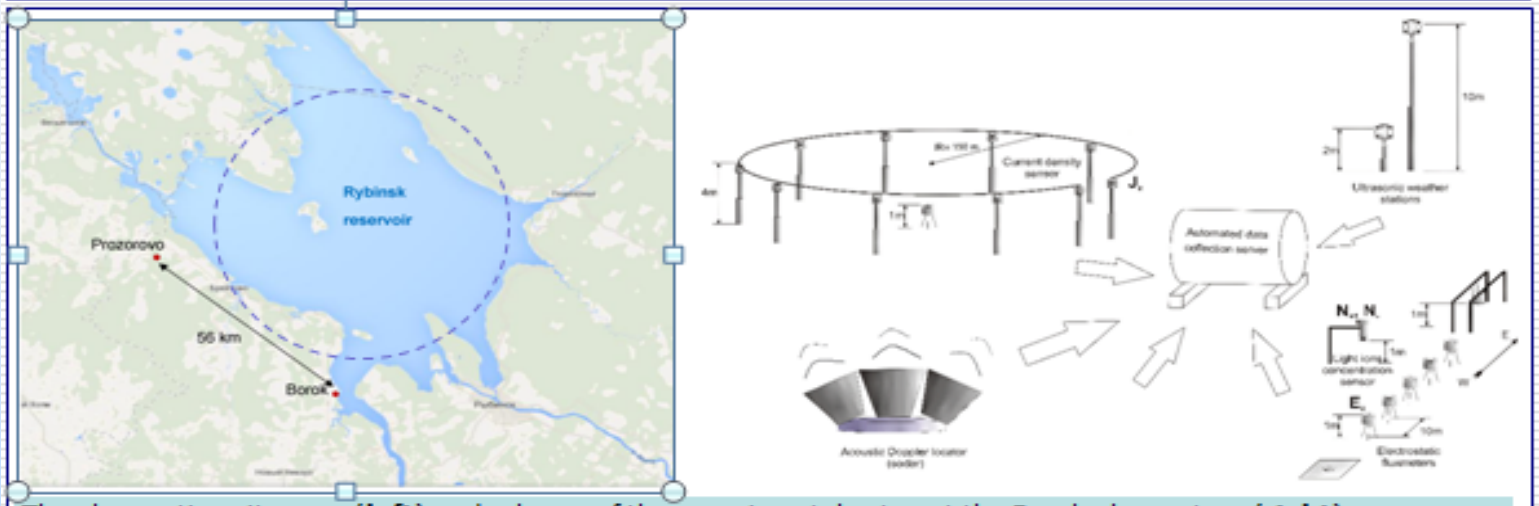

The observation site map (**left**) and scheme of the experimental setup at the Borok observatory (**right**).

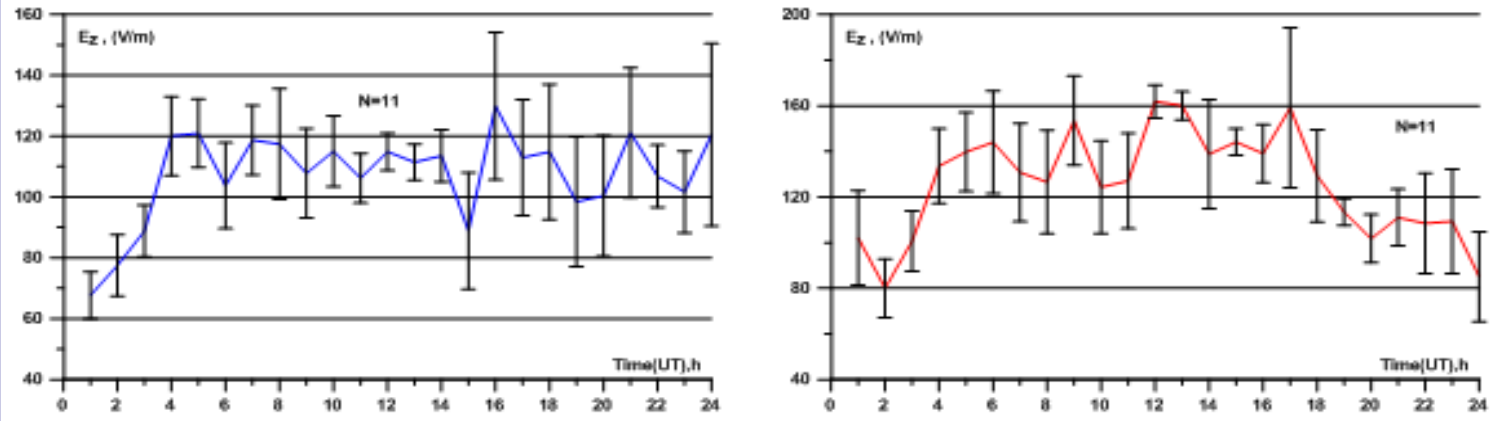

Diurnal variation of the fair weather electric field E_z as measured at the Borok (**left**) and Prozorovo (**right**) observation sites in July-August 2005. Local maximum of the field at about 09 UTC is well recognized.

LHR difference in the model in warm and cold ENSO periods

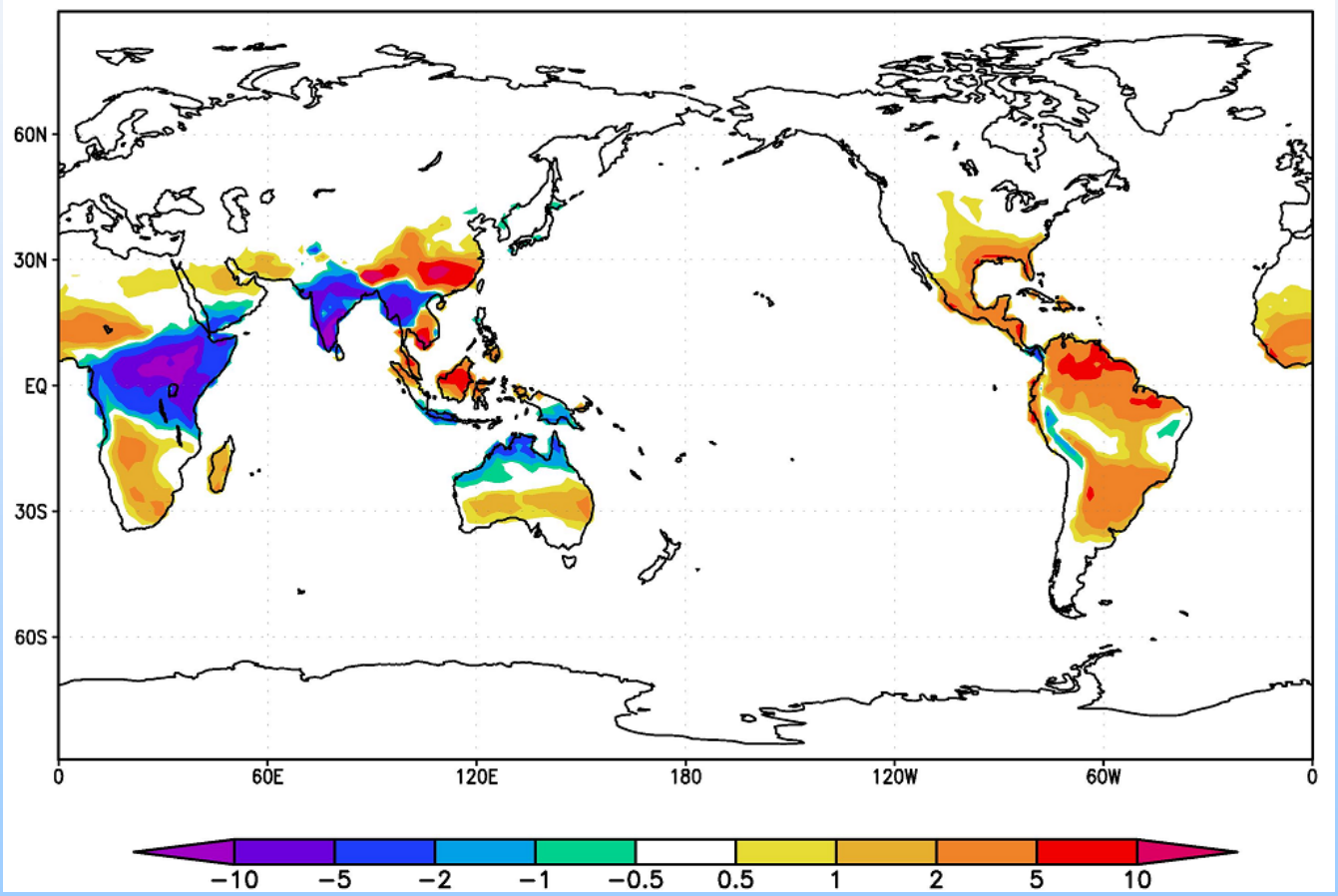

Without WS

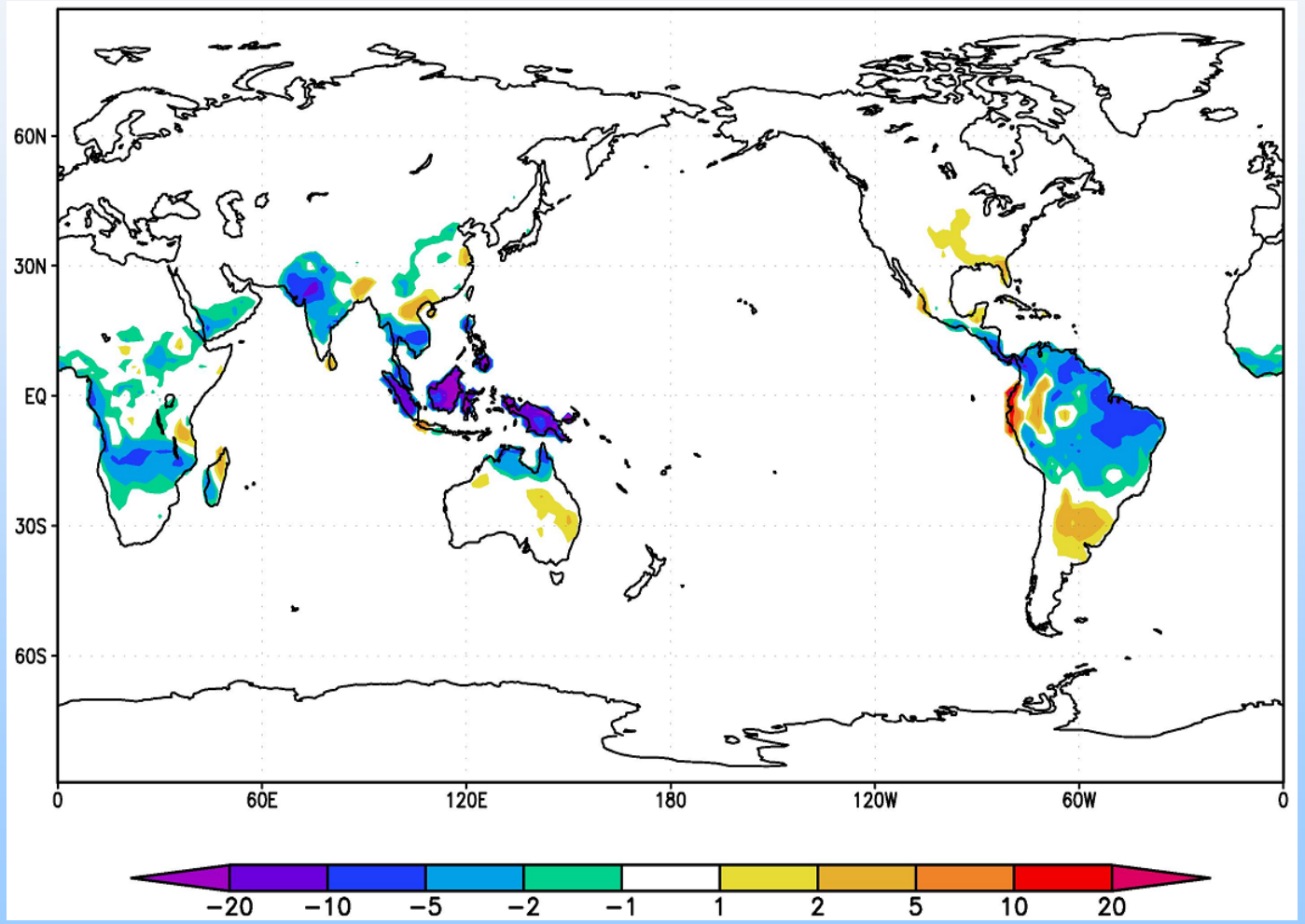

Parameter	Definition according to *Berger et al.* [1975]	Equation in terms of Figure 1*
Peak current	The maximum peak current during the return stroke	$i(C_k) = \max_{A_k \le t \le F_k} i(t)$
Stroke charge	The total charge in the stroke, transferred by both the "impulse" current and the continuing current	$\int_{A_k}^{F_k} i(t)\,dt$
Impulse charge	The charge transferred by the rapidly changing part of the stroke (*Berger et al.* [1975] note that it is not precisely defined)	$\int_{A_k}^{E_k} i(t)\,dt$
Flash charge	The total charge transferred by the flash	$\int_{A_1}^{F_n} i(t)\,dt$
Maximum current steepness	The steepest tangent on the front of the stroke	$\max_{A_k \le t \le C_k} \frac{di(t)}{dt}$
Front duration	The time interval between the 2 kA point on the front and the first peak	$C_k - B_k$
Stroke duration	The time interval between the 2 kA point on the front and the half-peak value point on the tail	$D_k - B_k$
Flash duration	The time interval from the beginning of the first stroke to the completion of the last stroke	$F_n - A_1$
No-current interval	The time interval between strokes during which no detectable current is flowing	$A_{k+1} - F_k$
Prospective stroke energy	The energy which would be dissipated by the stroke current flowing through a one-ohm resistor	$\int_{A_k}^{F_k} i^2(t)\,dt$

* When writing equations, we assume that the flash consists of n strokes; the subscript k indicates an arbitrary (kth) stroke; $i(t)$ stands for the current as a function of time.

Thunderstorm 1-2 June, 2015

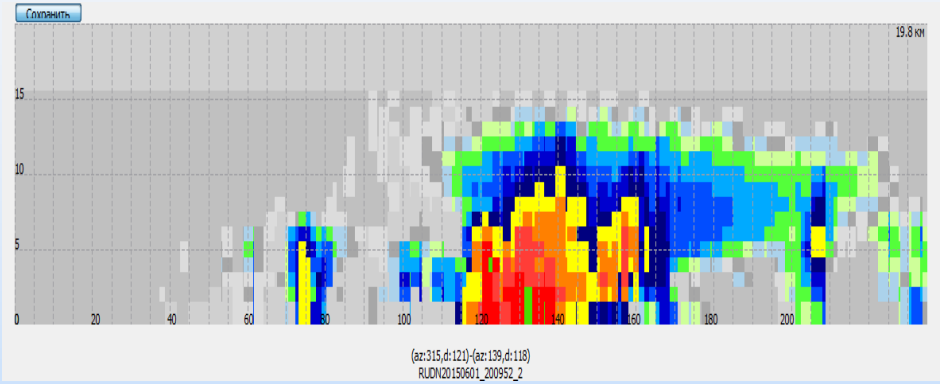

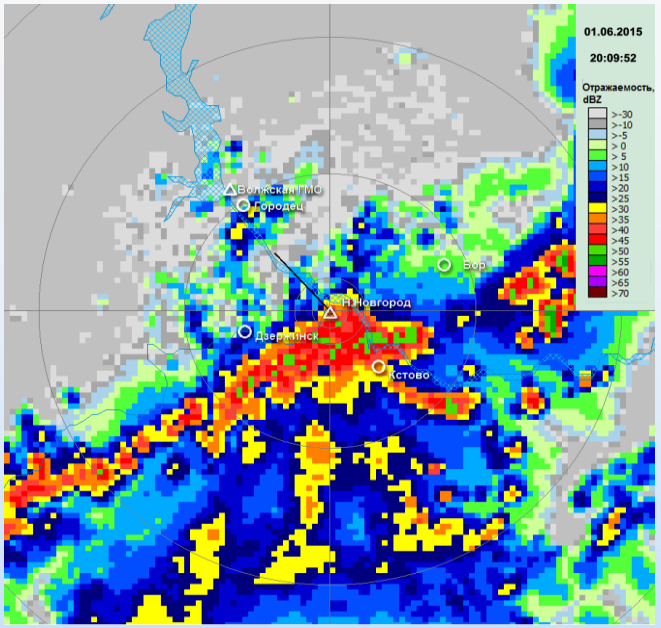

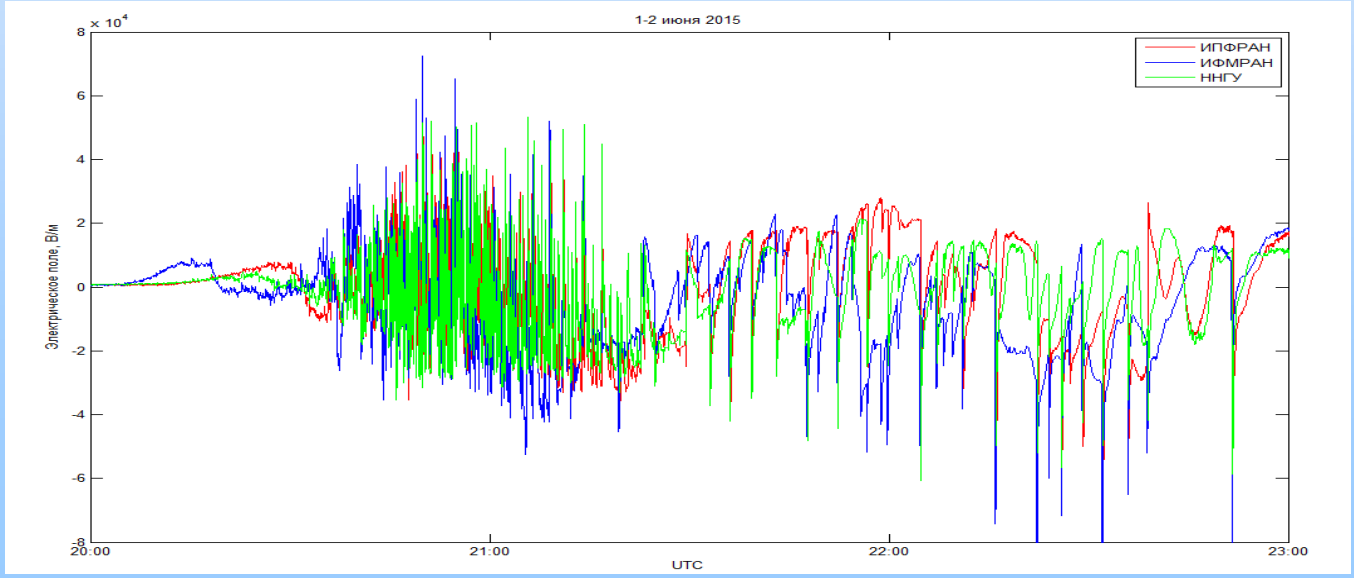

Lapierre et al., JGRD, 2014

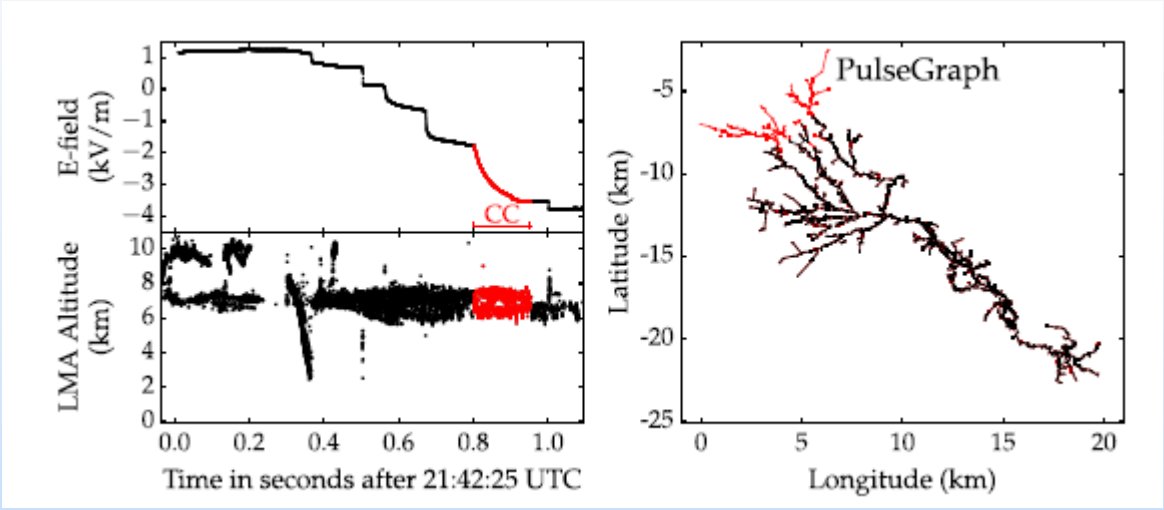

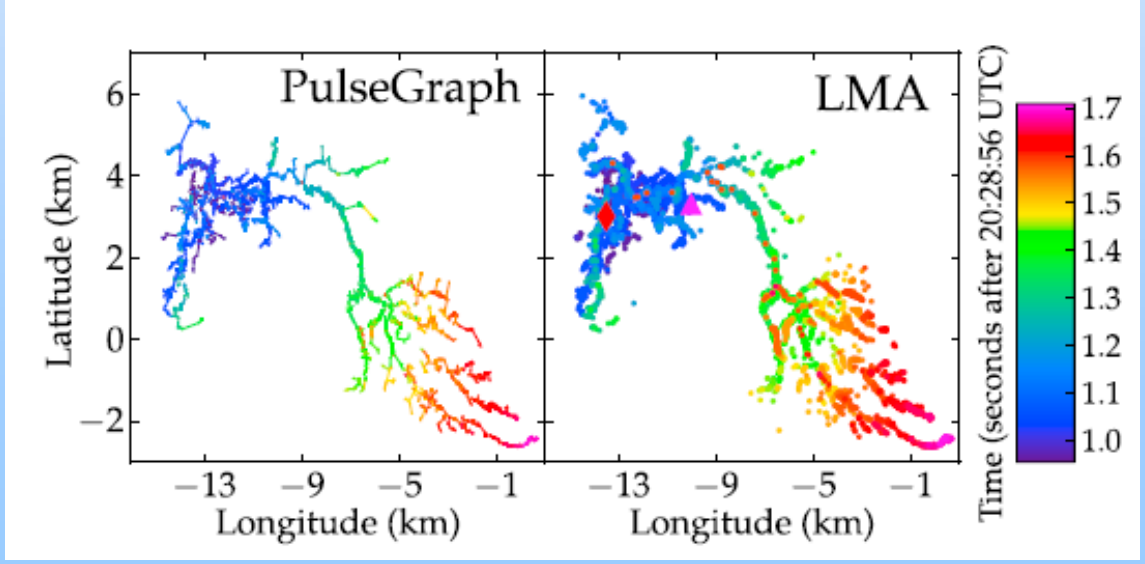

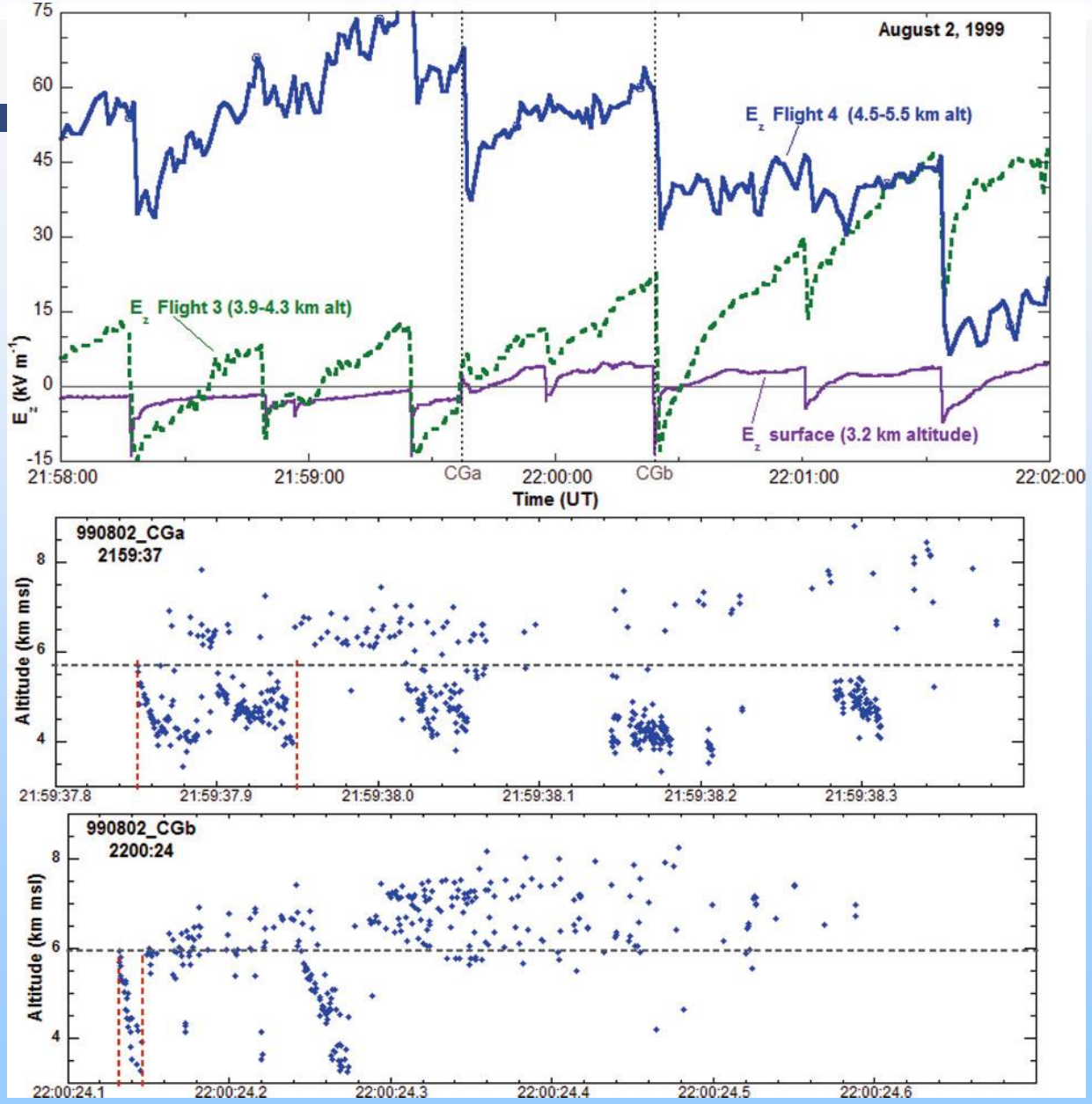

An example of a horizontal lightning channel traveling during a period of preliminary breakdown within a potential well (S&M, 2009)

Выводы

- Дан обзор актуальных и недостаточно исследованных проблем формирования так называемой главной стадии молнии, с которой связаны ее наиболее опасные проявления
- Показано, что данные современных систем грозопеленгации (NLDN) подтверждают логнормальное распределение вспышек по максимальному току
- Максимальный ток главной стадии формируется в результате быстрого последовательного подключения к высокопроводящему каналу молнии множества участков коронного чехла, образовавшихся при распространении предшествующего лидера
- Проанализированы физические процессы, формирующие статистику первой и последующих компонент отрицательной вспышки молнии по току, заряду и энергии

Моделирование длинного стримера

$$\frac{\partial n_e}{\partial t} + \nabla \cdot (n_e v_e - \mathbf{D}_e \nabla n_e) = (k_i N + k_i^* n^*) n_e$$
$$-(k_a' + k_a'' N) N_a n_e + (k_d N + k_d^* n^*) n_n - \beta_{ei} n_e n_p + S_f \quad (1)$$

$$\frac{\partial n_p}{\partial t} + \nabla \cdot (n_p v_p) = (k_i N + k_i^* n^*) n_e - \beta_{ei} n_e n_p$$
$$-\beta_{ii} n_p n_n + S_f \quad (2)$$

$$\frac{\partial n_n}{\partial t} + \nabla \cdot (n_n v_n) = (k_a' + k_a'' N) N_a n_e - (k_d N + k_d^* n^*) n_n$$
$$-\beta_{ii} n_p n_n \quad (3)$$

$$\frac{\partial n^*}{\partial t} = k^* N n_e - k_i^* n^* n_e - k_q^* N n^* - \frac{n^*}{t_l} \quad (4)$$

$$\nabla \cdot E = \frac{e}{\varepsilon_0}(n_p - n_e - n_n). \quad (5)$$

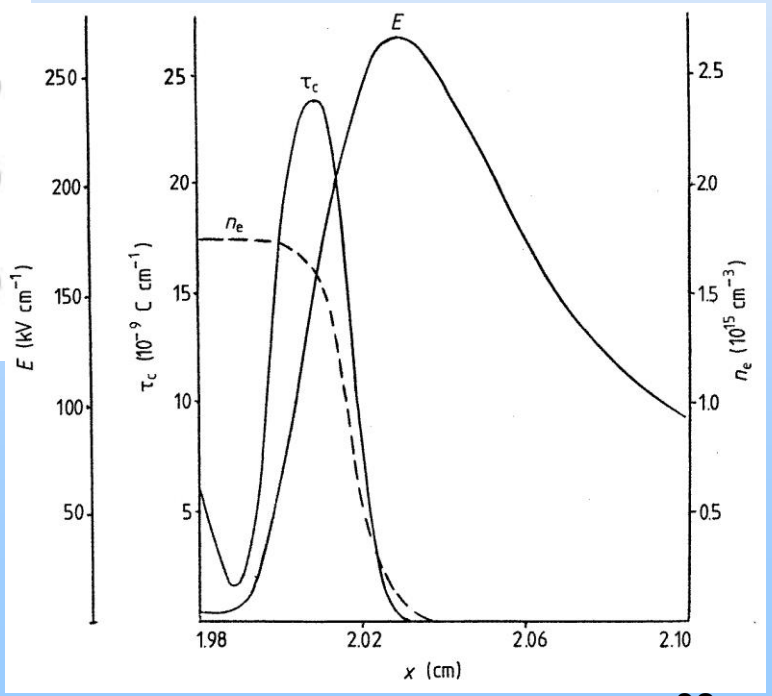

N.Aleksandrov, E.Bazelyan, 1996, 2007.

Формирование лидера

$$N(^4S) + O(^3P) \longrightarrow NO^+ + e$$

$$N_2(A^3\Sigma_u^+) + N_2(a'^1\Sigma_u^-) \longrightarrow e + N_4^+$$

$$N_2(a'^1\Sigma_u^-) + N_2(a'^1\Sigma_u^-) \longrightarrow e + N_4^+$$

Associative ionization

N.Popov, 2003.

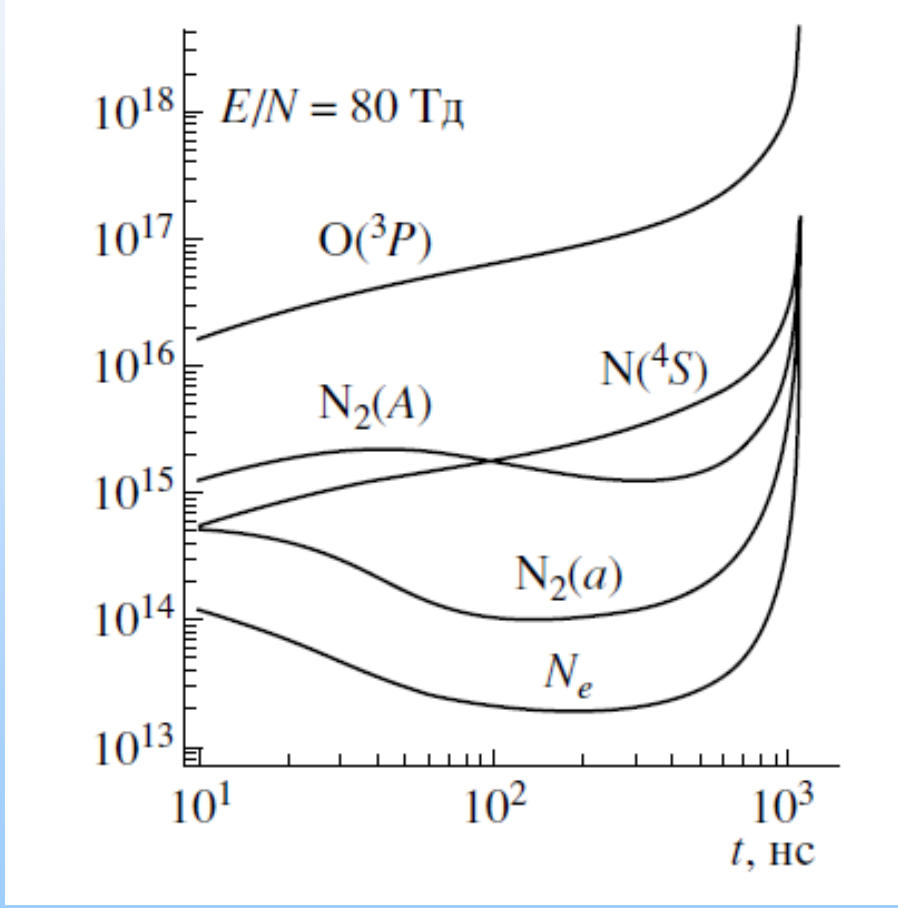

Формирование лидера. Быстрый нагрев

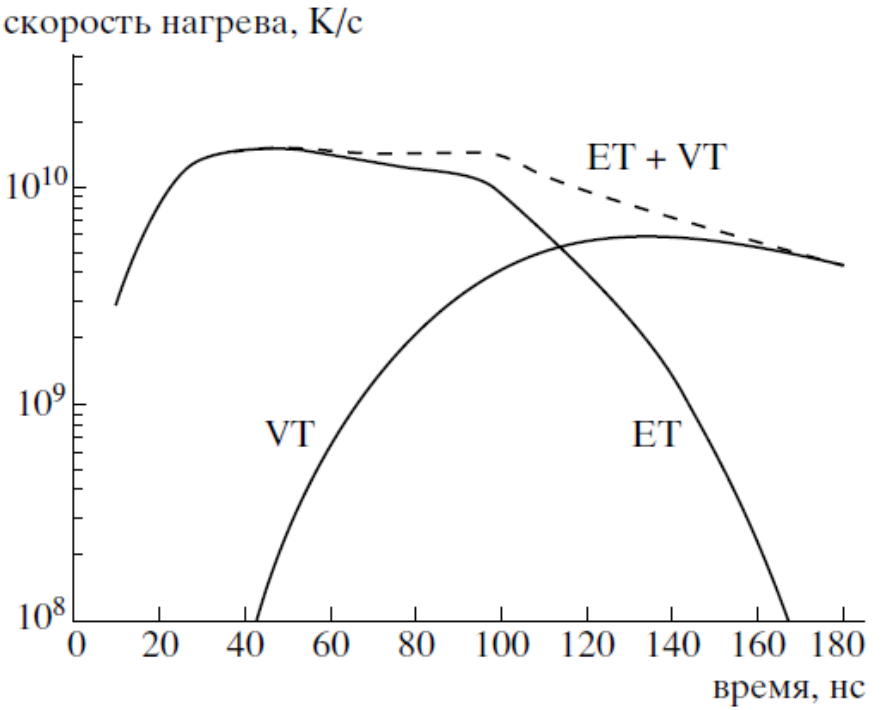

N.Popov, 2009.

$$\frac{\partial N_e}{\partial t} + \frac{1}{r}\frac{\partial (uN_e)}{\partial r} = \frac{1}{r}\frac{\partial}{\partial r}\left(rD_a\frac{\partial N_e}{\partial r}\right) +$$
$$+ N_e(\nu_{ion} - \nu_{att}) + Q_{ass} - Q_{rec} + Q_{det}$$

$$W_T = W_E + \frac{\varepsilon_V - \varepsilon_0(T)}{\tau_{VT}}$$

$$\frac{\partial \rho}{\partial t} + \frac{1}{r}\frac{\partial \rho ur}{\partial r} = 0$$

$$\frac{\partial \rho u}{\partial t} + \frac{1}{r}\frac{\partial \rho u^2 r}{\partial r} + \frac{\partial P}{\partial r} = 0$$

$$\frac{\partial \rho E_g}{\partial t} + \frac{1}{r}\frac{\partial \rho ur(E_g + P)}{\partial r} = \frac{1}{r}\frac{\partial}{\partial r}\left(r\lambda\frac{\partial T}{\partial r}\right) + W_T$$

Ионизационно-перегревная неустойчивость

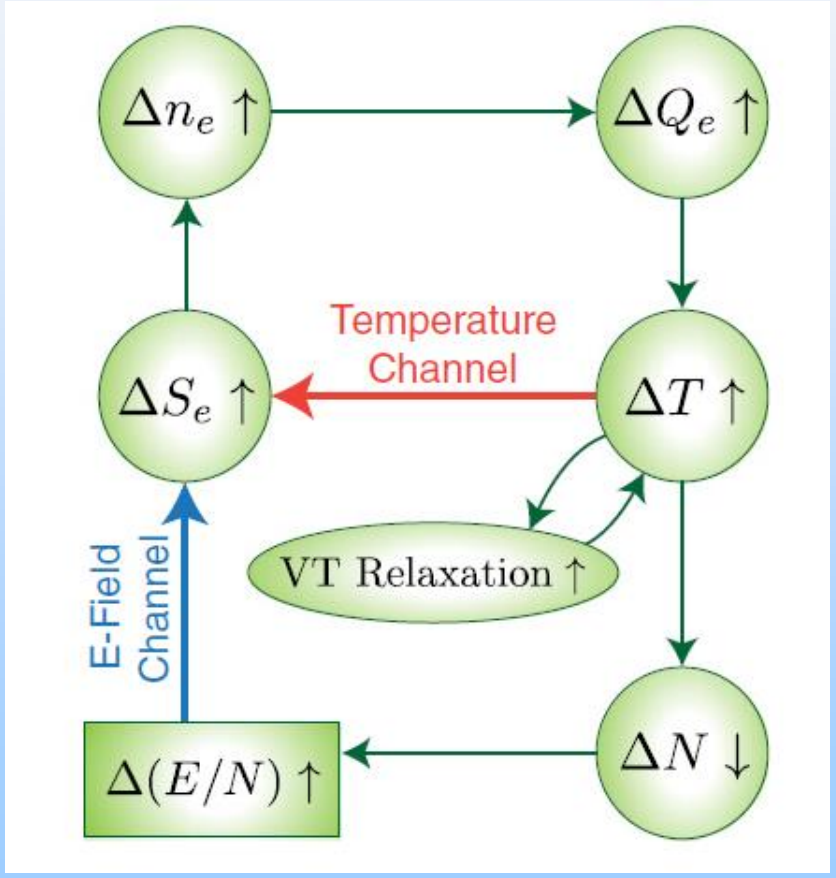

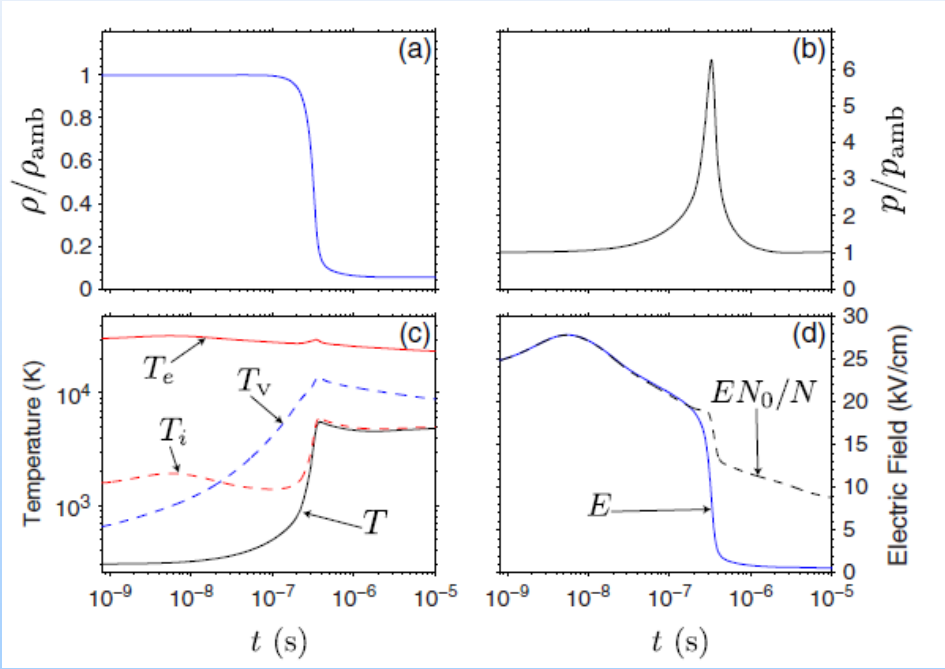

Raizer, 1992.

Da Silva and Pasko, 2013.

Conclusion

- The ionospheric potential (IP) and lightning flash rate (LFR) were calculated using INMCM4.0 model
- Global patterns of lightning activity on ENSO time scale in the model appear to be similar on observed patterns when taking into account the wind shear in LFR parameterization
- Numerical simulations suggest that the inter-annual IP variability is low and does not exceed 1% of the mean value, being tightly correlated with the mean SST in the Pacific Ocean (180W-100W, 5S-5N). The IP maximum corresponds to the SST minimum in model simulations
- During El-Nigno time in the model the mean aerosol content in the atmosphere decrease

Сквозная фаза

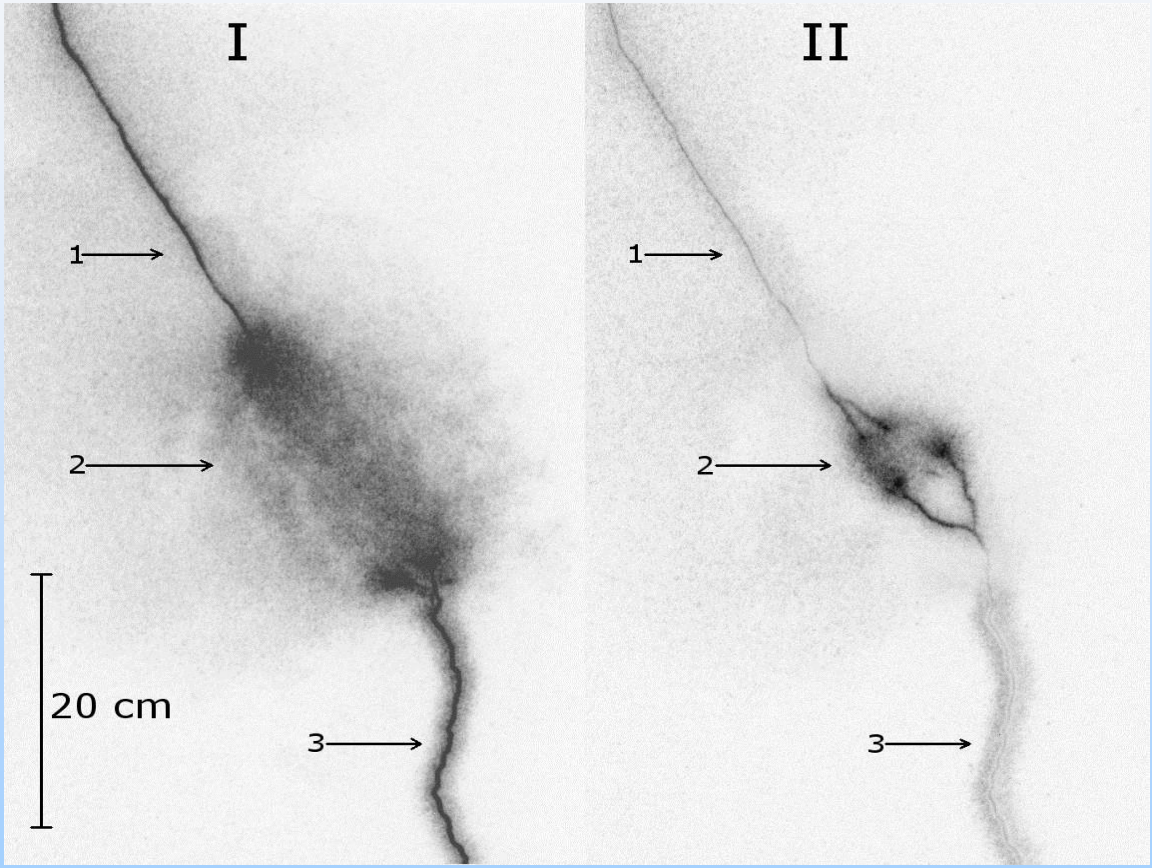

1 – отрицательный нисходящий из облака лидер, 2 – интенсивное взаимодействие стримерных зон, 3 – восходящий с токоприемника (шарика) положительный лидер. Выдержка кадра I – 100 ns, II – 50 ns. Время между кадрами – 2 мкс.

Циркуляция атмосферы

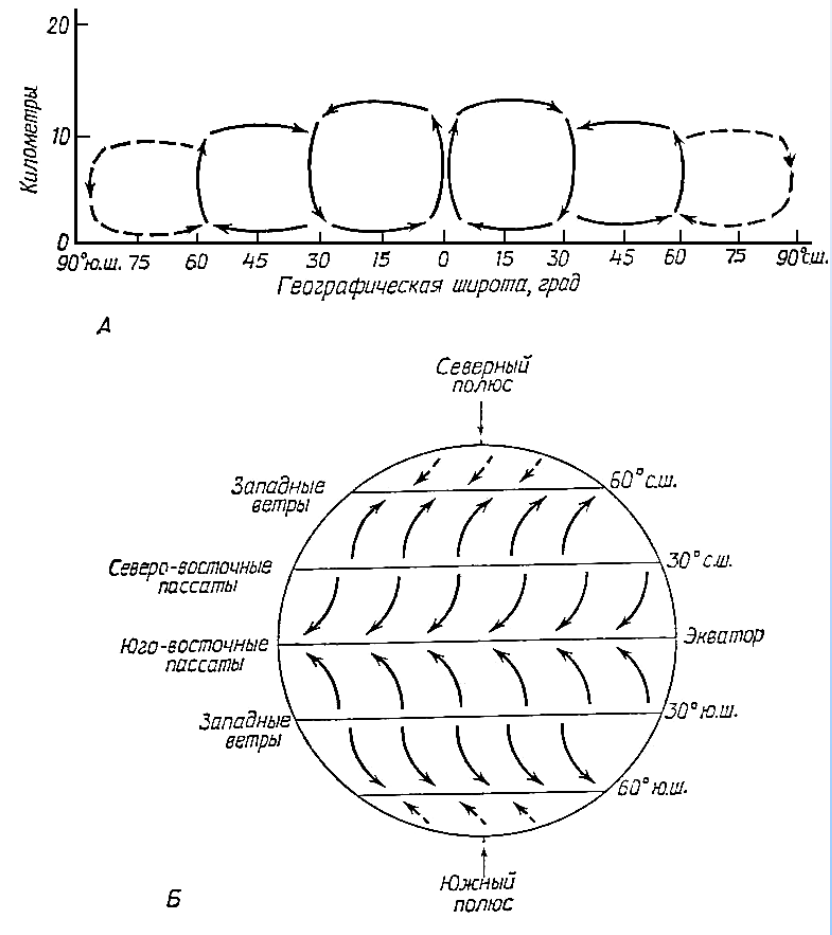

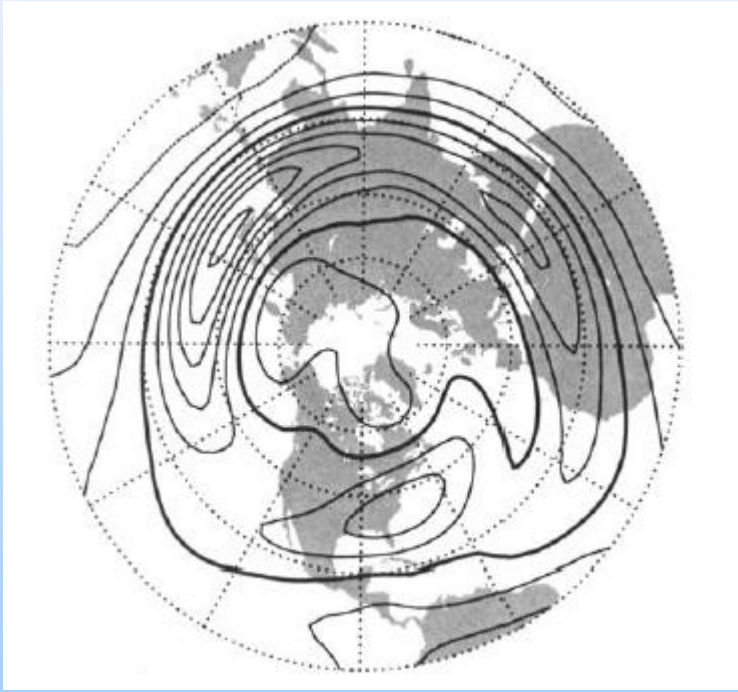

Циркуляция атмосферы

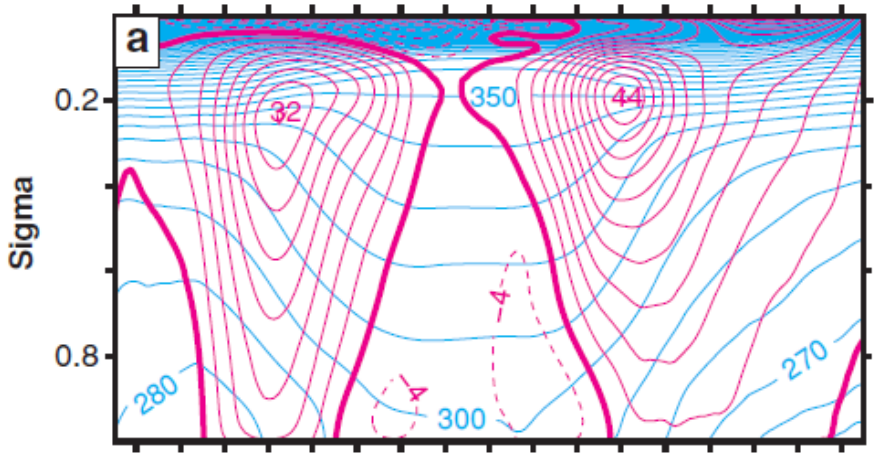

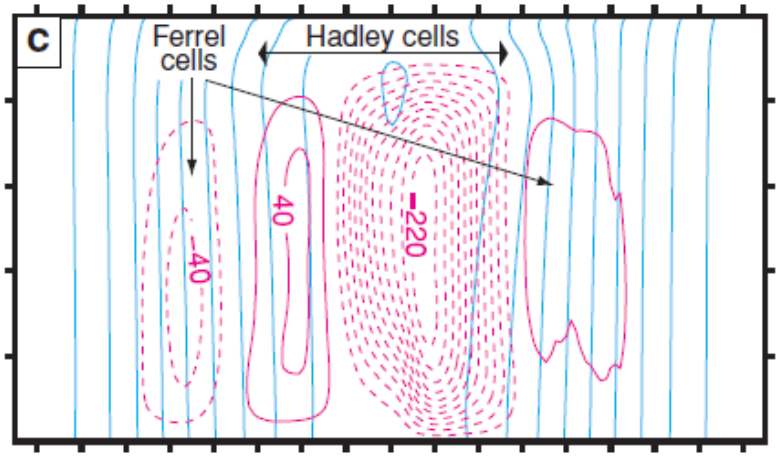

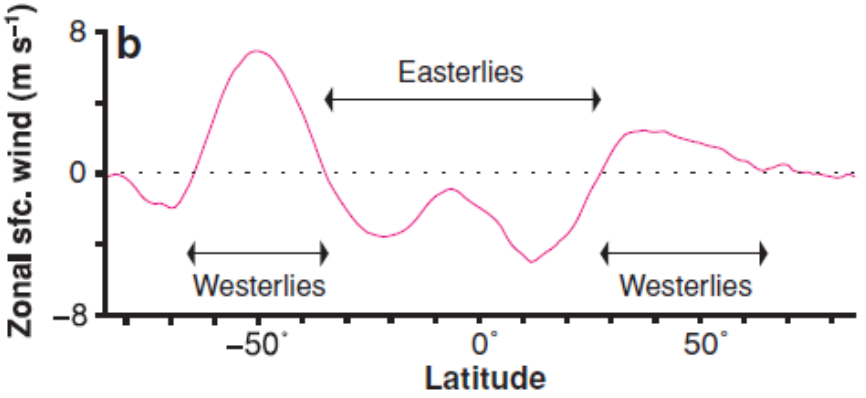

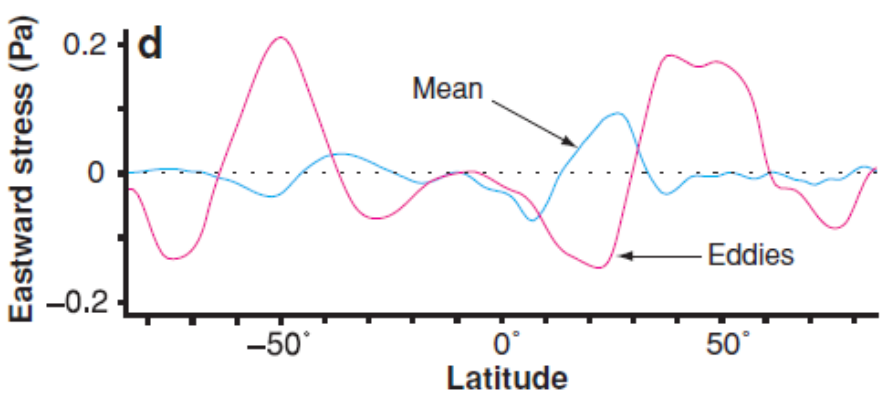

First and subsequent strokes

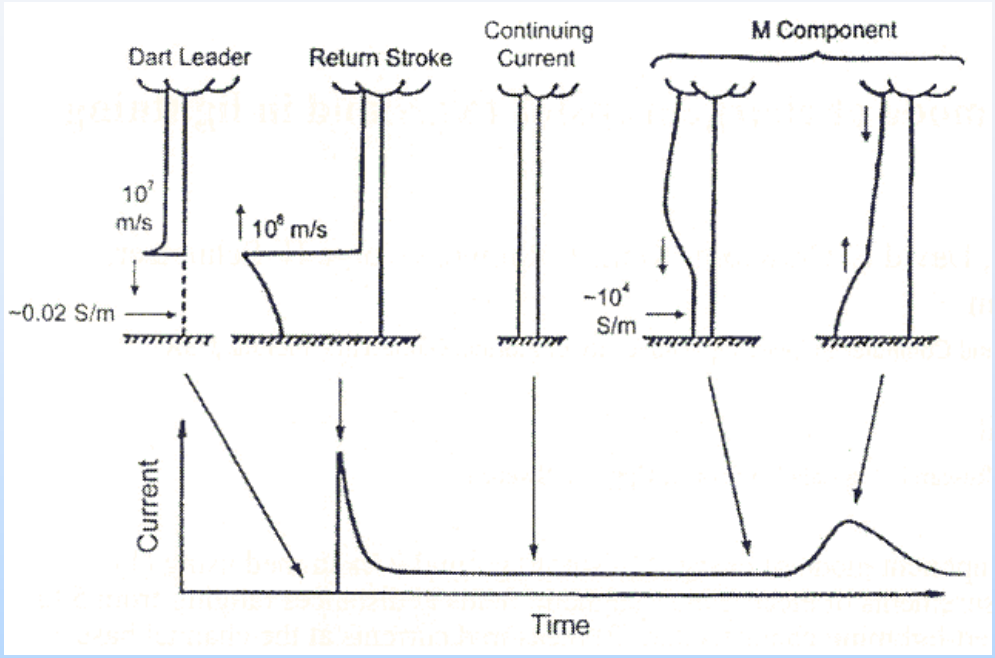

Rakov et al., JGR, 2001

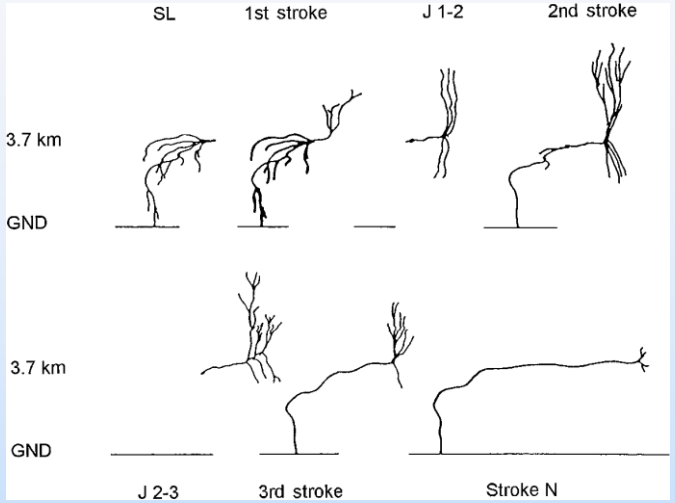

Proctor, JGR, 1988

Lapierre al., JGR, 2014

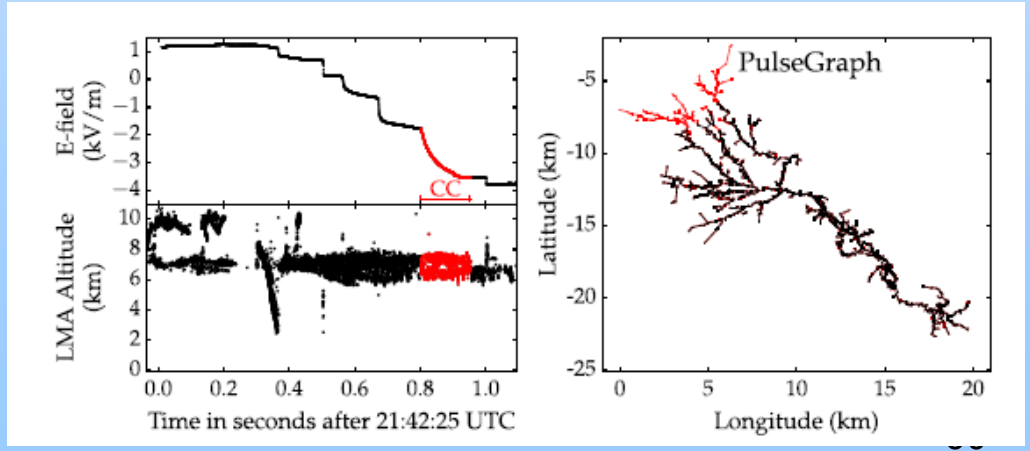

Корреляция эльфов и SST

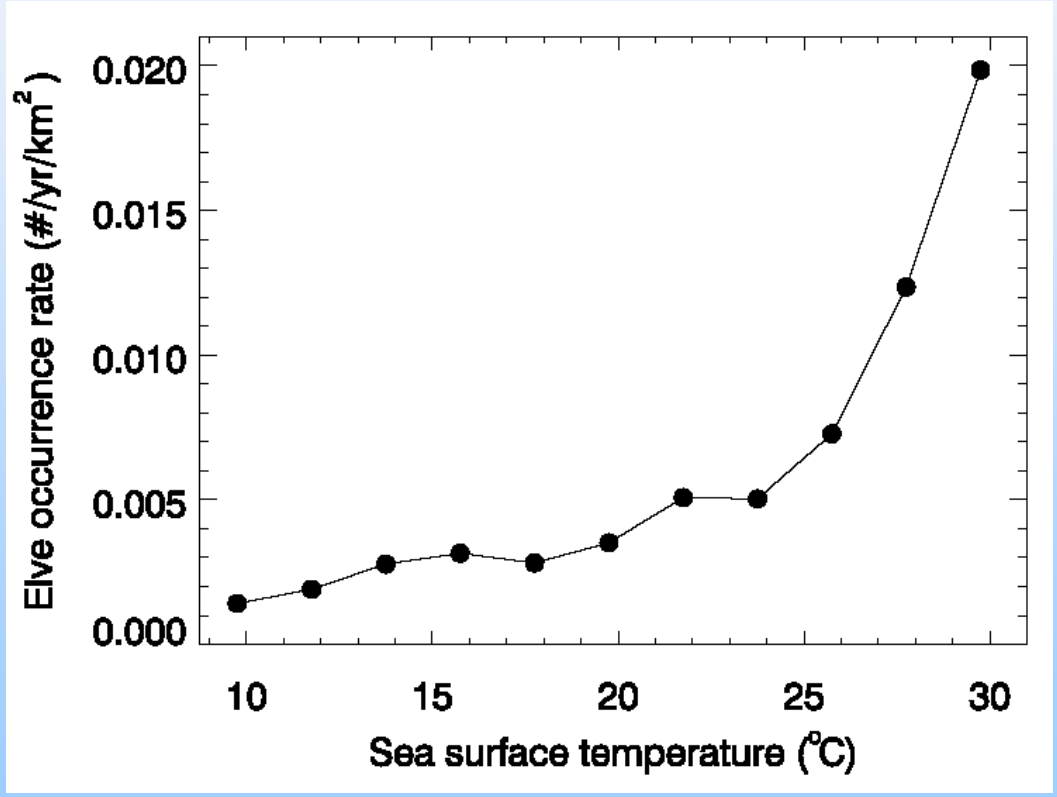

Field dynamics as measured at balloon and at ground

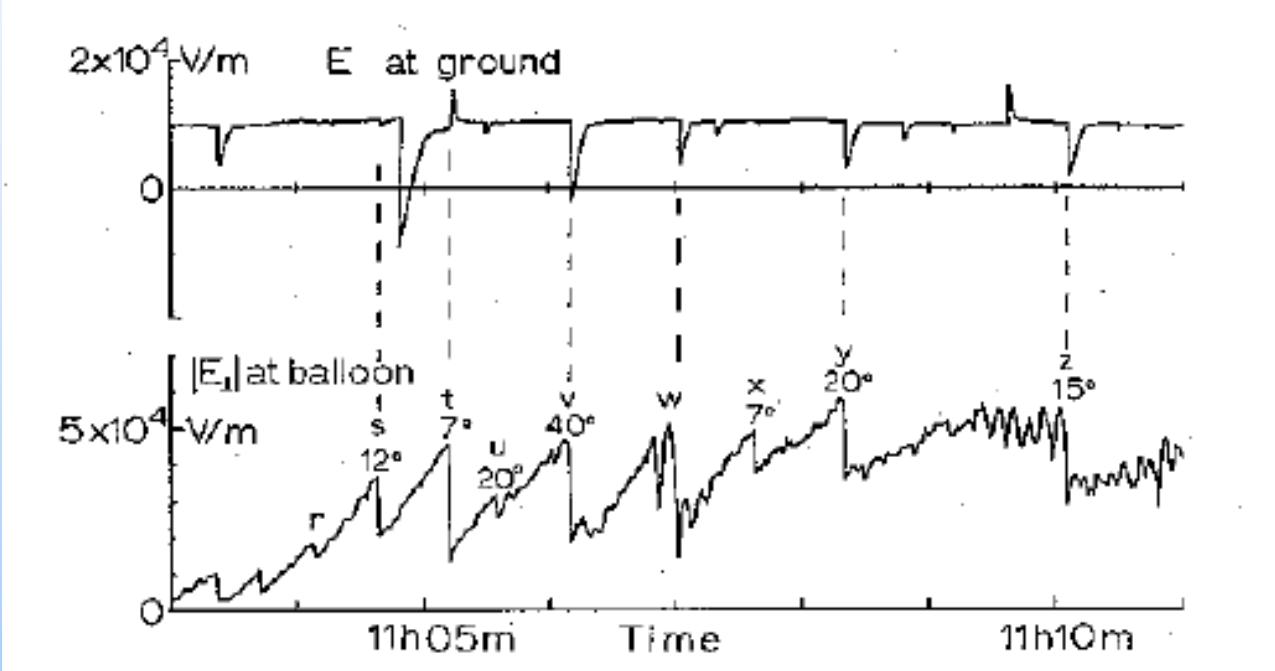

Winn and Bierley, QJRMS, 1975

Effect of corona layer near ground

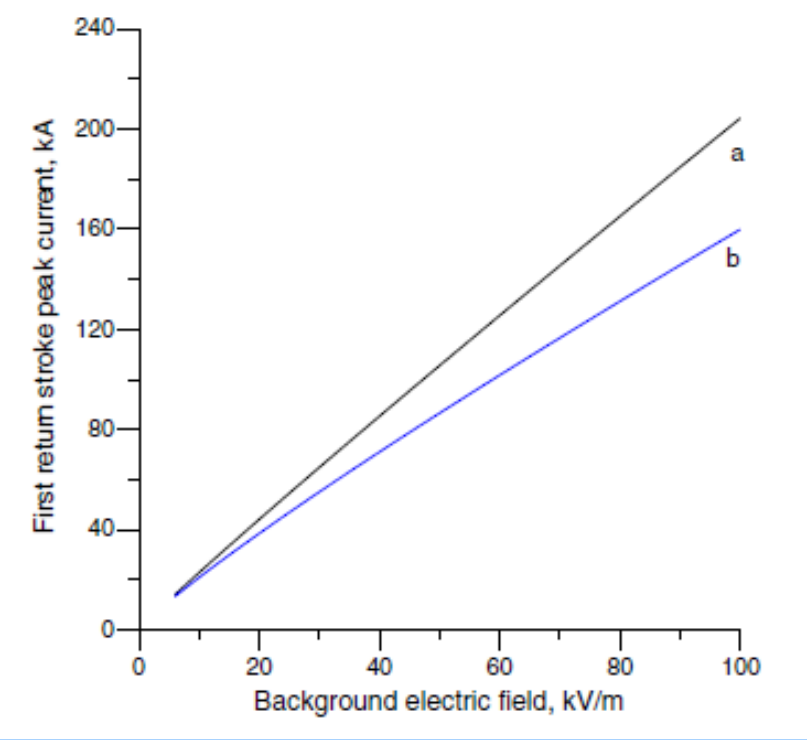

Cooray and Rakov, 2012

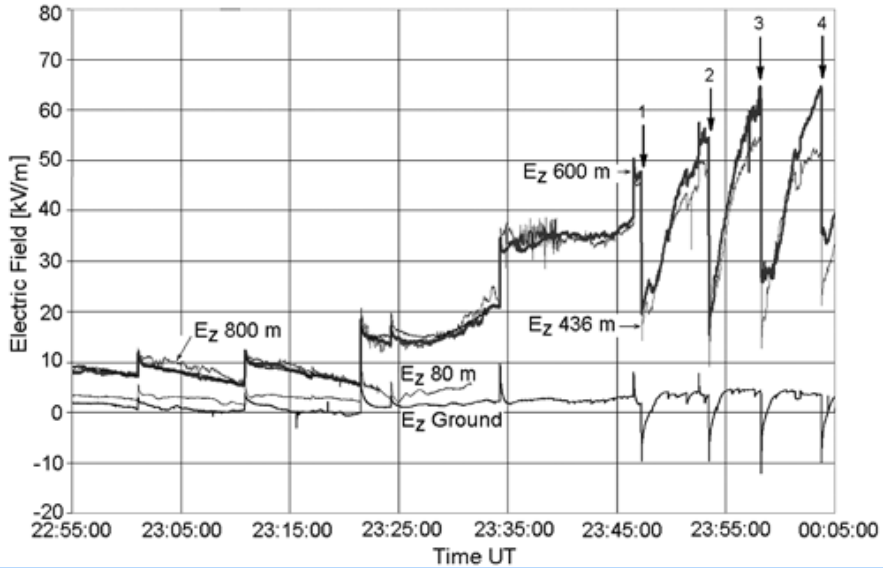

Electric field variations measured at ground and aloft beneath a thunderstorm on 10 August 1989, at Kennedy Space Center [Soula and Chauzy, 1991]. The numbered
arrows correspond to the triggered CG flashes.

Глобальная атмосферная электрическая цепь

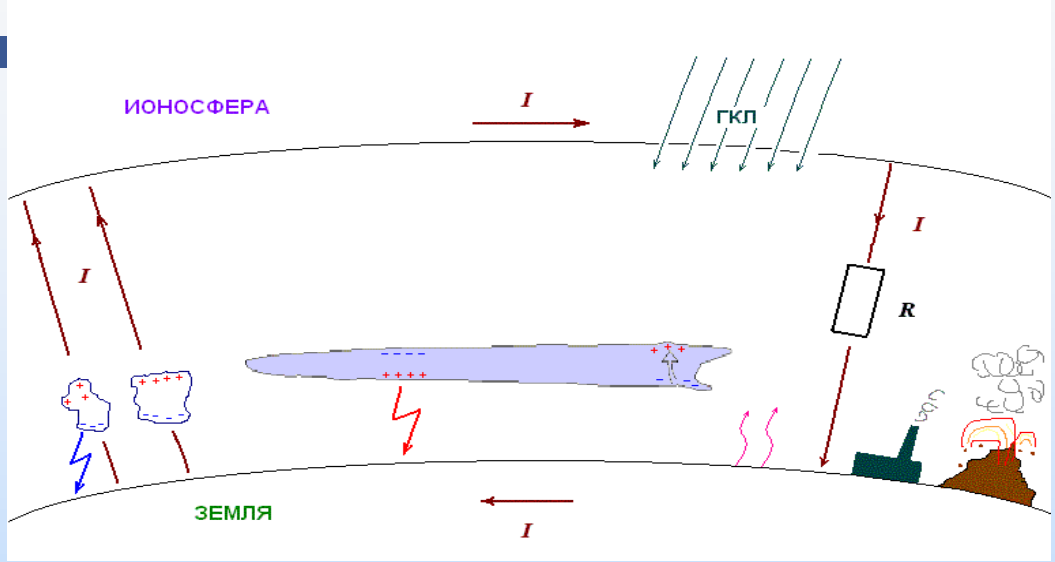

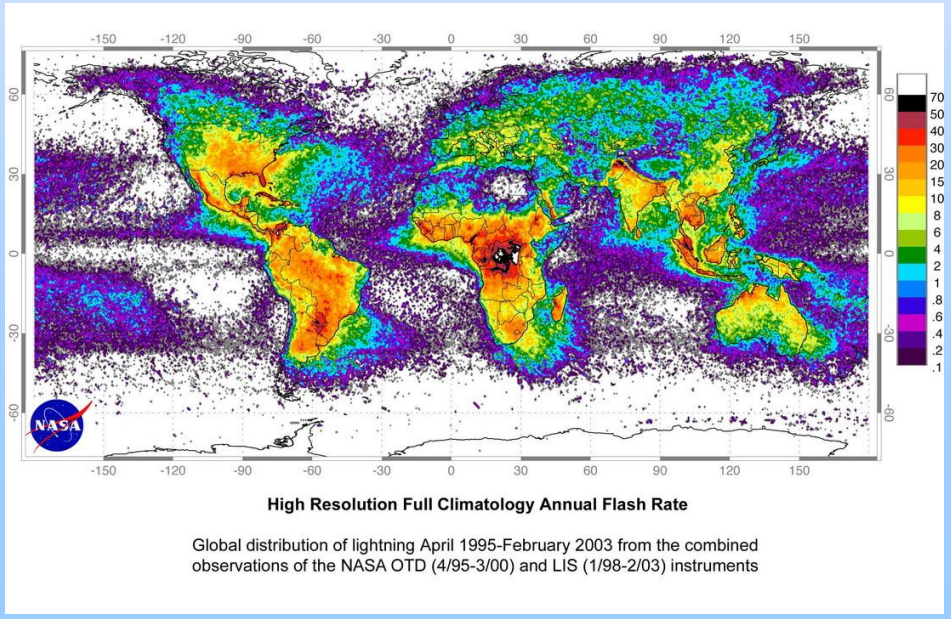

High Resolution Full Climatology Annual Flash Rate

Global distribution of lightning April 1995-February 2003 from the combined observations of the NASA OTD (4/95-3/00) and LIS (1/98-2/03) instruments

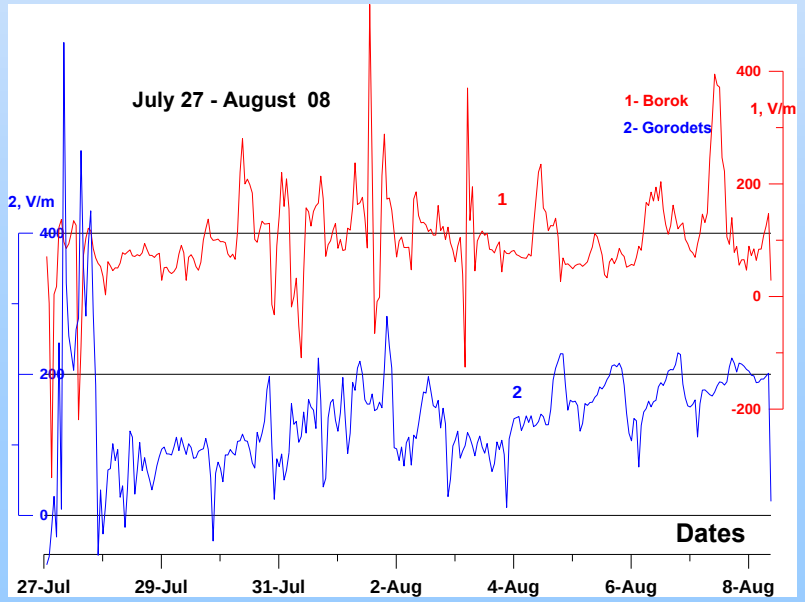

GEC evolution: mechanisms

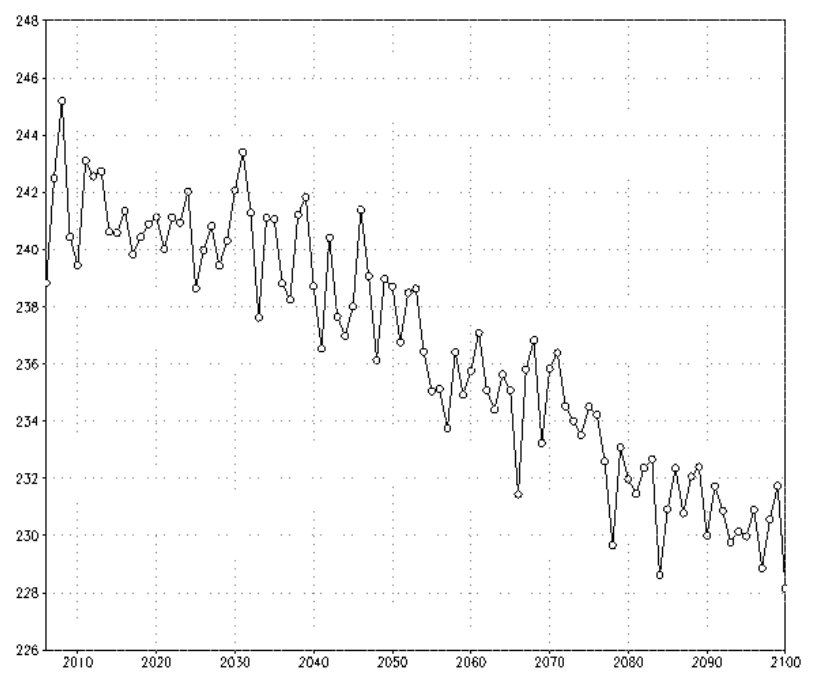

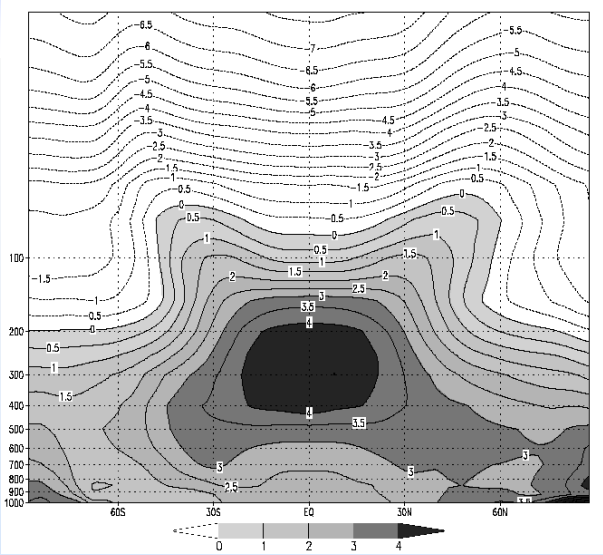

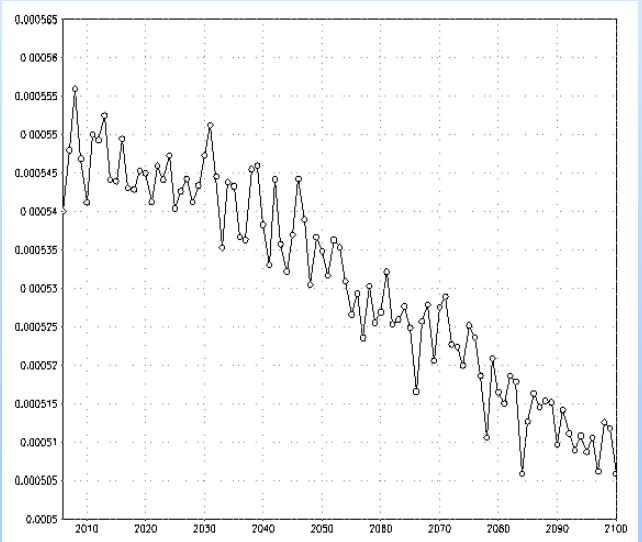

Vi mean-annual evolution in the model (left); latitude-altitude distribution of temperature perturbations; mean-annual square of convection (non-dimensional) calculated as the relation of convective precipitation over temporal step to the air-column moisture content

Перспективы

- Совершенствование банка данных характеристик атмосферного электричества средних широт и выработка рекомендаций по организации непрерывного мониторинга характеристик атмосферного электричества.
- Разработка моделей динамики глобальной электрической цепи в условиях изменяющегося климата на различных временных масштабах и прогноз эволюции атмосферного электричества в XXI веке.
- Исследование и выбор адекватных параметризаций глубокой конвекции и гроз для их использования в климатических моделях.
- Установление обратных связей между изменениями климата, атмосферным электричеством и газовым составом атмосферы на основе численных экспериментов с использованием химико-климатической модели высокого пространственного разрешения.

Спасибо за внимание!